Experiments on Quantum Turbulence within Superfluid ^{3}He-B.

Michael Robert Lowe BSc (Hons.)

October 2003

A thesis submitted in fulfilment of the requirements
of the degree of Doctor of Philosophy at
Lancaster University

Experiments on Quantum Turbulence within Superfluid ^{3}He-B.

Abstract

This thesis describes experiments conducted on B phase ^{3}He in the μK temperature regime to investigate the turbulent properties of quantised vortices created by driving a vibrating wire resonator above its superfluid pair breaking critical velocity.

By operating several resonators as highly sensitive vortex detectors the localised effects of vortex lines have been measured. The results have shown the vortices being of greater density in the directions of the generating wire motion and the rate of production being dependent upon the generator wire velocity. The rate at which the vortices decay spatially has been shown to approximate to a simple exponential and the decay length of this exponential has been measured.

Using a thermal quasiparticle beam emitted by a black body radiator, the temperature dependence of the vorticity has been investigated for several quasiparticle beam temperatures between 177μK and 275μK and several bulk superfluid temperatures between 171μK and 236μK. The vortex line density of the turbulence has been calculated using a mathematical model developed here at Lancaster and shows some dependence on the temperature of the superfluid. The method of using a quasiparticle beam emitted from a black body radiator may be developed to allow a higher resolution of investigation of vortex creation and decay.

To whom I owe my sanity...

During the past three years there have been good times and bad times. The people I will thank here have made the good times very good and the bad times few and far between. Firstly I would like to thank the love of my life Natasha for putting up with me for the past three years whilst I've worked late and worked the occasional weekend. Without her love and support all this may not have happened. Thank you. Secondly I'd like to thank my parents Phil Lowe and Gill Lowe for support both emotionally and financially, my brother David and little nephew George.

Studying for a PhD is not a solitary endeavour and the members of the research group have been at worst entertaining and at best wonderful colleagues so in no particular order I thank you all here. Thanks to my supervisor Ian Bradley and his fantastic selection of colourful T-shirts and his odd tastes in music. Thanks to Graeme Plenderleith and Rich Haley for first teaching me the incorrect way to do a helium transfer and correct way respectively. Thanks to Giorgi Tvalashvilli for showing me that the accelerator pedal is not necessary for driving and that an on-off switch works equally well.

Thanks to Ian Miller and Martin Ward for their fine technical support despite their reluctance to fill nitrogen dewars and thanks to Dave Clubb for just making me smile whenever I see his face. Thanks to Paul Reeves for looking far younger than me despite being several years older. Thanks to Marek Bartkowiak for just being so typically german. Thanks to Andreas Rahm to coming over from Germany for a year and doing all the weekend transfers. Thanks to Peter Skyba for the discussions on politics and finance and thanks to Becca Whitehead and Carolyn Matthews for their excellent

management of the Coffee Club.

Finally the last few members of the group and arguably the most important. Thanks to Shaun Fisher for proving to me that my patience knows no bounds and keeping me very well entertained on the way to Japan. Thanks to Tony Guénault for his initial supervision, for being the only one who understands LabView and for writing his very helpful book. Thanks to George Pickett for being an exemplary fluff headed figure head for the group and for his artistic wizardry with both Illustrator and Photoshop.

Lastly I'm going to thank the people who were not members of the group but have contributed to the last three years. Firstly I have to thank Owen Griffiths and Hamish Nichol for showing me how it all could have gone so horribly wrong. The technical support staff Ron and Tim and everyone who was a member of Coffee Club. Finally thanks to Dez "Statto" Wright, Brian "Big Bellied" Davies and the rest of the Graduate College Darts team. One day boys you may be as good as me.

With all the thanks, mentions and thinly vieled insults out of the way, enjoy the thesis.

Contents

List of Figures

Chapter 1

Introduction

Helium was originally of no great interest for science due to it being chemically inert. It has an atomic number of 2 and atomic weight of 4.0026[1]. The chemical properties of helium arise from the electrons which orbit the nucleus. Two electrons are located in the $1s^2$ electronic shell and balance the positive electric charges of the protons. With the $1s^2$ electronic shell being full these electrons are very reluctant to interact with any electrons from other atoms.

Helium is found to consist of two isotopes. The most common of these is helium-4. This isotope has two neutrons within its nucleus, is found commonly in air and is useful for floating balloons due to the gas being lighter than air. The gas, when cooled to a temperature below 4.2K condenses into a liquid and further cooling to below a temperature of 2.17K (SVP) undergoes a phase transition into a superfluid state, often refered to as HeII[2]. The superfluid transition is observable by a sudden cessation of boiling and a sharp peak in the heat capacity of the liquid. The shape of this heat capacity peak resembles the Greek letter lambda, λ, and gives the name of the transition.

Below T_λ the viscosity of the fluid reduces to an infinitesimally small amount and for a macroscopic volume of liquid it is very difficult to see any viscous effects.

The mathematics which have been developed to describe this new state of matter have one interesting consequence, *irrotationality*. This is where the liquid will not show any normal rotating flow and if the vessel in which the superfluid is contained is rotated, the bulk liquid will appear as though it is rotating like an ordinary liquid with the surface dipping in the center but the bulk liquid is actually stationary with small irregularities. These features are small vortex lines[3] where the total rotation of the vessel is compensated for by the liquid forming small lines where the superfluid is rotating around a core. The critical velocity V_c for spontaneous creation of vortices was first calculated for HeII by Feynman in 1955[4]. These vortex lines are of great interest to physicists due to their nature of being quantised. With the superfluid being a quantum system, the properties of the entire fluid can be described by a single wavefunction which applies to the whole system. The nature of this wavefunction gives rise to the fact that the vortex lines must be quantised with a quantum of circulation of $\frac{h}{m_4}$[3]. Since helium was first liquefied in 1908, it has become one of the most extensively studied chemicals.

The other isotope of helium, which is of interest to science, is helium-3. Identically to helium-4 it has two protons and two electrons but crucially it has only one neutron in the nucleus. This may be considered to be only a small difference, neutrons are very small, but this dictates that the properties of the two isotopes to be very very different at low temperatures. With helium-3 atoms being smaller, the zero point energy of the atoms is larger.

This reduces the temperature at which it condenses into a liquid to 3.2K (SVP) and this zero point energy of the helium-3 is sufficient to allow it to stay liquid like helium-4 even at absolute zero unless it is highly pressurised. Upon further cooling to temperatures below $\sim$ 1K, their physics can no longer be described merely by conventional theory, but we now have to consider quantum mechanics. This is where the differences in their atomic structure give rise to greatly different physical properties.

Helium-4 has two neutrons in its nucleus. With each nucleon having $\frac{1}{2}$ integer spin this gives the total atom an integer spin. Because of the zero integer spin, ^{4}He obeys Bose-Einstein statistics and is a Boson. Helium-3 has only one neutron in its nucleus. This gives the total ^{3}He atom a half integer spin and because of this it must obey Fermi-Dirac statistics and is a Fermion. Whereas Bosons can occupy any quantum state, fermions are governed by the Pauli exclusion principle which states that any quantum state can only be occupied by one fermion. This is explained more in Chapter 2.

With helium-3 being a fermion, in order to allow the transition into a superfluid at the temperature of 0.929mK and a pressure of 0 bar, it was discovered that two ^{3}He atoms with half integer spin will pair together to form a Boson with integer spin. Being an effective Boson this new particle can go through a phase transition and form the superfluid state. The mathematics for superfluids now apply to helium-3 and as such the superfluid is irrotational. Similarly, a rotating vessel of helium-3 will cause the superfluid to form quantised vortices to compensate for the rotation which have a quantum of circulation of $\frac{h}{2m_3}$[5]. The quantum of flow now has a mass factor of $2m_3$ rather than m_4 for ^{4}He. This is because the Boson like pair consists of

two ^{3}He atoms.

It has been discovered that a vibrating wire resonator driven above its critical velocity will generate vorticity in superfluid helium-3[6]. It is not the fact that vortices were produced that was surprising rather the fact as to how they were produced. It has been possible to produce vortices in this most novel of fluids for many years through more traditional techniques such as rotating the containing vessel. The discovery that inhomogeneous vortex lines could be produced so easily and without the need for expensive rotating cryostats has opened a new cheaper quicker avenue towards investigating this unique manifestation of quantum mechanics.

In comparison to the mathematically heavy NMR techniques, using a vibrating wire resonator to detect a region with a high density of vortex lines is relatively easy. Monitoring the damping experienced by the motion of the wire can provide a simple demonstration of the detectors recording vorticity. The main drawback of this method is an unfortunate lack of resolution, unlike with NMR, where single vortex lines have been observed[7], this technique can only provide qualitative information from a change in damping due to experiencing a tangle of vortex lines. The change in the damping can however provide some quantitative information if it is investigated with regards to how the tangle develops spatially or if a well defined beam of thermal quasiparticles is used to probe the vortices.

The Andreev reflection of quasiparticles by flow fields has been studied before using a paddle[8] to create the flow barrier. The work I shall explain will use the vortices recently found to be produced by a supercritical vibrating wire to provide the flow fields with which to reflect the quasiparticles.

Chapter 2 will describe the basic properties of ^{3}He at low temperatures and introduce the theory behind quantised vortices in ^{3}He, the mechanism of Andreev scattering of quasiparticles and a brief overview of investigations into turbulence within superfluids so far. Chapters 3 and 4 will introduce the equipment used for producing such low temperatures in the laboratory environment and the vibrating wire resonator that will be used extensively. In chapter 5 the first of the two experiments will be explained. This experiment will investigate how the vortices created by a vibrating wire resonator develop spatially. The temperature dependency of this will be investigated and a decay length for the vortex density will be measured.

Chapter 6 will detail the second experiment of this thesis. In this experiment a defined thermal ballistic quasiparticle beam is generated with a black body radiator and is used to probe a region of generated vortices. By using the radiator to resolve small changes in power, the fraction of the quasiparticles that interact with the vortices can be measured. A simple model which uses our calculated decay length is then introduced to relate the reflected fraction to a vortex line density, L_0. The results for the experiments are then summarised in chapter 7.

Chapter 2

Properties of Helium

2.1 Introduction

The ^{3}He nucleus contains only one neutron and two protons each having spin of $\frac{1}{2}$ resulting in the atom having a net spin of $\frac{1}{2}$. Thus the ^{3}He atom is described as a fermion similar to the free electrons found in a metal. Being fermions, ^{3}He atoms are forbidden, according to the Pauli exclusion principle, from occupying a common quantum state. Theory shows that in a system of free fermions at (or very close to) absolute zero, each allowed state will contain one fermion with spin up and one with spin down, to a maximum energy, E_F, known as the 'Fermi Energy'. A typical energy dispersion curve for a Fermionic system is shown in Fig 2.1 overleaf. Below the Fermi energy all available states on the curve are occupied and respectively all states above are empty. The Fermi energy also has an equivalent temperature, the 'Fermi Temperature', T_F, which are related thus:

$$T_F = \frac{E_F}{k_B} \tag{2.1}$$

For ^{3}He this temperature is of the order of 1K and is low compared to that of free electrons in a typical metal about 10^4K. As the temperature T of the fermions increases, this cut-off point becomes broadened by an energy k_BT, where k_B is the Boltzmann constant. The probability of an energy state being occupied within this broadened energy now lies between 0 and 1. At high temperatures where $k_BT \gg E_F$ this occupation probability tends towards the Maxwell-Boltzmann distribution and the system begins to obey classical mechanics. All the experiments within this thesis were done with ^{3}He at such low temperatures so that classical mechanics need not to be considered normally and only Fermi-Dirac statistics are needed to be used.

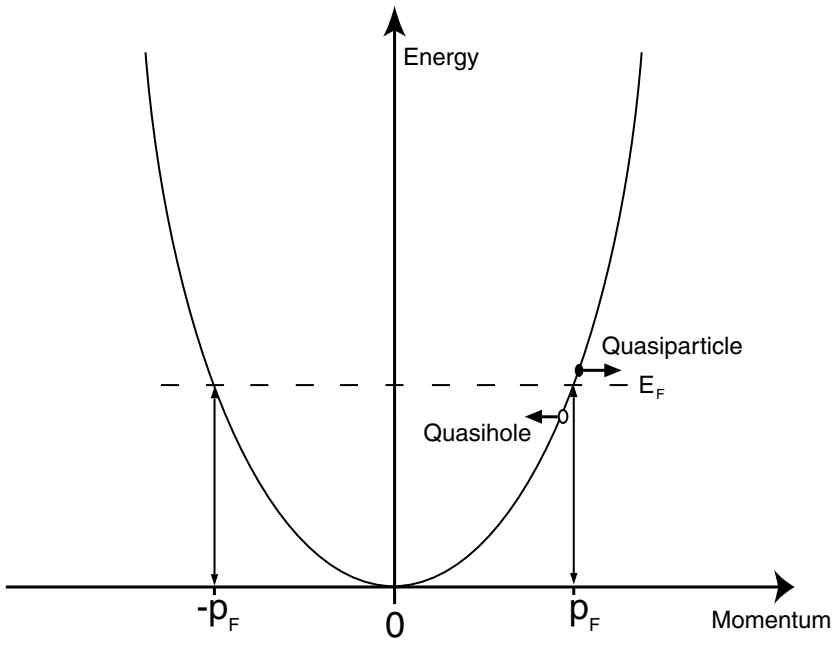

Figure 2.1: Excitation dispersion curve for a normal fermionic system.

Using the Fermi-Dirac distribution function the properties of the system can be derived, assuming that the system is an ideal case of non-interacting

fermions at low temperatures. The distribution function is:

$$< n(\varepsilon_i, T) >= \frac{1}{\exp\left[\frac{(\varepsilon_i - \mu)}{k_B T}\right] + 1} \tag{2.2}$$

where $< n(\varepsilon_i, T) >$ is the occupation number of a state i with energy ε at temperature T and μ is the chemical potential. The chemical potential is found to be equal to the Fermi energy.

Landau reasoned in his Fermi liquid theory, that for a system at such low temperatures the properties of a Fermi fluid will be governed exclusively by the excitations, as is the case for superfluid ^{4}He and superconductors[9][10]. It can be seen that for a system of fermions at low temperatures only the atoms with energies very close to E_F have available states within which to scatter. This renders atoms with their excitations in lower energy states effectively inert. Another of Landau's postulates is that to consider the interatomic forces between ^{3}He atoms they must be thought of as a weakly interacting 'quasiparticle' with a larger mass than a bare ^{3}He atom. The larger mass is due to the fact that with the interatomic interaction present, any perturbation of a ^{3}He atom will perturb all the neighbouring ^{3}He atoms.

With Landau's theory, the properties a Fermi liquid can be calculated from two sequences of Fermi liquid parameters, F_n^s and F_n^a. The full mathematical derivation of these parameters can be found in most texts on superfluid ^{3}He such as Wölfle[11], Tilley and Tilley[12] or Leggett[13]. In general practice only the parameters F_0^s, F_1^s and F_0^a need to be considered.

The parameter F_0^s correlates to the compressibility of the liquid and is found to be large and positive. F_1^s links the bulk flow and quasiparticle

momentum and allows the definition of the quasiparticle effective mass, $m^\star$:

$$\frac{m^\star}{m_3} = 1 + \frac{F_1^s}{3} \tag{2.3}$$

with m_3 being the bare mass of a ^{3}He atom. The last significant parameter, F_0^a, results in an enhanced magnetic susceptibility:

$$\chi = \frac{\chi_0}{1 + \frac{F_0^a}{4}} \tag{2.4}$$

where $\chi_0 = \mu_0^2 N_F$ and is the normal spin susceptibility of a Fermi gas of effective mass $m^\star$ with density of states N_F, and where μ_0 is the nuclear magnetic moment. At the low magnetic fields used the parameter F_0^a is not needed to be considered for the experiments conducted for this thesis.

2.2 B.C.S. Theory

After the experimental discovery of superconductivity at low temperatures, physicists started to work on the underlying theory behind this. In 1957 Bardeen, Cooper and Schrieffer first introduced the concept of electron pairing within superconductors[14] in order to explain superconductivity. The theory that they proposed was that as an electron travelled through the metal lattice it left a 'wake' which had a net positive charge. This wake then attracts an electron travelling in an opposite direction which leaves its own positively charged wake. The attraction between the two electrons then causes the creation of a 'Cooper pair'. An electron is of course a fermion and as such is governed by Fermi-Dirac statistics, like our friend the ^{3}He atom, but when paired with another fermion the pair behaves like a solitary particle. The new 'particle' is not a fermion but a boson and consists of two electrons interacting via phonon excitations in the lattice.

This new boson-like Cooper pair of two electrons can now undergo a second order phase transition into a new superconducting state. The transition into the superconducting state for the Cooper pair is characterised by the creation of an energy gap, Δ, between the Cooper pairs and the free electron excitations with the Fermi energy, E_F at the Fermi surface. This energy gap is due to the binding energy of the pair.

The interactions between the two electrons favour the formation of $L = 0$ pairs in order to maximise the interaction strength despite the considerable repulsive electrostatic forces. The respective wave functions of the electrons now overlap and this type of pairing is known as s-wave pairing. As the wave functions overlap the spatial component of the wave function must

be symmetric and, to conform with the Pauli exclusion principle, the spin component of the wave function must be anti-symmetric. The spins are therefore opposite and hence the total spin $S = 0$. Because of the s-wave nature of the pairs in superconductors the energy gap is isotropic.

After the paper was published physicists began looking for other systems which they could fit the theory to. An obvious target was ^{3}He. Being a fermion, like free electrons in metals, it was proposed that they too could create Cooper pairs. Since ^{3}He atoms have no lattice structure to propagate the interactions, any interaction must be spin based. If this is to be true then the spin component of the wave functions must now be symmetric and the spatial component anti-symmetric. Since ^{3}He atoms are not point charges and cannot pass through each other as required if $L = 0$, the next possible value is $L = 1$ although higher values of L are possible. This gives a ^{3}He Cooper pair consisting of two ^{3}He atoms orbiting around a common centre of mass with $L = 1$ and $S = 1$. This pairing mechanism is known as p-wave pairing. In the early 1960's papers were published by Balian and Werthamer[15], Anderson and Morel[16][17] and Anderson and Brinkman[18] which explored the theoretical properties of these p-wave states. The predicted BW[15] state has since been found to correspond to the B phase of superfluid ^{3}He and the ABM[18] state corresponds to the A phase. Finally in 1972 the superfluid transition of ^{3}He was discovered by Osheroff, Richardson and Lee[19] whilst studying the effects of pressure on liquid and solid ^{3}He within a Pomeranchuck cell.

Upon cooling to 0.929mK at a pressure of 0 bar, ^{3}He goes through a phase transition into the superfluid phase as shown in Fig 2.2. This phase tran-

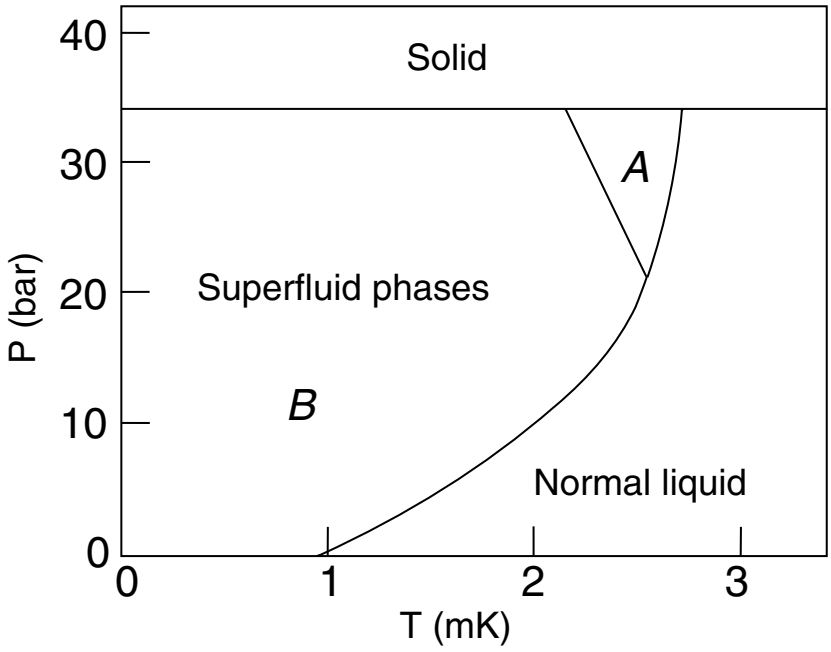

Figure 2.2: Phase diagram for helium-3 in zero magnetic field.

sition is analogous to the superconducting transition that has been studied extensively in metals that form superconductors. Unlike the s-wave pairing mechanism in this system, however, the p-wave pairing mechanism is more complex. The triplet nature of the $S = 1$ pairing allows three possible spin projections in ^{3}He, $S_z = -1, 0, 1$, and to fully describe the ^{3}He Cooper pair, the three possible angular projections due to the $L = 1$ triplet must be considered. Because of this the simple order parameter that is found in superconductors[11]:

$$\Psi_{SC} = \psi_0(|\uparrow\downarrow\rangle - |\downarrow\uparrow\rangle) \tag{2.5}$$

where ψ_0 is the amplitude of the wavefunction, needs to be replaced with a $3\times$ 3 matrix. The resulting parameter tensor $\hat{\mathbf{d}}$ now has 9 complex components representing the possible combinations of spin and angular momentum. This

results in many different superfluid phases; however only 3 of these are known to be stable. These are the B, A and A_1 phases. Figure 2.2 shows the main two phases found experimentally at zero magnetic field, the A and B phases. If a magnetic field is applied the A phase region will increase at the expense of the B phase region.

All the experiments conducted within this thesis are at such low temperatures and low magnetic fields that it is found that the B phase dominates the ^{3}He phase diagram and that there is no A or A_1 phase helium present within the cell. In this state all possible spin and angular momentum projections are found to be equally populated and because of this, the superfluid energy gap is isotropic with the BCS value of $\Delta = 1.76 k_B T_C$. This was first proposed by Balian and Werthamer[15] in their 1961 paper. The energy gap, Δ, is illustrated on the superfluid dispersion curve shown in figure 2.5.

The isotropic nature of the energy gap in k space means that as $T \rightarrow 0$, the number of quasiparticle excitations falls according to the Boltzmann factor $\exp(-\Delta/k_B T)$. At the lowest temperatures attainable in the laboratory, $\sim 80\mu$K, this exponential dependency leads to the quasiparticle density being so low that the mean free path of a quasiparticle is of the order of kilometres[20]. Since the mean free path is much larger then the dimensions of the experimental cell the quasiparticles are refered to as being 'ballistic' or in the 'ballistic regime'.

2.3 Quantised Vortices

2.3.1 Definition of a Vortex

A vortex is defined as a region where there is a circulating flow around a core. These are commonly seen when you pull the bath plug out and the water creates a 'tunnel' from the surface to the drain. Superfluids are also able to contain a vortex or vortices but these have a remarkable difference to the common ones observed in a body of water. This difference becomes apparent after examining the mathematical properties of flow in the superfluid.

In a classical viscous fluid there are several ways to describe a vortex or vortical flow. One definition defines a vortex as a finite volume of rotational fluid, bounded by irrotational fluid or solid walls[21]. A vortex line or a vortex tube can be defined by the equation

$$\omega = \nabla \times \mathbf{v} \tag{2.6}$$

where ω is the curl of the velocity field, known as the vorticity. A vortex filament is described as a vortex tube surrounded by irrotational fluid and a line vortex is a vortex filament with zero cross section. For HeII the vortex cross section is of the order of 1Å, so either vortex line or line vortex can be used. If a circular flow field is introduced by rotating a solid cylinder of radius a at a constant angular velocity Ω in an otherwise unbounded ideal fluid, a potential vortex is produced where the velocity distribution of the fluid v is given by

$$v = \frac{\Omega a}{r}. \tag{2.7}$$

This is described as a potential vortex. Replacing the cylinder with rotating fluid produces a Rankine vortex[3] where there is a velocity profile through

the core. These vortices are similar to the vortices found in ^{3}He since they have a thick core size in relation to the vortex size.

The proposal that superfluid ^{4}He could contain quantised vortices was first put forward in 1949[23] and Onsager postulated that the quantum of circulation would be h/m_4. This prompted activity within the experimental and theoretical groups. In 1961 the first experiment was performed to look for quantised circulation[24]. This experiment was successful in showing that quantised circulation and quantised vortex lines exist. Since this discovery the experimental methods to produce and detect vorticity have grown more sophisticated. These vortices found in HeII were seen to have a quantum of circulation h/m_4 where m_4 is the mass of a ^{4}He atom. Following on from the discovery that ^{3}He was found to form a superfluid at low temperatures the idea that it too could support quantised vortices has been investigated.

2.3.2 Vortices in ^{3}He

Since the ^{3}He superfluid condensate has a uniform quantum state the entirety of the superfluid can be described by a single macroscopic wave function[12]

$$\Psi(r) = \psi_0 \exp^{\mathrm{i}S(r)} \tag{2.8}$$

where $S(r)$ is the phase at position r and ψ_0 is the amplitude of the wave-function.

The consequence that this thesis is concerned with and shall be investigated is that since $\Psi(r)$ must always be single-valued, the phase of the wave function S itself must be single-valued or periodic. The requirement that S is periodic creates the phenomenon of quantised vortex lines in superfluid ^{3}He.

If we consider a loop of superfluid flowing in a circular way, the circulation, κ, of the loop of can be defined as:

$$\kappa = \oint v_s \cdot \mathrm{d}l \tag{2.9}$$

where the integral is taken around any loop wholly contained within the superfluid. The superfluid velocity of the flow, v_s, can be derived from the wave function in equation 2.8 and the definition of the mass current density, j_s[12]

$$j_s = \hbar \psi_0^2 \nabla S \tag{2.10}$$

which for ^{3}He, this superfluid flow velocity is then written as

$$v_s = \frac{\hbar}{2m_3} \nabla S \tag{2.11}$$

where $2m_3$ is the mass of the superfluid pair in ^{3}He.

Using this derivation it is now possible to express the quantity of circulation solely in terms of the phase S of the wave function by substituting equation 2.11 into equation 2.9 giving

$$\kappa = \frac{\hbar}{2m_3} \oint \nabla S \cdot \mathrm{d}l. \tag{2.12}$$

Solving this integral around the closed loop gives the result that

$$\kappa = \frac{\hbar}{2m_3} (\Delta S) \tag{2.13}$$

with ΔS being the change in phase of the superfluid wave function around the closed loop of flow. As the superfluid wave function is singularly valued, the phase S must be continuous around the loop. This sets the condition that the total change in S must be either zero or an integer multiple of 2π.

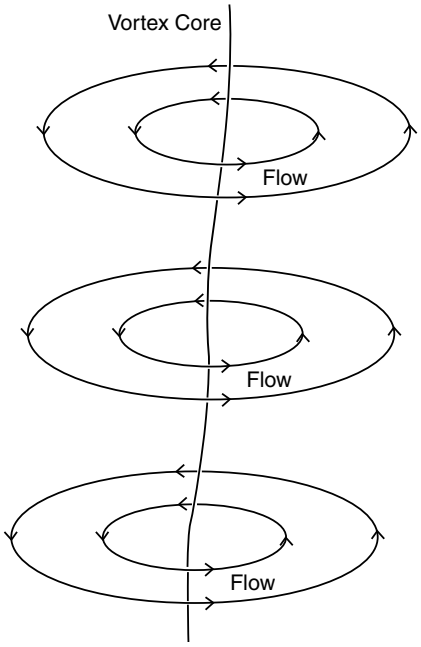

Figure 2.3: Vortex line in superfluid ^{3}He-B.

This defines the quantum nature of a vortex in superfluid ^{3}He where any enclosed loop of flow **must** have a quantum of circulation of

$$\kappa = n\frac{h}{2m_3} \tag{2.14}$$

where n is a positive integer.

From equation 2.9 it can be shown that the flow velocity of the vortex, v_s, reduces proportional to $\frac{1}{r}$ with distance r from the vortex core. Solving the integral around a closed loop gives

$$\kappa = \oint v_s \cdot \mathrm{d}l = v_s \cdot 2\pi r \tag{2.15}$$

therefore for a constant circulation κ it must be that $v_s \propto \frac{1}{r}$.

To calculate the energy per unit length of a vortex line it is necessary to integrate the kinetic energy associated with the velocity distribution between

Figure 2.4: Velocity of flow around a vortex line.

the core radius a and the vortex extent b. The vortex extent is taken to be the average intervortex spacing for a tightly packed tangle of turbulence. A term for the energy of a vortex line can be produced. This is shown in equation 2.16[3] where

$$\varepsilon = (\rho_s \kappa^2 / 4\pi) ln(b/a) \tag{2.16}$$

where ρ_s is the density of the superfluid and κ is again the circulation.

Substituting equation 2.14 into equation 2.16 it is shown that it is energetically preferential to have many vortices with $n = 1$ than to have vortices with $n > 1$. This means that if a vortex has twice the circulation it has four times the energy and is likely to breakup into four separate vortex lines.

With the quantum of circulation defined it is clear to see that vortex lines in superfluid ^{3}He must be quantised. Experiments conducted on superfluid ^{3}He contained within a rotating vessel at the Helsinki Institute of Technology have confirmed the sudden creation of a vortex line rather than the smooth

introduction of a vortex that a non-quantised system would produce and can even observe a single vortex line being created through NMR techniques[7].

Vortex lines in ^{3}He have a large core radius, typically of order of the coherence length ξ which is $\sim$ 77 nm at 0 bar and absolute zero, in comparison to vortices in ^{4}He, 0.1nm. The rotating superfluid around a vortex is responsible for a 'flow barrier' where the superfluid excitation energies undergo a galilean transformation when entering these associated flow fields. If the quasiparticle energy before entering the flow field is ε_0 and the energy is changed by $\mathbf{p} \cdot \mathbf{v}$ then the excitation spectrum of the quasiparticle is now shifted by

$$\varepsilon = \varepsilon_0 \pm \mathbf{p} \cdot \mathbf{v}. \tag{2.17}$$

The effect this transformation can have on the quasiparticle behaviour is quite dramatic due to the shifting of the excitation dispersion curve. Quasiparticles with energies less than $\Delta + \mathbf{p} \cdot \mathbf{v}$ are now unable to propagate through this flow barrier since there are no available states to propagate into causing the quasiparticle to be scattered. These scattering processes are explained in section 2.3.3.

2.3.3 Andreev Retro-reflection

If we examine the excitation spectrum for B phase superfluid ^{3}He, shown in Fig. 2.5, we can see that the quasiparticles have their momentum and group velocity in the same direction whereas quasiholes have their momentum in the opposite direction to their group velocity.

Let's consider what happens if a quasiparticle is travelling through the superfluid towards a region of localised flow in the superfluid such as around

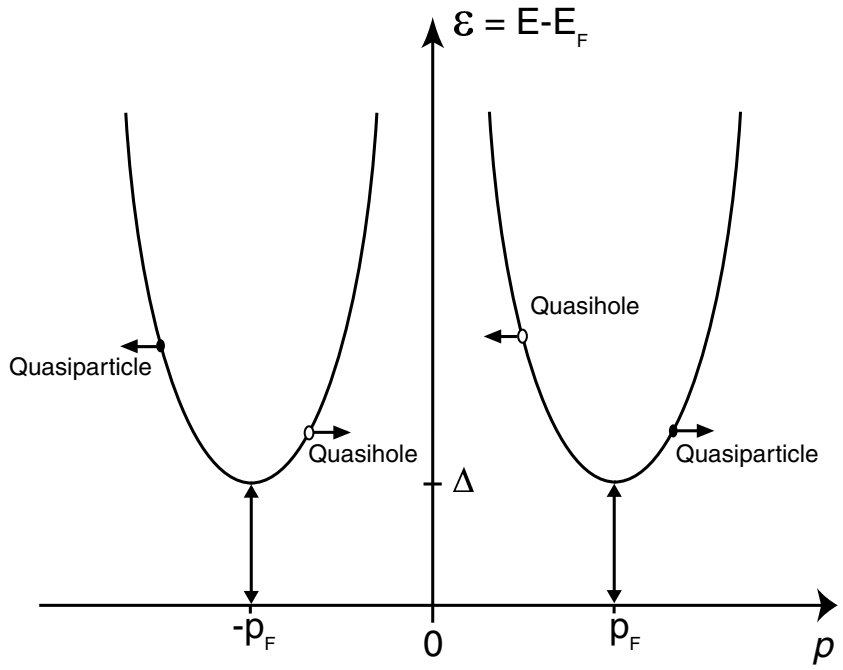

Figure 2.5: Excitation spectrum for stationary superfluid ^{3}He-B.

a vortex line. In the global rest frame of our laboratory the quasiparticle is moving towards a region of flow with a velocity, v. The flow field in the superfluid, can thus be assumed to travel towards the quasiparticle with velocity $-v$ in the rest frame of the quasiparticle. Since the fluid is moving, the excitation spectrum of the superfluid is changed with the quasiparticles and quasiholes in this region undergoing a Galilean transformation, which changes their group velocity to $v_g \pm v$ and their energies by $\pm p_F \cdot v$, depending on whether the quasiparticle is travelling into or away from the flow field.

Far away from the flow field the bulk superfluid is stationary in our laboratory rest frame and close to the flow field the superfluid has a velocity equivalent to the velocity of the flow field. In the rest frame of the flow field however the fluid next to the flow field is stationary and it is the fluid far

away from the flow field which has velocity v. This stationary dispersion curve is shown as the centre diagram in Figure 2.6. Under normal conditions an excitation will reach the 'surface' of the flow field and then propagate without interacting. What if there is no available state for the quasiparticle or quasihole to propagate through due to the excitation curves being shifted? This is where Andreev scattering occurs.

The process of Andreev scattering was first suggested by Andreev in 1964[22] in order to explain the conductivity of heat in intermediate state superconductors. The initial treatment was concerned with what happened to an electron with energy less than the superconductor energy gap attempting to propagate into the superconducting state from an adjacent normal state. His solution to this problem was that the electron combines with an electron of near identical opposite momentum from within the superconducting region forming a Cooper pair and leaving behind a hole within the normal region with identical momentum to the initial electron. Since the hole can be considered to have a negative mass equivalent to the electron mass the hole's velocity is in the opposite direction to the electron's and so is 'retro-reflected'. This argument can easily be applied to a quasiparticle in superfluid ^{3}He which is travelling into a region where due to flow fields the superfluid excitation curves are shifted and there are no available states in which for it to propagate.

If we look at Fig 2.6, and consider a quasiparticle on branch 5 with energy less than $\Delta + p_F v$. This quasiparticle has no states available within the flow field, shown by the centre curves, so cannot penetrate the flow field since the particle cannot create, or destroy, its own energy. Instead the en-

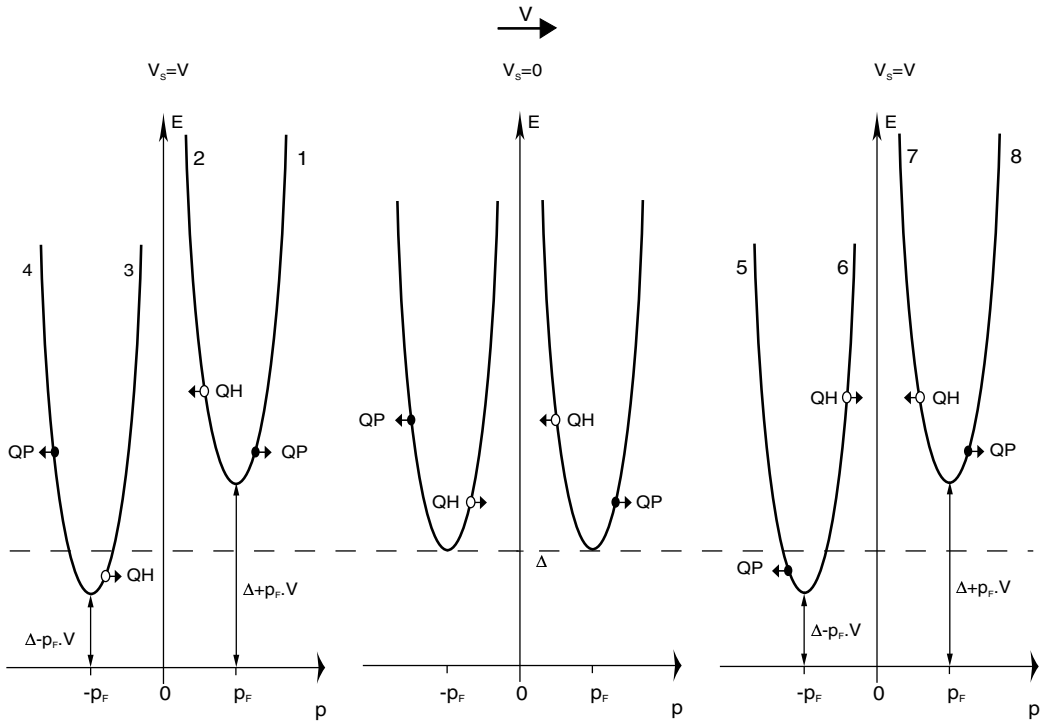

Figure 2.6: Excitation spectra for moving superfluid ^{3}He-B in the rest frame of the moving superfluid.

ergy and group velocity of the quasiparticle, in the moving superfluid frame, approaches the minimum in the excitation curve where the nature of the excitation changes. Quasiparticles effectively convert into quasiholes and vice versa for quasiholes approaching the minima. The group velocity of the excitation reverses at this point and the excitation travels away from the region of flow. During this process the excitation exchanges only a tiny amount of its momentum with the moving superfluid, $\sim (\Delta/E_F)p_F$[25]. Conversely, a quasiparticle approaching the flow from the other side of the flow field, such as a quasiparticle in branch 1 in Fig 2.6, has available states within which to propagate and will be able to travel through the flow flow field. In section

4.6 the consequences of these flow fields around a vibrating wire resonator will be discussed.

2.3.4 Quantum Turbulence

Quantum turbulence has been extensively investigated for HeII where it can be readily generated with counterflow maintained by an applied heat flux[26]. It was discovered that by applying more heat the counter flow velocity, $V = |v_n - v_s|$, increases until a critical velocity, V_{c1} is reached[27][28][29][30]. At this velocity a tangle of turbulence appears and is measured by the associated attenuation of second sound.

The Vinen experiments provided some great information on the dynamics of inhomogeneous quantum turbulence. The first interesting feature was the confirmation of a critical velocity V_{c1} above which turbulence is generated. This provided a numerical starting point for looking at the dynamics of vortex creation. Critical velocities are found in classical fluid dynamics regarding the creation of vortices. In classical mechanics the fluid flow is characterised by the Reynolds number, $Re = \frac{vL}{\nu}$ where L is a characteristic length, v the fluid velocity and ν the kinematic viscosity of the fluid. Typically $Re > 1000$ for turbulent flow. The generation of turbulence in ^{3}He by a vibrating wire resonator[6] also exhibited a critical flow velocity equivalent to the pair breaking critical velocity with an equivalent large Reynolds number due to the low viscosity.

The second result of the experiments of interest is the definition of the vortex line density, L_0, and the discovery of its relationship with the flow velocity shown in equation 2.18. The vortex line density, L_0, of this tangle

was found to have a quadratic dependence with the counterflow velocity, V, when $V > V_{c1}$

$$L_0 \approx \gamma V^2 \tag{2.18}$$

where γ is a temperature dependent parameter. Geometrically, L_0 gives the total length of vortex line per volume and so $L_0^{-\frac{1}{2}}$ represents the average spacing between the vortex lines.

The third result of the work was the creation of the 'Vinen's Equation' shown in equation 2.19.

$$\frac{dL}{dt} = -\chi_2 \frac{\kappa}{2\pi} L^2 \tag{2.19}$$

where κ is the quantum of circulation and χ_2 is a temperature dependent parameter found by recent computer simulation to be ~ 0.3 at zero temperature[31]. This equation provided a theoretical model of the rate of decay of the turbulence which is dependent on the vortex line density of the turbulence.

The work detailed in the experiments performed by Vinen, has been followed on by many groups[26][32][33][34] which yielded several different values for γ. It was found that at counterflow velocity $V > V_{c1}$ there is an initial turbulent state with moderate line density. If the counter flow velocity was increased a second critical velocity was found, V_{c2} above which the vortex line density suddenly becomes larger[35]. This puzzle was solved recently[36] when it was discovered that for the first turbulent state the superfluid is turbulent but the normal fluid is still laminar. Upon reaching the second critical velocity the normal fluid also becomes turbulent resulting in the increase in line density.

2.3.5 Computer Simulations

Computer simulations of the vortex dynamics within a tangle use the Magnus force[3] along with the Biot Savart law[37] in order to make approximations for the local superfluid velocity at any particular point. The simulations using these approximations were found to need an extra non-local effect to be considered. This effect is vortex reconnection. This occurs when two vortex lines come within a critical separation, then the two lines will reconnect. The critical separation used by different authors are found to be different[38][31] but the only consequence of this is an error due to vortices reconnecting when they should not. This approach towards modelling the intervortex dynamics has been moderately successful but there are limitations to this. With computer power being finite the vortex lines cannot be modelled as a line of infinite points but must be modelled as a string of discrete points. This introduces a finite spatial resolution below which effects cannot be seen.

Schwarz[38] showed that reconnections between vortex lines provided the mechanism that allowed smaller vortex loops to be created within the turbulence that could not be created by intrinsic nucleation. These reconnections however introduce kinks into the vortex lines which have a frequency ω given by

$$\omega = \frac{\kappa}{l^2} \tag{2.20}$$

where l is the length scale of the feature. These Kelvin waves form the mechanism of the turbulent energy decay into thermal excitations such as phonons and rotons in ^{4}He (in ^{3}He these excitations are presumed to be created quasiparticles.) The simulations done by Tsubota[31] in ^{4}He at $T = 0$ and a spatial resolution between $\frac{1}{4}$ to $\frac{1}{16}$ of the intervortex spacing show that

effects that have a length scale smaller than the spatial resolution, such as small Kelvin waves or small vortex loops, cannot occur and so in the simulations phonon radiation is not available.

The simulations also showed that the reconnections introduce a higher density of kinks into the vortex lines at lower temperatures than at higher temperatures. This was also observed by Schwarz[38]. The consequence of this is that if the reconnections create vortex loops smaller than the spatial resolution then the vortex loops will disappear. This smoothing of the vortex lines and loss of Kelvin waves are seen in the real physics of HeII as a loss of energy to higher Kelvin wavenumbers and the emission of phonon radiation. In reality the small vortex loops do not disappear since there is no mutual friction at low temperatures but reconnect into the tangle and produce more Kelvin waves. Using these effects the value for χ_2 of approximately 0.3 has been calculated[31].

To apply these numerical models to ^{3}He-B we need to note what the differences are. ^{3}He has a much larger core size than ^{4}He. Because of the finite core size, the Kelvin waves that radiate phonons in ^{4}He cannot be generated in ^{3}He-B as they are critically damped by the core. What is found though, is that the large core of the vortex contains a high density of bound quasiparticles[39] similar to superconductors. These bound quasiparticles provide the mechanism of mutual friction in ^{3}He, due to the scattering of free quasiparticles with these bound quasiparticles inside the core[40]. At low temperatures where there are no free quasiparticles there can still be dissipation however, if the vortex motion oscillates at a frequency close to the energy level spacing of the bound states.

It has been shown by calculations[41] that a Kelvin wave of this frequency, $\sim$ 10kHz, can be critically damped. This builds a model of the dissipation in ^{3}He where vortex reconnections dissipates a small amount of energy in quasiparticle production and generates Kelvin waves along the vortex. Since the core size is much larger than in ^{4}He it has been assumed that the effect of damping the Kelvin waves is more important than the quasiparticle emission during reconnection.

More recent simulations by Barenghi and Samuels[42] at temperatures approaching $T/T_C = 0$ of inhomogeneous turbulence within a superfluid shows a different behaviour with regards to the small vortex loops. The simulations show that small loops created near the surface of the tangle which have a radius R smaller than the average intervortex spacing, δ, can travel away from the tangle without reconnecting. It was shown that the velocity v_R of a vortex loop is related to the inverse of its radius R, thus the smaller the loops were, the greater their velocity and hence more probability of escaping the tangle. Since an escaping vortex will reduce the total length of vortex line, the resulting increase in δ, will thus enable more small vortex loops to escape. This shows a mechanism for the turbulence to decay by the 'evaporation' of small vortex loops created by reconnection rather than the creation and damping of Kelvin waves.

This model was then applied to the creation of turbulence in superfluid ^{3}He by a vibrating wire of diameter 4.5μm and leg spacing of 3mm. Using the values for the flow barrier calculated by Fisher *et al*[6], the velocity of the expansion of turbulence created by a vibrating wire, was calculated to be of the order of 1mms^{-1}. This is in good agreement with the measurements

taken by Fisher and unpublished measurements by Bradley *et al.*

2.4 Previous Investigations of Turbulence in ^{3}He-B

As has already been mentioned vorticity in ^{3}He has been studied for many years using rotating cryostats. Vortices have also been shown to be created by a vibrating wire resonator in ^{3}He[5]. In this experiment the driving force on a vibrating wire resonator was increased and the velocity response of the wire was measured. Typically a vibrating wire resonator's velocity will increase rapidly with time until a critical velocity V_{c1} is reached. Above this velocity the wire causes pair breaking in the superfluid and the production of thermal quasiparticles. Simple theory would dictate that as the pair breaking occurs the velocity of the wire would not change since the quasiparticles being highly ballistic would move away from the wire and not cause any additional damping but the rate of increase in velocity with drive is reduced. What was found in the experiment however was that the velocity actually dropped to a second velocity V_{c2} whereupon the velocity would increase back to the initial critical velocity V_{c1} and oscillations between the two velocities were observed.

Upon closer examination of the wire velocity as it switches between the two velocities, the wire behaviour displayed some interesting features. Upon initially reaching V_{c1} the wire velocity drops almost instantaneously to V_{c2} then the 'recovery' back to V_{c1} is considerably slower than the initial drop. As the driving current is increased the wire velocity continues to switch between the two velocities where just before the effect ends the drop in velocity becomes slower and the recovery near instantaneous. The mechanism for

this that was considered is that upon reaching V_{c1} the laminar flow around the resonator wire had a relative velocity sufficient to produce a vortex loop. This vortex then reduced the velocity of the wire to V_{c2} where the vortex was either shed from the wire or annihilated.

After the discovery that a resonator could produce a tangle of vortices[6] and discussions with Krusius *et al.*[43] the assumption that a single vortex loop is connected with the wire, was found to be unreliable. The suggestion was put forward that the wire creates an unstable turbulent tangle and that the switching between the two critical velocities is due to intermittent laminar and turbulent flow. This intermittent switching between laminar and turbulent flow has been observed in measurements involving a vibrating microsphere in superfluid ^{4}He[44][45]. This suggestion prompted further investigation into the lower critical velocity V_{c2}.

The reply from Bradley *et al.*[46] to the suggestions from Krusius *et al.*, considered that since the resonator is at rest twice per cycle perhaps the amplitude of the wire motion and not the velocity is a contributing factor. The argument put forward is that the vorticity is produced at the maximum of the wire velocity and moves away as the wire slows, but if the vorticity has not moved far enough away from the wire it is recaptured by the wire and vortex production immediately ceases until the wire slows to V_{c2} where the wire amplitude is small enough for the vorticity to escape. This produces a localised tangle of vortex lines rather than a homogeneous loop.

The experiment in which the generation of turbulent vortices by a supercritical vibrating wire resonator was discovered[6] consisted of two adjacent vibrating wire resonators. The generator resonator when driven above its

critical velocity affected the second resonator and a reduction in the incident quasiparticle flux on this wire was measured. The full extent of this effect was measured with different source wire velocities above and below the pair breaking critical velocity. The experiment was also conducted at temperatures above $0.185T_C$ where T_C is the superfluid critical temperature for ^{3}He. At these temperatures the damping on the detector resonator due to the thermal background quasiparticles was ~ 300 times larger than the intrinsic damping due to the wire stiffness, providing a clear measure of the quasiparticle density.

At velocities just above the critical velocity the detector wire saw only an increased quasiparticle flux from the produced quasiparticle beam since the vorticity was not of a sufficient density to reach the detector wire. Increasing the generator velocity increased the density of the vortex tangle and the detector wire response began to see a shielding effect. The shielding effect then rose rapidly until the velocity reached $\sim 2.0V_c$ where the shielding effect stabilised. Increasing the driving velocity further saw the shielding effect begin to diminish.

From these results an effective flow barrier due to the vortex lines was calculated using the fractional change in the damping of the detector as

$$f = 1 - \exp[-(p_F v_b)/k_B T] \tag{2.21}$$

where v_b is the effective flow barrier causing the reflection of incident quasiparticles through Andreev processes.

The experiment clearly showed the production of turbulent vortex lines and the shielding of the detector wire from background thermal quasiparticles by Andreev processes. The experiments I shall describe in this thesis expand

upon this experiment by providing a greater range of generator-detector separations in order to measure how the density of the vortex tangle changes with displacement from the generator.

Chapter 3

Refrigeration Techniques

3.1 Approaching Absolute Zero

According to the third law of thermodynamics it is only possible to reach absolute zero in an infinite number of steps. Fortunately for physicists it is possible to get really quite close in a finite number of steps. The steps performed commonly at Lancaster in the pursuit of absolute zero shall be described in this chapter.

The experiments described here are conducted on superfluid helium-3 at temperatures approaching absolute zero or more typically in the order of $\sim$ 200μK. To reach these temperatures, which are not found naturally in the universe, it is necessary to remove large amounts of heat energy from the sample helium. Most of the equipment to do this can be easily bought from commercial companies but it is found that purpose built machinery often produces better results in both temperatures reached and hold times at those temperatures.

The machine that was used for these investigations is a Lancaster style

helium dilution refrigerator[47][48] which can routinely achieve temperatures of around 2mK under constant operation. Dilution refrigerators have become common equipment for low temperature research since their inception in the 1960's and their working has been described in various journals and papers so I shall not describe them in too much detail here. Using the dilution refrigerator to 'precool' the experiment to temperatures approaching 7mK it is then possible to conduct the final stage of cooling. This final stage is called 'Adiabatic Nuclear Demagnetisation' and utilises the ordering and relaxation of the nuclear spins of copper atoms. This is explained in greater detail in the demagnetisation section and can be used to cool our experimental liquid, ^{3}He, to temperatures below 100μK.

3.1.1 The Dilution Refrigerator

Getting from room temperature of $\sim$ 300K to temperatures of a few millionths of a degree Kelvin takes many stages. The initial stages simply use cryogenic liquids of nitrogen and helium to cool the refrigerator. This can easily cool the equipment down to temperatures of around 4K in the helium 'bath' in only a couple of days. Next the dilution section is cooled down further to $\sim$ 1K by pumping on a helium pot which is replenished through a trickle feed from the helium 'bath'. Once down to this temperature it is possible to commence full refrigeration to cool further.

The refrigerant used is a mixture of ^{3}He and ^{4}He. This liquid is used due to the solubility of ^{3}He in liquid ^{4}He even when ^{4}He turns superfluid. When a mixture of the two isotopes is cooled below about 0.8K there is a phase separation into two separate phases. In the first phase, known as the 'dilute'

phase the ^{4}He superfluid attempts to expel ^{3}He atoms but has a saturation concentration of around 6% at temperatures approaching absolute zero as shown in Fig 3.1. The second phase, refered to as the 'concentrated' phase, however is ^{3}He rich containing a much much larger concentration than 6% and when $T \to 0$ the concentration of ^{3}He $\to 100\%$.

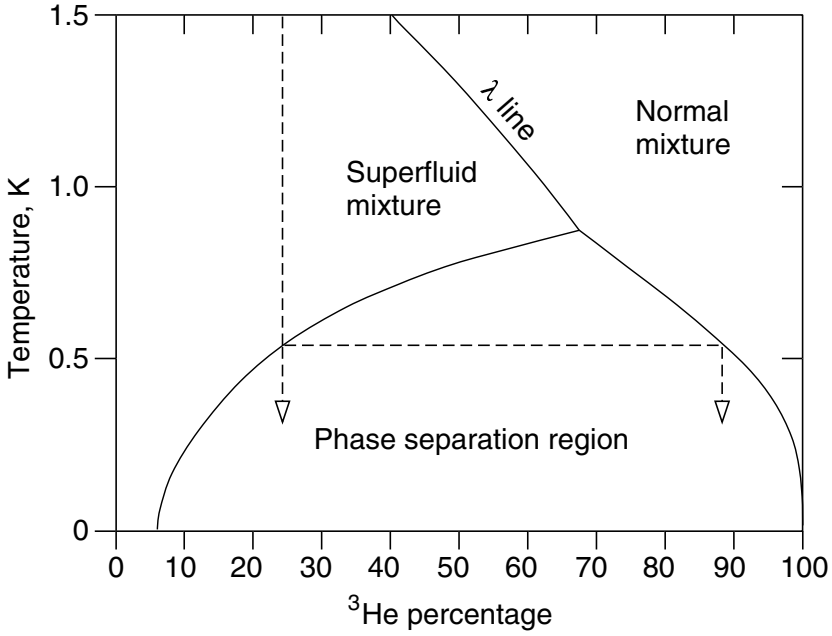

Figure 3.1: Phase diagram for a mixture of ^{3}He and ^{4}He.

In a gravitational field the lighter concentrated phase will sit happily on top of the heavier dilute phase. Since ^{3}He is a Fermion and obeys Fermi-Dirac statistics, the entropy of a simple Fermi gas, at temperatures much lower than the Fermi temperature T_F, can be given by

$$S = \frac{\pi^2}{2} N k_B \frac{k_B T}{E_F}. \tag{3.1}$$

The concentrated phase, containing a much larger fraction of ^{3}He than the dilute phase, has, as a result of Fermi-Dirac statistics, a much higher Fermi

energy, E_F. If ^{3}He atoms can be coerced into crossing the phase boundary they will go from a low entropy phase into a higher entropy phase[49]. When there is a flow of ^{3}He atoms across the boundary between the concentrated mixture to the dilute mixture there is a resulting cooling power of $dQ = TdS$ per particle which gives for the whole system

$$\dot{Q} = \dot{N}_3 T[S_D(T) - S_C(T)] \tag{3.2}$$

where T is the temperature and $\dot{N}_3$ is the molar flow rate of ^{3}He atoms. It should be made clear though that this is for an ideal case which does not take into account the warmer returning ^{3}He gas. The flow of ^{3}He atoms can be considered to be analogous to simple evaporation of a liquid. Putting in the numbers for the entropies into equation 3.2 we get a cooling power[50] of

$$\dot{Q} = 84\dot{N}_3 T^2. \tag{3.3}$$

To ensure that the phase boundary, and hence the cooling power, is located within the mixing chamber the concentration and volume of mixture is carefully controlled.

The next problem is how to coerce the ^{3}He atoms to cross the phase boundary inside the mixing chamber. As can be seen in the Fig 3.2 the ^{3}He atoms are pumped through the still. Inside the still there is a free liquid surface and due to the larger vapour pressure of the lighter atoms the vapour above the surface consists predominantly of ^{3}He atoms. To maintain a higher vapour pressure a small amount of heat is applied to the still with a small resistor. This evaporation of the ^{3}He creates an osmotic pressure gradient between the still and the mixing chamber mixtures which encourages the atoms to cross the boundary or 'evaporate'[51]. It is this 'evaporation' that

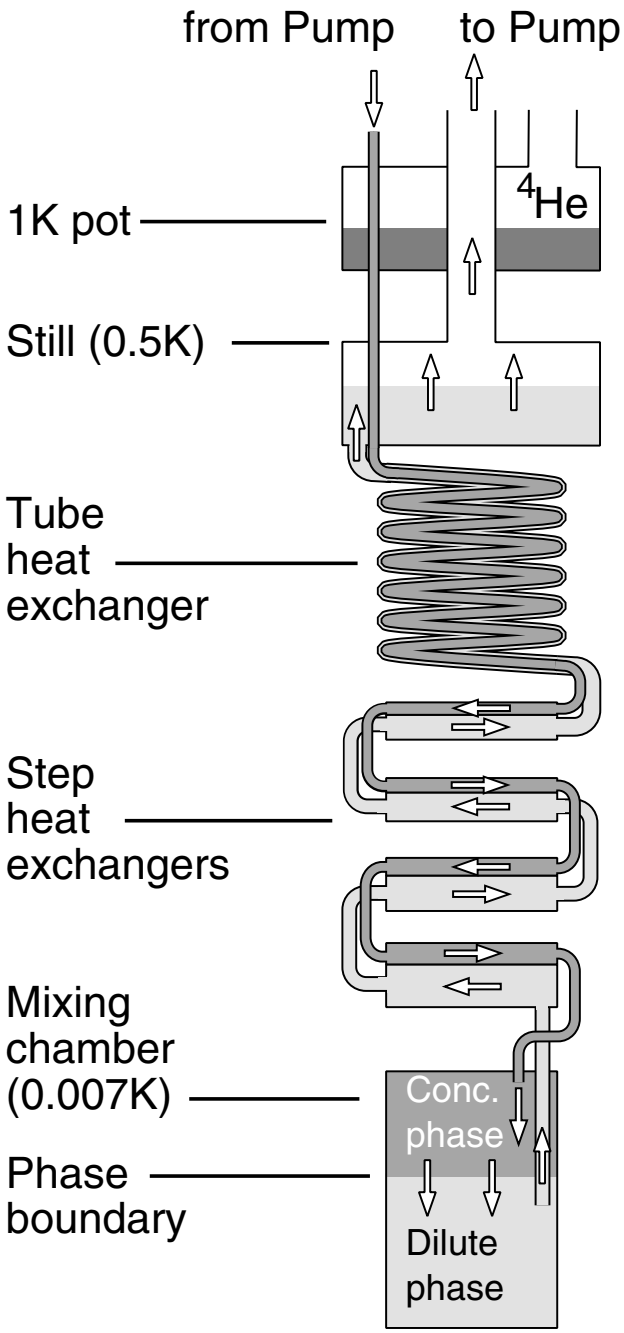

Figure 3.2: Schematic diagram of circulating dilution refrigerator.

provides the cooling power so that the more that evaporation can take place the colder we can achieve.

If there is only a finite volume of mixture then all the ^{3}He will be soon pumped out of the mixture so there is a need to replenish the mixture in the mixing chamber. To do this the pumped gas is returned, passing through the 1K pot to remove most of the heat and then through several heat exchangers in order to cool the returning gas entering the mixing chamber. The limit of what temperatures we can reach is governed by the efficiency of the heat exchangers. The more the returning gas can be cooled the less heat there is entering the mixing chamber. Typically the refrigerator used for these results 'pre-cooled' the cell to approximately 7mK before demagnetisation.

3.1.2 Adiabatic Nuclear Demagnetisation

Using the dilution refrigerator at its maximum capacity it is possible to achieve a minimum temperature of around 2mK. This is easily cold enough to turn ^{4}He superfluid but the transition temperature for ^{3}He is 0.929mK at 0 bar. If we wish to turn this liquid into a superfluid for investigation then a final cooling stage will need to be performed which is known as 'Adiabatic Nuclear Demagnetisation'. The theory for adiabatic nuclear demagnetisation was first proposed by Gorter in 1934 and also Kurti and Simon in 1935 independently. In 1956 Kurti, Robinson, Simon and Spohr[51] demonstrated the first application of this new method by succeeding in reducing the nuclear spin temperature of copper to about 1μK.

The theory behind this technique shall be briefly discussed here. To explain the principles behind it, it is best to consider a solid of N atoms.

Each atom has a nuclear spin of 1/2 which are weakly interacting, meaning that the solid is 'paramagnetic'. With each atom having a spin of 1/2 there are two states that the atom could be in, spin up and spin down. In a magnetic field, B, these states have an energy $+\mu B$ and $-\mu B$, where μ is the appropriate magnetic moment due to the z-component. If the solid is in thermal equilibrium, which we shall assume, at a temperature T the Boltzmann distribution[49], $\exp(-\Delta E/k_B T)$ where $\Delta E = \pm\mu B$, can be used to calculate the occupation of the two states and with that the thermal properties.

At high temperatures where $k_B T \gg \mu B$ the nuclear spins in the solid are completely disordered. This results in an entropy of $S = N k_B \ln 2$ as each atom could be in one of two states. If the temperature is lowered towards $\Delta E/k_B$ the atoms will find it preferential to be in the lowest energy state reducing the entropy towards zero. If this system is made to be adiabatic the entropy cannot therefore change and since the entropy is solely a function of $\mu B/k_B T$ this ratio cannot change. This leads nicely onto the process of demagnetisation.

As has already been shown if the system is thermally isolated, hence adiabatic, the ratio $\mu B/k_B T$ cannot change. By applying a large magnetic field, typically 8 Tesla, the spins become highly ordered and are then cooled by the dilution refrigerator already discussed. Once the cell achieves a temperature of $\sim$ 7mK demagnetisation can commence. The cell is thermally isolated from the refrigerator by activating a 'heat switch' constructed from aluminium. When placed within a high magnetic field the superconductivity of the switch is suppressed which allows thermal transfer across the switch.

As the magnetic field is then reduced the fringing field inside the switch reduces allowing the switch to revert to its superconducting state and denying thermal transfer. This process of demagnetisation occurs over a period of typically 14 hours to a final field of 80mT. This final field is required, rather than removing the entirety of the field, for the operation of the resonators as described in chapter 4.

Since the ratio $\mu B/k_B T$ is constant, to a first approximation, the final temperature of the cell can be calculated from the equation

$$\frac{B_i}{T_i} = \frac{B_f}{T_f} \tag{3.4}$$

or

$$T_f = \frac{B_f\, T_i}{B_i} \tag{3.5}$$

where B_i is the initial field, B_f the final field and T_i our cell temperature before demagnetisation. This gives a final temperature after demagnetisation of 70μK for the copper nuclei. Although the theory seems to indicate that removing the field entirely would reduce the temperature to absolute zero there occurs self ordering of the copper nuclei due to nuclear spin interactions between the atoms. This interaction results in an equivalent field of around 0.3mT.

Plates of sintered copper metal is used as the refrigerant for demagnetisation at Lancaster. The reason for this choice is that the copper nuclei have spin 3/2 within a cubic lattice. Since these nuclear spins are about 2000 times smaller than electronic spins[49] temperatures into the nK range are theoretically possible. The minimum temperature reached in the helium however is governed mainly by how efficiently the cold copper nuclei can extract heat from the helium liquid via the orbiting copper electrons. The

thermal resistances between the nuclei and electrons of the copper with the helium superfluid is refered to as the Kapitza[51] resistance. To minimise this resistance, which is caused by acoustic mismatching between the helium and a solid, the surface area of the copper is made as large as possible by using very fine sintered powders. Although this resistance limits how cold the superfluid can be cooled it also has the advantage of leaving the copper nuclei colder than the fluid, hence providing a 'cooling power' for several days after demagnetisation. For the refrigerator and cell used for the experiments I shall describe, a 'hold time' of around 6 days was obtained with the superfluid being suitably cold for investigation.

3.2 The Experimental Cell

The experiment built for the investigations described in chapters 5 and 6 consists of a Stycast impregnated base with six vibrating wire resonators constructed from 4.5μm NbTi wire aligned in a linear array along the base. A seventh wire is placed at the side of the array and orientated perpendicularly. This array of wires will be used for the experiment described in chapter 5. On a second Stycast and paper plate suspended above the array is a Lancaster style black body radiator with a solitary 4.5μm NbTi vibrating wire resonator situated approximately 1mm away from and facing the radiator hole. Inside the 'box' is a 4.5μm NbTi vibrating wire resonator and a 13μm NbTi vibrating wire resonator. The 'Box' experimental setup is described in greater detail in chapter 6. Also inside the experimental cell is a Tantalum resonator used for thermometry inside the inner cell prior to demagnetisation.

The experiment is nested inside several sintered copper plates, the design of which is used for all 'Lancaster style' demagnetisation cells. These sintered plates are thermally connected through an aluminium heat switch to sintered silver plates which are placed inside the mixing chamber of the refrigerator. The heat switch will only allow heat transfer through whilst in the normal state, with no heat transfer possible in the superconducting state, and is used so that once demagnetisation of the copper begins heat does not leak into the cell from the mixing chamber. At the low temperatures that the heat switch is operated at, the superconductivity of the aluminium is suppressed by the fringing field from the main demagnetisation magnet. The transition field to the normal state for the switch used is about 10mT which is removed

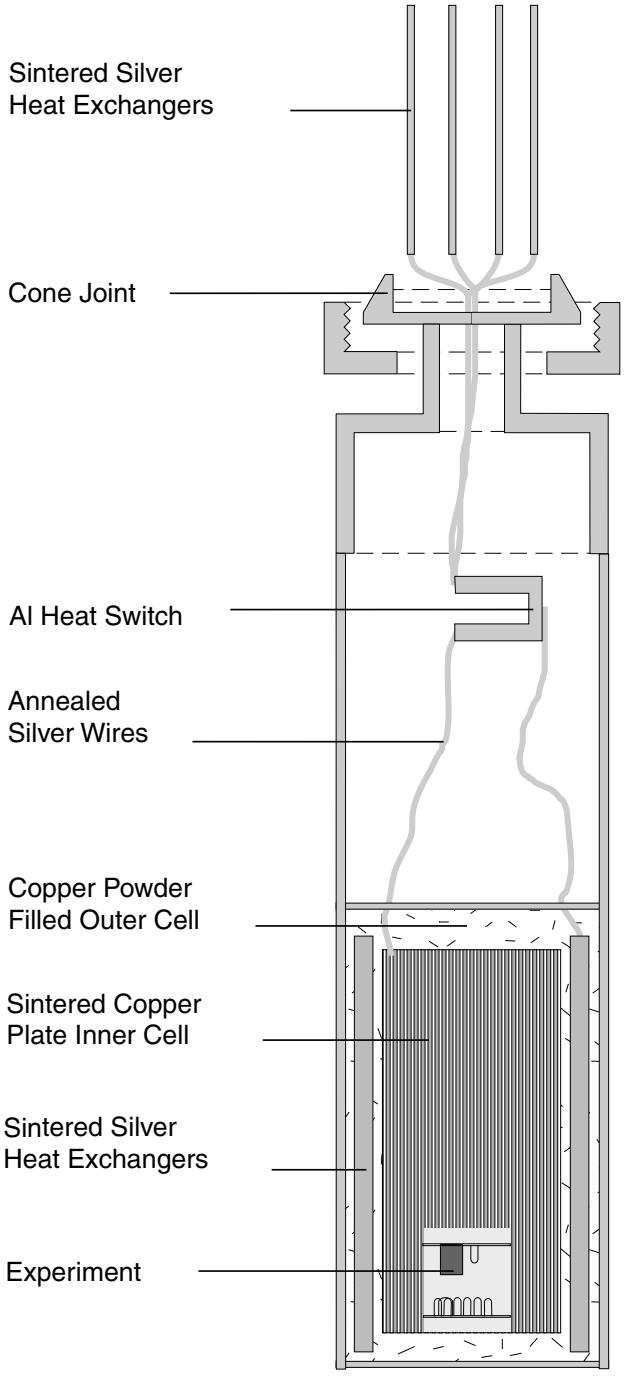

Figure 3.3: Diagram of the experiment nested inside the copper refrigerant plates with heat switch and mixing chamber silver plates.

almost shortly after demagnetisation is commenced. The sintered copper plates inside the inner cell are surrounded by a very fine copper powder in the outer cell to increase the volume of copper nuclei available as a refrigerant and to also act as a thermal guard against heat leaks into the innner cell and the experimental region. The cell body is made from Araldite and attached to the mixing chamber with a high precision cone joint. The cone joint is made superfluid leak tight by priming the connecting surfaces with an aqueous glycerine solution forming a 'soap seal'. A diagram of the cell body is shown in figure 3.3.

3.3 Laboratory Arrangement

Being at such an extreme end of the temperature scale, the experimental cell is extremely sensitive to any kind of energy be it kinetic or electromagnetic. One consequence of this sensitivity is that the cell can behave as an extremely sensitive cosmic ray detector[52] and occasionally a cosmic ray will upset measurements being taken. When a cosmic ray hits the cell the resulting heating effect dissipates quickly and is easily removed from the measurements being taken. It can be a minor nuisance though and repeat measurements may have to be done.

Any electromagnetic radiation which manages to enter the room could cause radical heating of the experimental cell due to the high sensitivity of the experiment to energy fluctuations. This noise is stopped from entering the experimental chamber by locating the entire refrigerator within a large Faraday cage. The walls of the 'shielded room' are lined with tin plate including the windows which are covered in a fine metal mesh. This mesh has the added advantage of keeping the postgraduate students caged in also. To reduce electromagnetic noise during the demagnetisation and data acquisition all network connections are closed and portable telephones are left outside the shielded room or switched off.

The refrigerator is not exclusively susceptible to EM radiation though. It is also very sensitive to mechanical vibrations or shocks. The transmission of this mechanical energy can be stopped by making the damping of any movement as large as possible. To facilitate this the refrigerator is mounted on three 1500kg concrete pillars and the whole structure is then floated on three pressurised air springs. The combination of the soft airsprings and the

large mass of the concrete legs act to suppress any mechanical energy that may attempt to enter the cell through the fridge. This is especially necessary as the laboratory is only a few hundred yards from the M6 motorway. All the pumping equipment and cold traps are situated outside the shielded room with the helium lines passing through the shielded room concrete wall and connecting to the top of the refrigerator through a flexible length of hosing. The end of the pumping lines are mechanically anchored to the top of one of the concrete pillars.

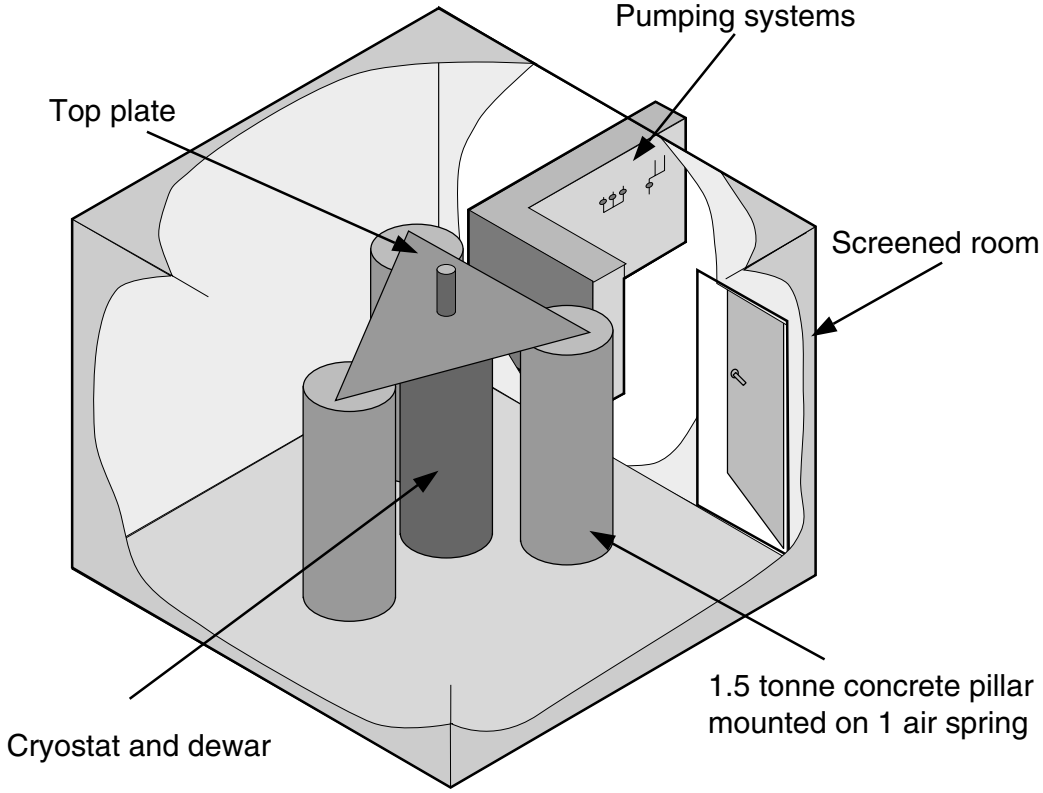

Figure 3.4: Schematic diagram of dilution refrigerator located within a shielded room.

Chapter 4

Vibrating Wire Resonators

4.1 Introduction

Having such a cold fluid we will need some method of probing the liquid without creating undue heating or disturbance within the liquid. The method used within my research group at Lancaster is to use a Vibrating Wire Resonator. The vibrating wire resonator consists of a single loop of superconducting Niobium-Titanium wire of diameter $\sim 4.5\mu$m. These vibrating wires have a high sensitivity to temperature, typically a resolution of $<$ 1nK at $T \sim 100\mu$K, and cause almost no heating to the sample. Superconducting wire is used to avoid Ohmic heating of the wire and resistance signal losses. Other uses for the vibrating wires aside from thermometry will be explained later and form the basis of the experiments conducted and described in this thesis. The principles behind a vibrating wire resonator are quite simple. Using the Lorentz force created when a current is passed through a magnetic field, the resonator is made to oscillate at the frequency of the driving AC current. As the frequency approaches the resonant frequency of the vibrating

wire the velocity of oscillation will increase. This velocity is then recorded by using the effect of Faraday induction where a moving conductor in a magnetic field will induce a voltage across the conductor. By measuring the voltage induced for a range of frequencies from below to above the resonant frequency the damping on the wire can be measured and inferred and as will be shown, this damping can be used to measure directly the temperature of the superfluid.

4.2 Vibrating Wire Theory

We use the method described in detail by Fisher[53] to describe the motion of the vibrating wire. A resonator is considered to be a long homogenous cylinder with mass m per unit length along an axis in the y-direction and free to oscillate rigidly in the x-direction. The restoring force upon the wire is $m\omega_0^2$ per unit length per displacement x. The wire sits in a magnetic field B orientated along the z-direction and an alternating current $I = I_0 e^{i\omega t}$ is passed along the cylinder. This creates a Lorentz force of BI per unit length, in the x-direction which can be seen in figure 4.1.

As the cylinder is moving within a fluid we can describe the equation of motion as such

$$m\ddot{x} + m\lambda\dot{x} + m\omega_0^2 x = BI_0 e^{i\omega t} \tag{4.1}$$

where λ is a complex variable which describes the damping force experienced by the wire due to the fluid. This damping force has been shown to be linear with velocity provided the velocity is small and so λ is independent of velocity and may be expressed as

$$\lambda = \lambda_2 + i\lambda_1 \tag{4.2}$$

where λ_1 describes the out of phase component of the force and λ_2 describes the in-phase dissipative component. The out of phase component is attributed to fluid back-flow and has the effect of increasing the effective mass of the cylinder.

To convert equation 4.1 into a more useful form it is necessary to add a constant, C, to the equation to describe how the maximum displacement relates to the force. This constant depends on the fact that the magnitude of

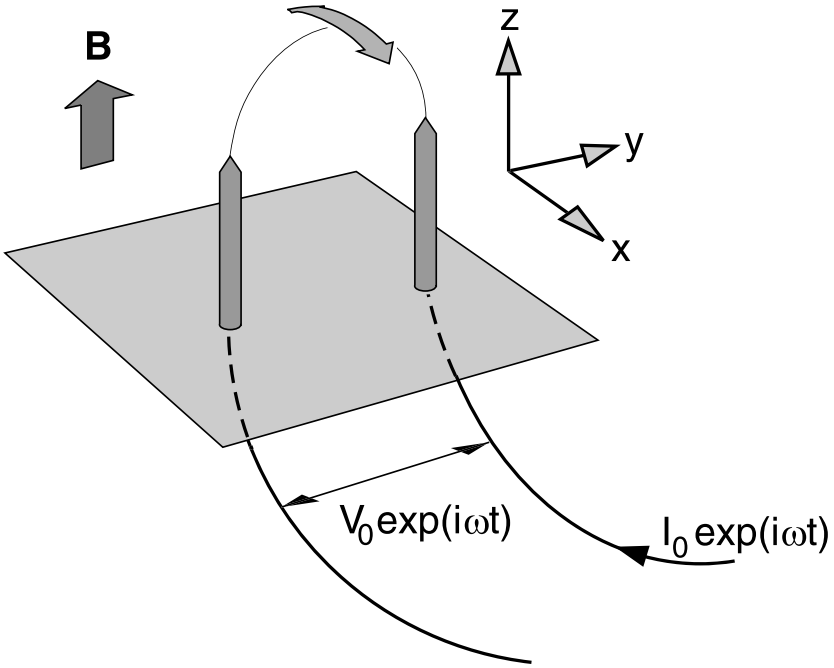

Figure 4.1: Operation of a Vibrating Wire Resonator.

motion is small such that the motion is, to the nearest approximation, linear. This gives

$$\ddot{x} + \lambda_2 \dot{x} + i\lambda_1 \dot{x} + \omega_0^2 x = C\frac{BI_0}{m}\mathrm{e}^{i\omega t} \tag{4.3}$$

where x now describes the maximum displacement of any point on the wire, typically being the centre point of the loop.

Equation 4.3 has a solution in the steady state in the form of

$$\dot{x} = \dot{x}_0 \mathrm{e}^{i\omega t} \tag{4.4}$$

and combining this into 4.3 results in

$$\dot{x}_0 = C\frac{I_0 B}{m}\left(\frac{i\omega}{\omega_0^2 - \omega^2 - \omega\lambda_1 + i\omega\lambda_2}\right) \tag{4.5}$$

This equation can now be split into the in-phase and out of phase components. The component in-phase with the driving force, $Re\{\dot{x}_0\}$ is described

by a Lorentzian as shown in Fig 4.3,

$$Re\{\dot{x}_0\} = C\frac{I_0 B}{m}\left(\frac{\omega^2\lambda_2}{(\omega_0^2-\omega^2-\omega\lambda_1)^2+\omega^2\lambda_2^2}\right). \tag{4.6}$$

The component out of phase with the motion (the quadrature) is denoted by,

$$Im\{\dot{x}_0\} = C\frac{I_0 B}{m}\left(\frac{\omega(\omega_0^2-\omega^2-\omega\lambda_1)}{(\omega_0^2-\omega^2-\omega\lambda_1)^2+\omega^2\lambda_2^2}\right). \tag{4.7}$$

The maximum of the in-phase velocity is thus,

$$Re\{\dot{x}_0\}_{max} = C\frac{I_0 B}{m\lambda_2} \tag{4.8}$$

when the resonant frequency, ω_0' is given by,

$$\omega_0^2 - \omega_0'^2 - \omega_0'\lambda_1 = 0 \tag{4.9}$$

$$\Rightarrow \omega_0 - \omega_0' \simeq \lambda_1/2 \tag{4.10}$$

where ω_0 is the vacuum resonant frequency and equation 4.10 is valid assuming that $(\lambda_1/\omega_0) \ll 1$, which holds true for the wires we use during our experiments. The effect of the inertia of the ^{3}He back flow is small in comparison to the density of the wire so the resonant frequency of the wire is shifted by

$$\Delta\omega_1 = \omega_0' - \omega_0 = -\frac{\lambda_1}{2} \text{ or } \Delta f_1 = -\frac{\lambda_1}{4\pi} \tag{4.11}$$

The quadrature term at this point is zero.

Using a similar set of assumptions we can calculate the half height resonant width. The in-phase velocity is half its maximum value at a frequency $\omega_{1/2}$. At this frequency the quadrature is also at its maximum or minimum. $\omega_{1/2}$ is given by

$$(\omega_0^2 - \omega_{1/2}^2 - \omega_{1/2}\lambda_1)^2 = \omega_{1/2}^2\lambda_2^2 \tag{4.12}$$

and using the assumption that $\lambda_2 \ll \omega_0'$, which is valid for the range over which our measurements are taken, we can say

$$\omega_0 - \omega_{1/2} \simeq (\lambda_1 \pm \lambda_2)/2. \tag{4.13}$$

From this we can define the in-phase half height resonant width as

$$\Delta\omega_2 = \omega_{1/2}^{+} - \omega_{1/2}^{-} = \lambda_2 \text{ or } \Delta f_2 = \frac{\lambda_2}{2\pi} \tag{4.14}$$

Having clearly defined the spatial maximum over which the wire velocity changes it is now possible to relate this to a physical property which we can measure, the induced voltage across the wire, with a factor dependent on the wire geometry. As described by Faraday's law a voltage is induced as the wire moves through a magnetic field, $\mathbf{B}$

$$V = -\frac{d(\mathbf{B} \cdot \mathbf{A})}{dt} \tag{4.15}$$

where $\mathbf{A}$ is the vector area bounded by the wire loop and its supports. The wires we use are actually a rigid semi-circular loop of diameter D where the area bounded by the wire and the legs is $\pi D^2/8$ hence the rate of change of angle with the field direction is $2\dot{x}/D$, thus a more accurate voltage amplitude is,

$$V_0 = \frac{\pi}{4} BD\dot{x}_0 \text{ (rigid semicircle).} \tag{4.16}$$

This is generally written as

$$\dot{x}_0 = K\frac{V_0}{BD}. \tag{4.17}$$

The wires used for the experiments described within this thesis are similar but not ideal nor identical. Because of this the actual values of K vary but

it is assumed that the value is close to the rigid semi circle value of $\pi/4$. The uncertainty in this is estimated to be around 10 per cent.

Combining equation 4.17 with equations 4.14 and 4.8 we get

$$\frac{V_0 \Delta f_2}{I_0} = \frac{C}{K} \frac{B^2 D}{2\pi m} \tag{4.18}$$

where the ratio C/K is a constant depending on the actual wire but typically of order unity[53] for the wires used. Equation 4.18 is an incredibly useful equation as if the field remains constant then the parameters governing the wire motion do not change. This gives us a constant by which to use the wires known as the 'Height Width over Drive' or $H \times W/D$ where H refers to the signal height, W the resonant damping width and D the driving current. This shall be explained further in the sections explaining fixed frequency operation.

4.3 Construction

Construction of a vibrating wire resonator begins with a length of multi-filamentary Nb-Ti superconducting wire embedded in a copper matrix. A length of this wire is wrapped around a former consisting of a cylindrical metal bar of diameter equal to the required leg spacing and threaded through two holes punched in a sheet of Stycast-impregnated paper. For the wires described and used during the experiments explained herein, the leg spacing is $\sim 3\,\mathrm{mm}$. The wire is securely fastened to the paper by running liquid Stycast into the holes. This creates a firm, rigid joint to the paper base which is superleak tight. Once the legs are secure the cylindrical former can be removed and the resulting shape of the wire is of a semicircular loop.

Once the wire shape has been created the copper matrix can be etched away from the semicircular portion. This is achieved using a small volume of nitric acid and submerging the portion of wire where etching is required. The removal of the copper cladding exposes the Nb-Ti strands whose diameter, depending on type of wire used, ranges from 13μm to 4.5μm. The filaments described here are 4.5μm in diameter and are referred to as triple micro's or $\mu\mu\mu$'s. Typically there are around sixty of these filaments looping between the rigid legs after etching. Using a microscope these are removed with care by plucking with tweezers and hopefully a single undamaged filament will be left. This filament forms the active part of the vibrating wire. To secure this filament two caps of Stycast are deposited at the top of the legs. This also captures the remaining shards of the removed filaments and stops them interfering with the wire. The resonator is now ready for installation in an experimental cell after attachment of the drive current and voltage sense

leads. The single micro wires are made in an identical manner but have filaments of 12.4μm diameter. Tantalum wires are also made the same way but are considerably easier having no filaments.

4.4 Operational Modes

The wires are driven using, typically, an Agilent 33120A signal generator which provides an alternating sinusoidal voltage ranging up to $3.5\mathrm{V}_{\mathrm{rms}}$. This is converted into a drive current by using a 'drive box' which contains a $1 : 0.155$ step down transformer and a selectable range of resistances between 100Ω and $1\mathrm{M}\Omega$ in decades to allow a larger range of drive currents. The transformer is for the purpose of breaking earth loops but also has the advantage of matching the input impedance of the drive box with the output impedance of the signal generator.

$$I_{drive} = \frac{0.155 V_{drive}}{R_{drive}} \tag{4.19}$$

The wires are monitored using a four point probe technique where the voltage induced by the motion is measured using a separate pair of leads to the leads supplying the drive current and is recorded using a SR830 lock-in amplifier. The signal generator and lock-in amplifier are controlled by a PC running the LabVIEW software suite via a GPIB interface. A reference signal for the lock-in amplifier is taken from the signal generator. The voltage sense wires are taken through the cryostat via a low temperature transformer, which is thermally anchored to the 4K plate, to increase the signal voltage and to match the low impedance of the resonator with the high impedance of the lock-in amplifier. This increases the signal to noise ratio of the data by up to 30 times but is also responsible for a small shift in the resonant frequency. There are also two RF SQUIDs available which were used for the measurements involving the black body radiator which are described in chapter 6.

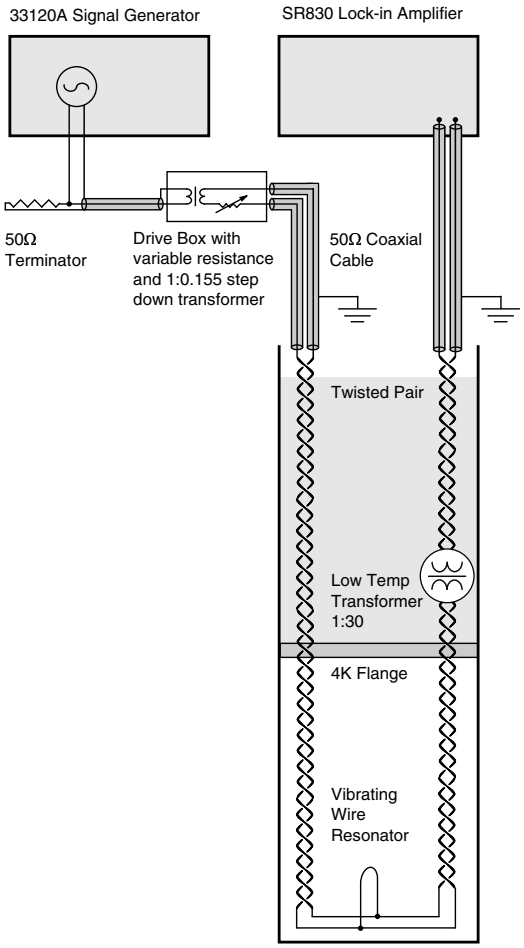

Figure 4.2: Diagram of circuit used to drive a vibrating wire resonator.

There are three main modes of operation used; frequency sweep, amplitude sweep and fixed frequency. Each of these methods is used to obtain information on different parameters of the resonators. Frequency sweep operation is used to quantify the $H \times W/D$ constant described in equation 4.18. Amplitude sweep operation is conducted to measure the 'pair-breaking' critical velocity of the wire. The final mode of operation, fixed frequency, is the most commonly used mode for taking the data used in these measurements. Fixed frequency measurements allow a fast quantification of the damping

experienced by a wire and hence the temperature.

4.4.1 Frequency Sweep

The frequency sweep mode is the initial mode of operating a VWR and consequently the simplest. The vibrating wire resonator is driven at a constant drive current, set by applying a known AC voltage through a drive box. The frequency of the alternating current is smoothly increased by the LabVIEW software whilst the in-phase, equation 4.6, and quadrature signals, equation 4.7, are read from the lock-in amplifier. When these values are charted against the AC drive current frequency, the resulting in-phase response curve follows a Lorentzian shape with a distinct peak. This peak occurs at the resonant frequency, f_0. The half height resonant width, Δf_2 is then calculated from the frequency difference between the two points either side of the resonant peak, where the height is $f_0/2$.

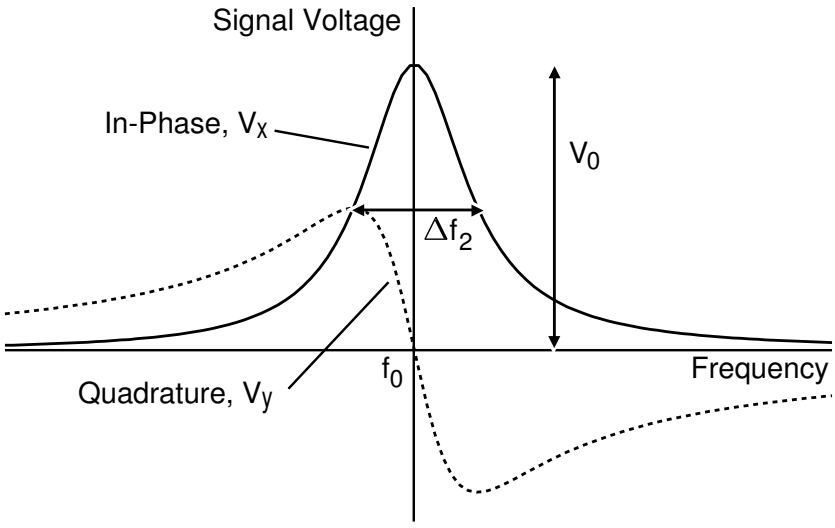

Figure 4.3: Typical frequency sweep chart for a vibrating wire resonator.

Having measured the resonant height, width and the driving current, a value for the $H \times W/D$ constant can be calculated. To calculate this value it is typically necessary to 'sweep' the wire at least 20 times. The more times the wire is swept the more accurate the final value for the constant will be but too much time should not be expended on this as a demagnetisation has only a limited hold time. This constant is calculated anew for each demagnetisation as the constant can be affected by small changes in the operating magnetic field as shown in equation 4.18 as being $\propto B^2$ and although the settings for the final demagnetisation field on the equipment are not changed there can be discrepancies by a few percent. At the beginning of each demagnetisation each wire that is to be used during the data acquisition is frequency swept and has the $H \times W/D$ constant, resonant frequency and relative phase measured and recorded. This frequency sweeping technique can also be used for slow thermometry but with a typical sweep taking 300 seconds this is not fast enough for the data acquisition needed for some of the later experiments.

4.4.2 Amplitude Sweep

The amplitude sweep mode is used to characterise the parameters of the wire such as the pair-breaking critical velocity where the wire imparts enough kinetic energy into the local superfluid to break a superfluid pairing. The peak wire velocity is measured as before by measuring the induced Faraday voltage created when a conductor moves in a magnetic field. This Faraday voltage correlates to the wire velocity and hence the pair-breaking velocity can be defined in terms of the in-phase resonant signal voltage. A typical pair-breaking velocity for a 'triple micro' wire is around 9mms^{-1}. Herein the

critical velocities for the resonators will be refered to in units of microvolts.

To amplitude sweep a resonator the resonant frequency is first measured using the frequency sweep technique. The resonator is then driven at this frequency with a small drive, typically the smallest drive possible with the signal generator, which is then smoothly increased until the resultant signal levels out. To avoid any loss in signal due to the wire resonant frequency shifting the lock-in amplifier is changed to R, θ operational mode where R is the scalar signal voltage and θ the phase angle. In this mode the in-phase signal and the quadrature signal are both used to calculate the maximum signal voltage. The signal measured shows a smooth nonlinear increase until the wire velocity approaches the critical velocity.

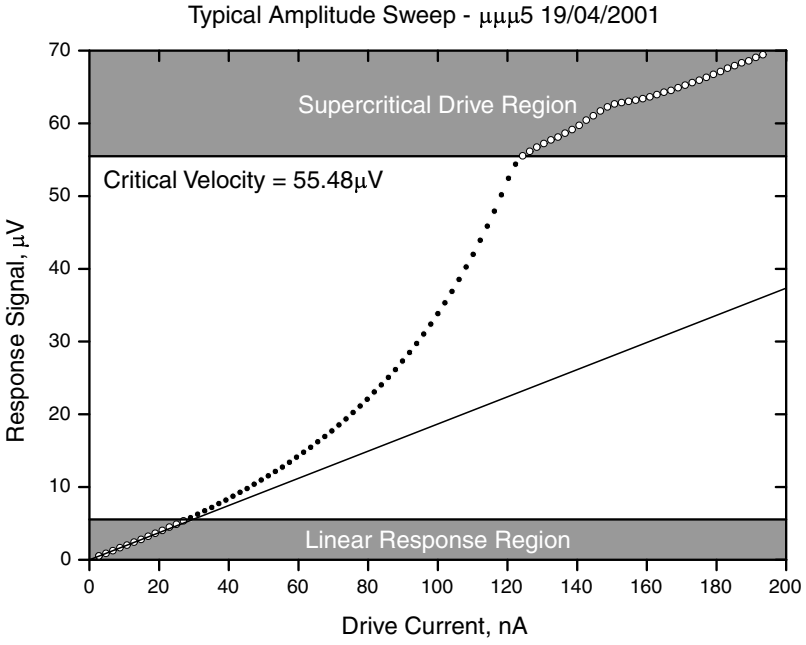

Figure 4.4: Amplitude sweep chart for a vibrating wire resonator $\mu\mu\mu$ 5.

At this drive the extra damping experienced from the breaking superfluid pairs inhibits the rapid increase in signal and so the wire signal levels off.

According to superfluid theory[11] the change to vortex creation should be a sharp kink although the amplitude sweeps done on a real wire show a more 'rounded' transition. This rounding is attributed to microscopic defects on the surface of the wire causing increased flow velocities in localised regions. A more detailed investigation of this by Bradley[5] has shown the breaking of the pairs and creation of quantised vortex lines which can be assumed to be due to the increased flow velocity of the superfluid around microscopic asperities and defects on the wire surface. As can be seen from the amplitude sweep diagram once the wire velocity exceeds approximately 10 per cent of the critical velocity, V_c, the wire no longer exhibits a linear relationship with drive. For the resonators used for the purpose of vortex detection, the drive velocities are kept low so that the resonator signal stays within this linear region.

When the temperature of the superfluid ^{3}He is increased and the amplitude sweep repeated it can be shown that the critical velocity does not change but as would be expected the drive current will need to be increased to counteract the extra damping experienced by the wire due to increased thermal quasi-particle collisions. This enables us to use the obtained value for the critical velocity for a wire for the entirety of a demagnetisation even when the superfluid is heated to take measurements at higher temperatures.

4.4.3 Fixed Frequency

After measuring the resonant frequency, the $H \times W/D$ constant described in section 4.4.1 for the wires and their pair-breaking critical velocity all the information needed to use the wires for more than slow thermometry is ready.

By keeping the wires on resonance with a known drive current the width and hence the temperature can be derived from the signal height. With this method the temperature and hence the quasi-particle density incident on the wire can be measured instantaneously rather then once every 5 minutes as with the frequency sweep mode. To ensure that the calculated width is a reasonable and accurate value the wire velocity is kept at or below $0.1v_c$ well within the linear region described in section 4.4.2. To calculate the resonant width, or damping, of the wire,

$$\Delta f_2 = (H \times W/D) \times \frac{V_{Drive}}{V_x} \tag{4.20}$$

where V_{Drive} is the drive voltage into the 'drive box' and V_x is the measured in-phase signal. During their operation the resonators are kept as close as possible to their resonant frequency during data taking but if there is a large change in the damping of the wires the frequency may 'drift'. It is possible to correct for this drift as simple mathematics can show that

$$V_x' = V_x + \frac{V_y^2}{V_x} \tag{4.21}$$

where V_x' is the value for the in-phase voltage on resonance and V_x and V_y are the measured signal voltages. The resonators can now be operated in a manner which can record the damping width on a fast time scale. Typically the widths are logged every second for normal data taking but to enable a higher temporal resolution the width, and hence the quasi-particle density, can be sampled at rates up to 0.05 seconds per point. The computer programs used to operate the resonators can be set to calculate automatically the widths 'on the fly' to provide a real time measure of the temperature. The resolution of this however is restricted by the digitisation of the data sent

through the GPIB bus. Recording the analogue voltages output from the lock-in amplifiers separately with a data acquisition card and calculating the widths after the experimental run has ended allows full corrections for equipment crosstalk and other background voltages to be performed. This provides a much more accurate value for the damping widths.

4.5 Vibrating Wires as Heaters

Although much effort has gone into getting the experiment as cold as possible it is often necessary to perform experiments at a slightly hotter temperature. To control the temperature it is found that a 13μm resonator makes a very effective heater. If the wire is driven above its critical velocity the superfluid Cooper pairs can be broken creating thermal quasiparticles effectively raising the temperature of the superfluid. The power dissipated by a 'heater' wire can be simply found by the product of the drive current shown in equation 4.19 and the in-phase signal voltage:

$$\dot{Q} = I_{drive} V_x = 0.155 \frac{V_{drive} V_x}{R_{drive\ box}} \tag{4.22}$$

where V_{drive} is the drive voltage into the drive box, $R_{drive\ box}$ is the resistance of the drive box and V_x is the in-phase signal voltage. The factor of 0.155 is due to the step down transformer inside the drive box for breaking any earth loops and impedance matching.

4.6 Vibrating Wires as Thermometers

Thanks to the phenomenon of Andreev Scattering it is possible to use a vibrating wire resonator to evaluate a necessary real world quantity. It is found to be very useful to be able to convert the resonant width, Δf_2, into a temperature. To do this conversion it is necessary to consider what processes happen to the wire whilst it is being driven. Earlier in this chapter it was described how the fluid acts upon the moving wire causing a restoring force (equation 4.1). This force is due to the quasiparticles colliding with the flow fields in the fluid around the wire and transferring momentum to the wire.

If we examine the excitation spectrum for the superfluid Fig. 2.5 shown in section 2.3.3, we can see that quasiparticles have their momentum and group velocity in the same direction whereas quasiholes have their momentum in the direction opposite to their group velocity. This results in a 'pulling' force upon an object when a quasihole collides with it and a 'pushing force' when a quasiparticle collides. A simple supposition would be that when a wire moves through the fluid the pushing and pulling forces would virtually cancel each other out but experimental data shows otherwise[25].

Consider the moving wire as a paddle of cross sectional area A which has a velocity v through the superfluid and suppose that the quasiparticles are constrained to only move forwards or backwards in the direction of the paddle motion. If there are n quasiparticles per unit volume of average velocity v_g and momentum p_F, then the number hitting the forward facing side of the paddle can be shown to be $An(v_g + v)/2$ per unit time and conversely the number hitting the rear to be $An(v_g - v)/2$. Since each quasiparticle exchanges a momentum $2p_F$ with the paddle the opposing force per unit

area is

$$F = p_F n(v_g + v) - p_F n(v_g - v) = 2np_F v. \tag{4.23}$$

This damping force is however three orders of magnitude smaller than the measured force[53]. The reason for this difference is that incident quasiparticles will be Andreev scattered before reaching the wire surface. This scattering is due to the fluid close to the wire moving at a velocity equivalent to the wire velocity and causing the excitation dispersion curve of this moving fluid to undergo a galilean transformation $\Delta \pm p \cdot v$ as described earlier in section 2.3.3. Under these conditions quasiparticles with energy less than $\Delta + p \cdot v$ are unable to propagate through to the wire surface in order to undergo normal scattering and are thus scattered by Andreev processes.

Before we begin it is necessary to make some assumptions about the wire and the excitations. The wire is considered to be a flat moving paddle with direction of motion normal to the surface. The quasiparticle excitations are also considered to be moving parallel to the wire velocity and in the ballistic regime where there are no quasiparticle-quasiparticle interactions.

Since the force on the paddle from normally scattered excitations can now by modelled it is possible to calculate this force. To get the number of quasiparticles and quasiholes active in the system the product of the density of states $g(E)$ and double the distribution function $f(E)$, since there are two different types of excitation, is integrated with respect to energy within the limits of Δ and $\Delta + p_F v$. To calculate the quasiparticle flux per unit area this is then multiplied by the excitation group velocity v_g and since the excitations exchange $2p_F$ momentum with the paddle of width $2a$ the force

on the paddle can be evaluated as such[25]:

$$F = -\int_{\Delta}^{\Delta+p_F \cdot v} 8ap_F g(E)\exp(-E/k_B T)v_g dE \tag{4.24}$$

where at low temperatures the Fermi function approximates well to a Boltzmann factor $\exp(-E/k_B T)$.

Using the identity that $g(E)v_g(E) = g(p) \simeq g(p_F)$ and integrating we find that:

$$F = -(8ap_F g(p_F)k_B T)\exp(-\Delta/k_B T)[1 - \exp(-p_F \cdot v/k_B T)] \tag{4.25}$$

Now let's consider conditions of driving the wire at high velocities at low temperatures so that $(k_B T \ll p_F v)$ we find that:

$$F = (8ap_F g(p_F)k_B T)\exp(-\Delta/k_B T) \tag{4.26}$$

The damping force on the wire in this regime is velocity **independent** since the temperature is low enough to ensure that all excitations are with the thermal variation $k_B T$ of the dispersion curve minimum. Therefore all low energy excitations are Andreev reflected before being incident upon the paddle.

The other condition where $(k_B T \gg p_F v)$, i.e. high temperatures and low velocities the force is reduced to:

$$F = (8ap_F^2 g(p_F))\exp(-\Delta/k_B T)v \tag{4.27}$$

Under these conditions some of the lower energy excitations as shown in branches 3 and 5 of Fig. 2.6 reach the paddle cancelling a proportion of the damping due to higher energy excitations such as those in branch 1 and 7. The resonators used are operated in this regime.

Now the model has been defined and evaluated it is time to relate it to observed wire behaviour. The resonators used however are not the flat paddle

which has been modelled but fully three dimensional wires so a geometric factor has to introduced to the model. With this factor in place equation 4.27 becomes:

$$F = (8\lambda' a p_F^2 g(p_F))\exp(-\Delta/k_B T)v \tag{4.28}$$

Where λ' is the dimensionless geometric constant experimentally found to be about 0.95[25]. So how does this then relate to the damping on the wire measured as the resonant width Δf_2?

Since the resonators are always driven in the low velocity linear regime the damping force can be equated to the fluid damping component from the initial equation of motion, equation 4.1, and in terms of Δf_2 from equation 4.14, hence

$$F_{fluid} = m\lambda_2 v = m(2\pi\Delta f_2)v = 8\lambda' a p_F^2 g(p_F)\exp(-\Delta/k_B T)v \tag{4.29}$$

and rearranging gives

$$\Delta f_2 = \left(\frac{8\lambda' a p_F^2 g(p_F)}{2\pi m}\right)\exp(-\Delta/k_B T) = A\exp(-\Delta/k_B T) \tag{4.30}$$

where A is a constant found numerically to evaluate to 1.691×10^{-5} for a 4.5μm resonator at a pressure of $P = 0$. This simple relationship can be evaluated and the theoretical damping-temperature relationship for such a resonator is plotted in Figure 4.5.

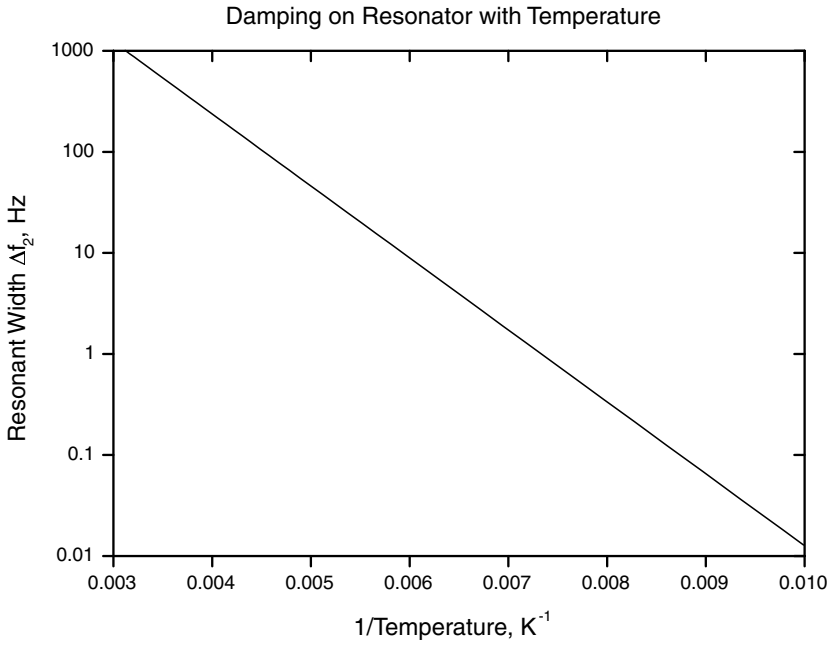

Figure 4.5: Chart showing damping on resonator as a function of temperature.

4.7 Vibrating Wires as Vortex Generators

Historically there were three main ways in which vortices could be studied in superfluid ^{3}He. By rotating a vessel containing a sample of superfluid a build up of counterflow from the rotation of the normal component is relaxed by the creation of an ordered lattice of vortex lines. These vortex lines can then be detected and probed by their NMR signatures[54]. This 'rotating bucket' technique is the most commonly used method of creating ordered vortices. The second way in which vortices are commonly created is when a fluid quenches rapidly through the superfluid transition due to intense local heating. To facilitate the Kibble mechanism[55] the localised heating is created by neutron capture processes. The final method for vortex creation

is during oscillatory flow when a superfluid is forced through an orifice or weak link[56]. At the orifice a large phase gradient is created which can be relaxed by 2π upon the creation of a vortex line.

It was recently discovered that a vibrating wire resonator could be used for a more interesting purpose than simple thermometry. Fisher *et al*[6] observed that when a resonator was driven above the pair-breaking critical velocity v_c an inhomogeneous localised region of quantised vortex lines will be created. These vibrating wire resonators have been used by various research groups and primarily the Lancaster group for many years for purposes such as thermometry and as heaters, by driving them above their pair breaking velocity. The side effect that the wire was also producing a tangle of vortices was not discovered until a second resonator was placed in close proximity to the hypercritical resonator.

When the second wire was monitored it was observed that as the drive velocity of the 'source' wire increased the quantity of thermal quasiparticles incident on the 'detector' resonator increases and then rapidly decreases by up to 20%. This 'shielding' of the quasiparticles is attributed to Andreev processes reflecting the quasiparticles from the flow field around a vortex line.

The mechanism of creating the quantised vortex line with a vibrating wire resonator has not yet been completely studied so the exact mechanisms are as yet unconfirmed. Since the initial discovery[6], it has been found that the results from previous studies[5] show the vortex creation results from an increased flow velocity in the localised region around a defect on the resonator surface. These defects could be caused by a simple kink in the wire, a section

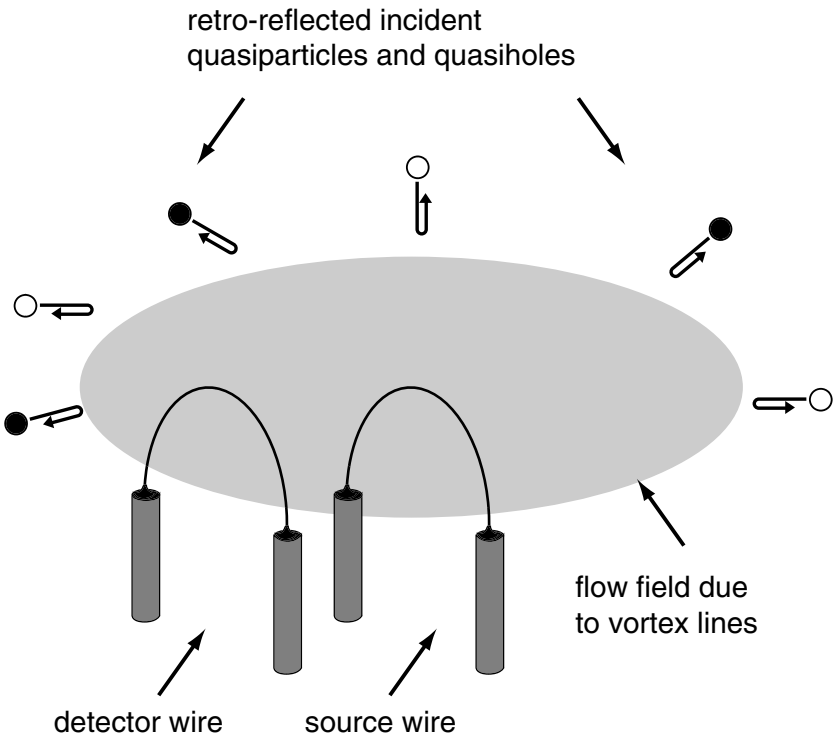

Figure 4.6: Diagram showing a vortex 'cloud' shielding a detection resonator.

of the matrix not removed during the manufacturing process or some piece of 'debris', most probably powdered copper refrigerant or detached sinter, which has become attached.

4.8 Black Body Radiators

Most of the recent experiments conducted by the Lancaster group have utilised black body radiators. Inside this cell is a single Lancaster style Black body radiator referred to as a 'box'. These boxes can be used as very sensitive bolometers capable of resolving energy changes far lower than 1pW. A box contains two resonators, a 13μm NbTi resonator and a 4.5μm NbTi resonator, and has walls made from stycast impregnated paper. The superfluid inside is weakly thermally linked to the 'bulk' superfluid with a small aperture, 0.33mm diameter for the box used, in one of the walls. Without any heat being applied into the box via the 13μm NbTi resonator the temperature inside the box, measured with the 4.5μm NbTi resonator, is due to heat leaks from the paper walls, $\dot{Q}_{leak}$. This heat leak is balanced with heat exiting the box through the aperture $\dot{Q}_{out}$.

Before the box can be of any use it needs to be calibrated. If a known quantity of heat is applied by driving one of the resonators the temperature inside the box can be measured with the second resonator. From simple kinetic theory[57] this gives

$$\dot{Q}_{out} = \frac{1}{2} A < n v_g > \tilde{E} \tag{4.31}$$

where A is the aperture cross sectional area, $\tilde{E}$ is the mean quasiparticle energy and $< n v_g >$ is the 'quasiparticle' flux. $< n v_g >$ is defined as the integral product of the density of states function for a given energy E, the excitation distribution function and the group velocity for energy E. Solving this integral for our experimental conditions[57] enables us to measure the calibration constant c for the black body radiator in terms of the damping

on the wire as

$$(\Delta f_2 T\tilde{E}) = c\dot{Q}_{out} \tag{4.32}$$

where $\dot{Q}_{out}$ was previously shown to equal to the heat entering the radiator, due to the applied heat and the heat leak, and $\Delta f_2 T\tilde{E}$ is a newly defined quantity known as the 'width parameter' where Δf_2 is the resonator damping inside the radiator, T is the temperature inside and $\tilde{E}$ is average quasiparticle thermal energy. By measuring changes in the width parameter, $\delta(\Delta f_2 T\tilde{E})$, from the base value we now have a calibration allowing us to convert any increases in the measured width parameter into powers entering the radiator. Figure 4.7 shows the calibration of the box used in this cell over several orders of magnitude and over a period of $\sim$ 24 months.

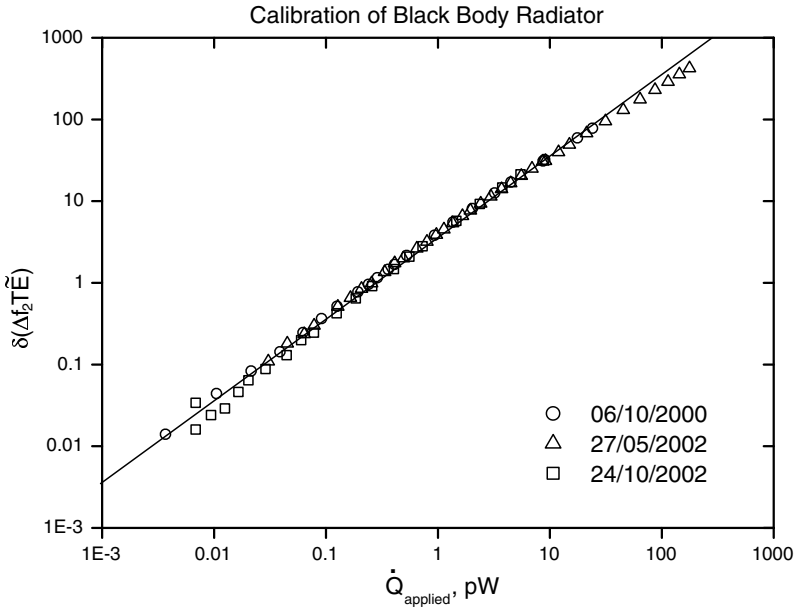

Figure 4.7: Calibration diagram of black body radiator.

Chapter 5

Spatial Extent of Turbulence

5.1 Experimental Technique and Theory

Vorticity was recently discovered to be produced in superfluid ^{3}He B phase when it was shown that a vibrating wire resonator is driven at velocities exceeding its pair breaking critical velocity, and this vorticity could be detected by a second resonator in close proximity[6]. This experiment proved useful in establishing that a vibrating wire resonator could indeed produce a tangle of quantised vortex lines in ^{3}He but it could not provide a great deal of quantitative information upon the phenomenon. The experiment conducted and described in this chapter expands upon this work by observing the development of the vortices over a larger range of separations between source and detector resonators. To enable a range of separations having a moveable wire for which the separation could be varied would be ideal. Unfortunately design and engineering have conspired to make this unworkable. The solution to this problem was to construct an array of several wires. Although this will only provide a limited selection of separations the construction was,

in contrast to other ideas, relatively simple. In addition to this it was also thought necessary to try to investigate the sideways extent of this vorticity. For this purpose a vibrating wire resonator was added at the side and positioned perpendicular to the array. This resonator can then be used to detect any vorticity generated by wires in the array or be used to generate vorticity itself to be detected by the array. An eighth wire is located 1.02mm above wire $\mu\mu\mu\,2$ in the array.

5.1.1 The Experimental Arrangement

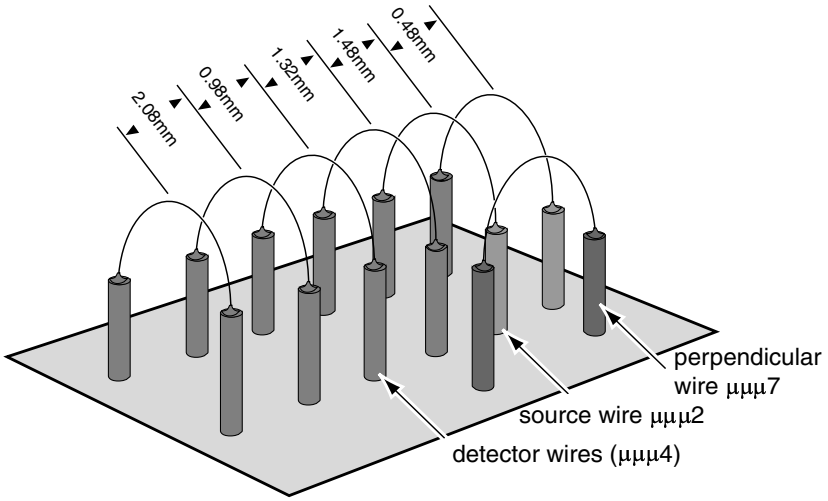

Figure 5.1: Linear array of six vibrating wire resonators measuring the extent of a vortex tangle with the seventh wire shown.

To be able to detect and measure the vorticity at several different separations from the source wire a linear array of six $4.5\,\mu$m vibrating wire resonators was constructed. The resonators were created in the standard way described in section 4.3. The typical separation between adjacent wires within the array is $\sim 1\,$mm. The exact separations of the linear wires are

shown in Fig 5.1. Alongside the linear array of the six resonators is a seventh 4.5 μm vibrating wire resonator perpendicular to the orientation of the initial six. This seventh wire was added to detect and measure the sideways growth of the region of vorticity and is used during the linear investigations to examine if the quasiparticle beam or the vorticity extends in the directions transverse to the source wire motion or whether the vorticity is directionalised along this x axis. Also using the seventh wire as a generator wire would allow initial measurements on the transverse extent of the vorticity.

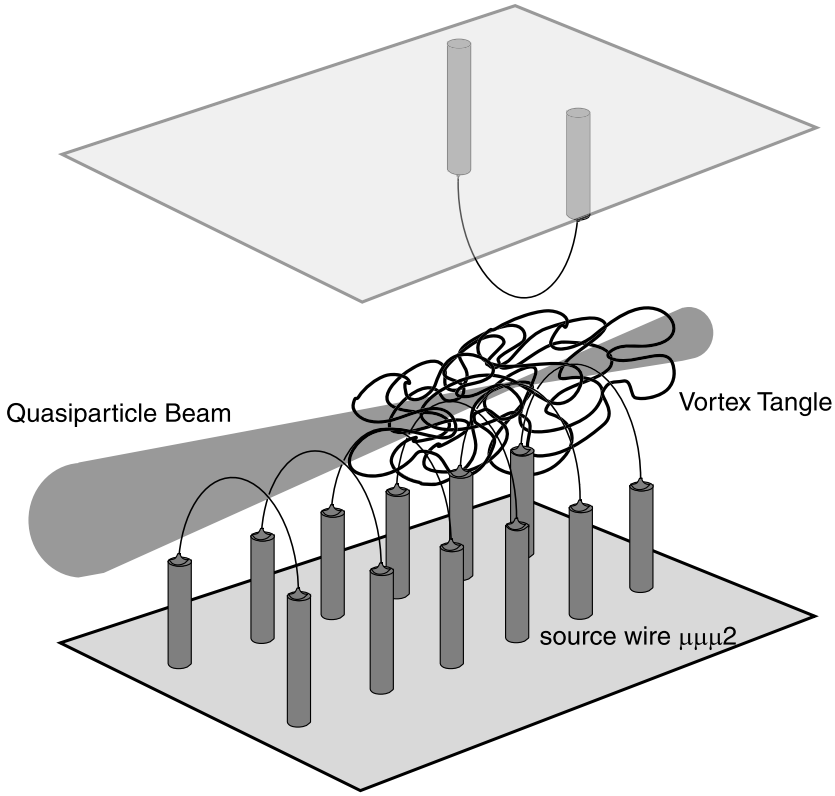

Figure 5.2: Diagram of the beam being produced as vorticity is generated with the seventh wire removed for clarity.

During the experiment a resonator in the array is designated as the generator wire and will be used to create a localised region of vorticity where the flow fields around the vortex lines will shield neighbouring resonators from incident thermal quasiparticles through Andreev scattering processes as described in section 2.3.3. This wire, refered to herein as the 'source' wire, is driven at a velocity above its pair breaking critical velocity and, as was explained in chapter 4, will thus generate a tangle of quantised vortex lines.

As the mechanism of creating the vortices is presumed to be as a result of breaking the superfluid Cooper pairs, this will also have the effect of producing a directionalised beam of ballistic thermal quasiparticles along the axis of the generator wire motion. This effect of the beam can then be measured, and subsequently compensated for, by driving the source wire through the normal operational range of drive velocities whilst the cell is at the bulk superfluid base temperature, $\sim 110\,\mu$K, where there are negligible background thermal quasiparticles and hence negligible shielding due to the vortex lines.

5.1.2 The Ballistic Quasiparticle Beam

As was briefly mentioned in section 4.5 a vibrating wire resonator driven above its critical velocity will break the Cooper pairs of nearby superfluid and create a directionalised beam of thermal ballistic quasiparticles. This beam can also be detected with a secondary vibrating wire resonator placed in the direction of the produced beam[58]. The mechanism for this is due to the moving wire causing changes to the excitation dispersion curves. If we consider a microscopic object moving through B-phase ^{3}He the critical

velocity can be easily shown to be given by the Landau velocity,

$$v_L = \frac{\Delta}{p_F} \tag{5.1}$$

where the energy of the moving fluid equates to the superfluid energy gap. When this occurs it is no longer energetically preferential for the ^{3}He atoms to be in Cooper pairs and so they split creating a quasiparticle-quasihole pair which have almost equal momenta. This was confirmed experimentally by Ahonon *et al*[59].

Unfortunately this simple relationship cannot be applied to a vibrating wire resonator since they are not a microscopic object but macroscopic. For these objects we also need to consider the effects of the energy gap being suppressed within a few coherence lengths of the wire surface and the fluid backflow around the wire. For this real object the critical velocity is found to be of the order of $v_L/3$[53]. The full mathematical derivation and proof of this can be found in the PhD Thesis by S. N. Fisher(1992).

So it has been shown that driving a resonator at or above the critical velocity V_c will create a beam of thermal quasiparticles. For this beam to have an effect on neighbouring vibrating wires two criteria need to be fulfilled.

The first criterion is that the mean free path of the quasiparticle needs to be long enough for it to travel from the source wire to the detector wires without being scattered. This mean free path of a quasiparticle (or indeed a quasihole) is found to be as large as several hundred meters at our cell base temperature of $\sim$ 110 μK ($\Delta f_2 \simeq$ 1.0Hz) but drops as the superfluid temperature increases to a length of $\sim$ 1cm at $\sim$ 210μK ($\Delta f_2 \simeq$ 70Hz). Because of this, the experimental cell is designed and built to be smaller dimensionally than 1cm. Figure 5.3 shows the calculated mean free path of

a thermal quasiparticle over a large temperature range.

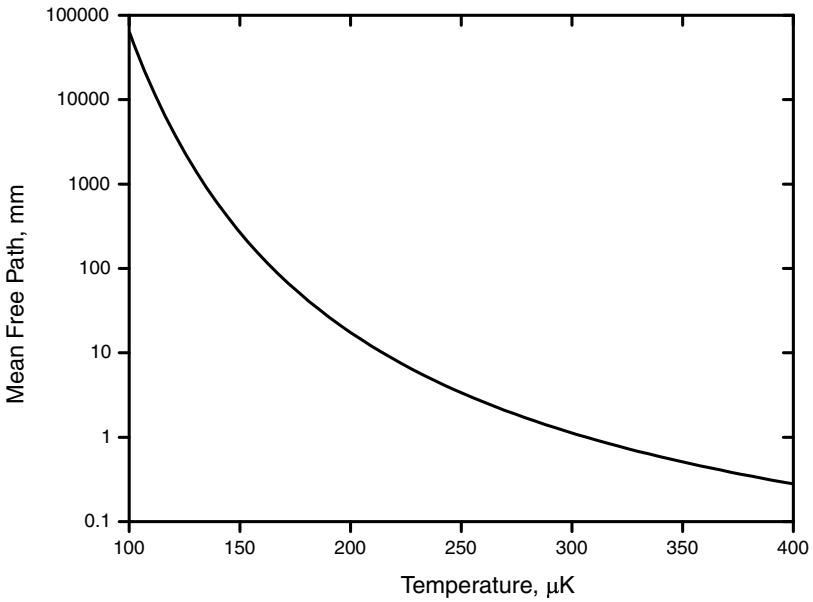

Figure 5.3: Mean free path of thermal quasiparticle as a function of superfluid temperature.

The second criterion is that the intensity of the generated beam is greater than the intensity of the surrounding thermal quasiparticles in the bulk superfluid. To ensure this, the bulk superfluid temperature is kept as low as possible whilst the effect of the beam is being measured and the heating effect of the beam on the bulk superfluid is minimised by the extra cooling power of the surrounding copper refrigerant.

5.1.3 Dynamics of the Vortex Tangle

Any changes in the density of the vortex lines can be inferred from a decrease in the damping of the detector wires. Since the quasiparticle collisions are the dominant source of the damping experienced by a vibrating wire resonator at

these low temperatures, changes in the vortex line density will reflect less or more of the background thermal quasiparticles. By measuring the damping of a detector before and during a pulse, we can define the change in the damping as

$$\delta\Delta f_2^T(v) = \Delta f_2^T(v) - \Delta f_2^T(0) \tag{5.2}$$

where Δf_2 is the wire damping, v refers to the source wire velocity and T denotes the cell temperature above the base temperature. Since the process of creating vortex lines with a resonator also creates a thermal quasiparticle beam, the effect of this beam must be first measured at the cell base temperature where there are minimal thermal quasiparticles in the bulk superfluid to be shielded and calculated with the equation;

$$\delta\Delta f_2^0(v) = \Delta f_2^0(v) - \Delta f_2^0(0). \tag{5.3}$$

The measurements taken at temperatures above the base temperature contain both of the components due to the quasiparticle beam effect and the component due to the shielding effect. By subtracting the damping change due to the beam at the base temperature from the change in damping at the higher temperatures the direct heating effect of the quasiparticle beam can be compensated for. Scaling the result of this by the initial damping of the detector before the pulse commences, it is possible to evaluate the fractional change in the damping as

$$F(v) = \frac{\delta\Delta f_2^T(v) - \delta\Delta f_2^0(v)}{\Delta f_2^T(0)}. \tag{5.4}$$

Here $F(v) = 0$ is true when there is no change in the damping, and $F(v) = 1$ when all the background thermal quasiparticles are shielded by the vortex lines. The data can now represented as the fraction change in damping

against the source wire velocity in units of the critical velocity. This fractional change in damping is related to the vortex line density and can be used as an arbitrary measure of this.

5.2 The Experiment

The experiment is mounted inside a Lancaster style nested demagnetisation cell which uses sintered copper plates as a nuclear magnetic refrigerant. The cell is then mounted onto a dilution refrigerator as described in section 3.1.1. The dilution refrigerator takes approximately ten days to cool to around 7mK after a 'remagnetisation' whereupon it is possible to again demagnetise the cell. More information on the demagnetisation cycles is found in section 3.1.2. Demagnetisation reduces the temperature of the superfluid inside the cell to its base temperature of $\sim 110\mu$K. The superfluid is now cold enough to perform the experiments and will stay at this temperature for around four days. The time difference between demagnetisations of fourteen days is convenient as it allows an experiment to be performed every two weeks (when everything is working correctly).

The first procedure to perform once the cell is cold is to frequency sweep the resonators that will be used. This allows the calculation of the 'Height Width over Drive' constant, described in section 4.4.1, which shall be used for the fast measurement of the damping width Δf_2. Once the $H \times W/D$ has been measured for each wire, the pair breaking critical velocities, V_c, for each wire can be measured by 'amplitude sweeping' the resonators as detailed in section 4.4.2. Finally after collecting all of these resonator parameters it is now possible to commence the investigations of the vortex tangle.

After selecting the 'source wire', typically $\mu\mu\mu 2$ as the separations between this wire and the other detectors wires are the most even, the detector wires are driven at a drive velocity approximately 10% of their critical velocity to ensure the wire responses are well within the linear limit. The

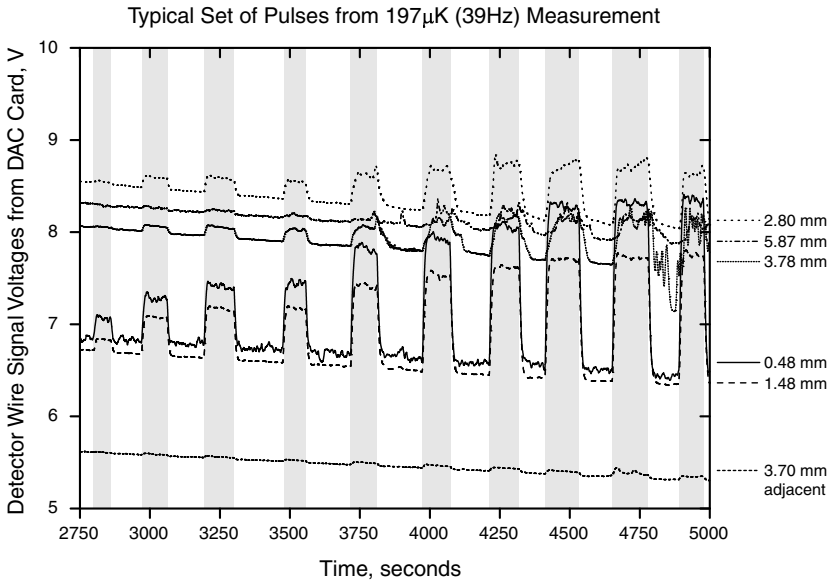

Figure 5.4: Section of raw captured data at temperature of $\sim 197\mu$K.

source wire is now driven at a range of velocities between $< 1V_c$ and $\sim\ 3V_c$ to measure the effect of the pair breaking quasiparticle beam on the detector wires. Once this is completed the cell is heated with a 13μm diameter resonator wire, known as a 'single micro', to a designated temperature to increase the density of the thermal quasiparticles in the bulk superfluid. The drive current on the detector wires has to be increased at this point back up to $\sim\ 10\%\, V_c$ since the larger quasiparticle flux increases the damping measured by the wires and reduces the measured signal voltage. Now the source wire is driven at velocities within the range of the velocities used for the pair breaking quasiparticle beam measurements.

To be able to capture all the data from multiple detectors at a suitable resolution the signal heights V_x from the detector wires are logged at a rate of 10 points per second with a 16−bit PCI data acquisition card (DAQ card) by National Instruments. The analogue output from the SR830 lock-in am-

plifiers outputs a voltage between -10 and 10V which is calibrated to the full scale deflection of the amplifier reading. For example if the full scale deflection is 5.0μV and the signal is 2.2μV the analogue output into the DAQ card will be 4.4V. This allows a high level of precision at a faster rate than logging the data through the GPIB bus would be able to provide. These signal heights are then easily converted to a damping width by using the $H \times W/D$ constant and the drive voltage. A typical pulse lasts for approximately 50 seconds and after a pulse has been removed, the cell is left for approximately 100 seconds to allow all the vorticity to decay and the quasiparticle beam to thermalise with the superfluid. The source wire drive current is then increased incrementally and the next pulse is conducted.

The process of measuring the response of the detectors takes around 4 hours for a set of approximately 50 pulses of drive velocities between $0.5\,V_c$ and $3.0\,V_c$. With a data resolution of 10 points per detector per second the raw data files can quickly become very extensive.

5.3 The Results

The data files collected are read into the Microcal Origin software program which allows the easy manipulation of large data files. Before any manipulation of the data is commenced the data has to be corrected for any 'cross talk' that may have occurred between the detectors and amplifiers. The effect of this cross talk is measured by removing all of the applied magnetic field from the experimental magnet and measuring the response of the detectors over the range of drive currents used in the experiment. Removing the magnetic field isolates the cross talk interference from any signal due to the induced Faraday voltage since with there being no magnetic field present there can be no voltage induced from the motion of the wires. This effect is found to vary for each demagnetisation and so at the end of each demagnetisation they are measured anew.

Next the data is corrected to take into account any drift in the resonant frequency of the resonator as detailed in equation 4.21. Now for each pulse, the response of the detector wires can be converted into a measure of the damping experienced by the wire. This in turn can be used as a measure of the 'density' of the vortex lines in that region as was described earlier but it should be stated that the exact correlation between the change in damping and the vortex line density is unknown but it does provide us with a simple effective technique for resolving changes in the quasiparticle density. The equation used to convert the signal responses into the damping width is:

$$\Delta f_2 = (H \times W/D) \times \frac{V_{drive}}{V_x}. \tag{5.5}$$

These measured widths are then applied to equation 5.4 along with the measured effect of the generated ballistic quasiparticle beam to calculate a value

for the reflected fraction of the incident background thermal quasiparticles. Using the assumption that the vortex line density will affect the amount of quasiparticles incident upon the resonators, this fractional change in the quasiparticle density can be used to measure the change in the vortex line density.

5.3.1 Linear Quasiparticle Beam

At the cell base temperature the effect of the beam on the neighbouring wires is quite dramatic. Typically at this temperature the resonators have a half height resonant width, Δf_2, less than 0.1Hz without the beam applied, which is solely due to the inherent damping arising from the internal friction within the wires and the background quasiparticle density. The inherent stiffness of a resonator is found by operating the wires in a vacuum where there is no damping from thermal quasiparticles or from the fluid motion. When the generated quasiparticle beam is incident upon the resonators the damping of these detectors exceeds by several times the measured damping without the beam. The effect of the beam at the base temperature is shown in Fig 5.5.

In this figure we can see some interesting features. The first and most obvious is that there is no change in the response of the resonators whilst the source wire velocity is below its critical velocity. This is to be expected since whilst this is so, there is no breaking of the superfluid pairs and so no ballistic quasiparticles are being created. The second expected feature is that as the source wire velocity increases the amount of quasiparticles incident on the detectors increases. Again theory suggests that this will be, since there will be more quasiparticles created the faster that the source wire is driven.

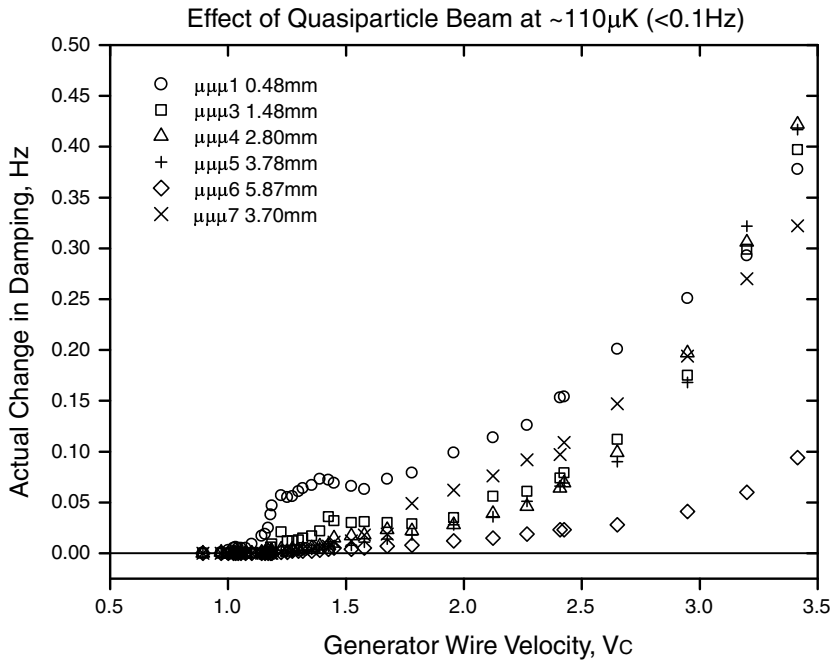

Figure 5.5: The effect of the linear pair breaking quasiparticle beam on the detector damping.

One interesting feature is the abnormal peaks in the wires closest to the source wire at velocities of $\sim 1.2V_c$ and $\sim 1.4V_c$. This is clearly illustrated in Fig 5.5 by wire $\mu\mu\mu 1$. The reasons for these features are not known at present although I believe work is planned in the future to investigate what the mechanics behind these are and whether the separation between source and detector has an effect.

5.3.2 Detection of Vorticity with a Linear Orientated Wire

The measurements are now ready for examination. Firstly the raw changes in the detector damping are plotted against the source wire velocity. The

source wire velocity is scaled by its critical velocity so that pair breaking occurs at $1.0V_c$. The results for the measurements taken at a temperature of 39Hz or 197μK are shown in Fig 5.6. Here we can see that all of the detectors

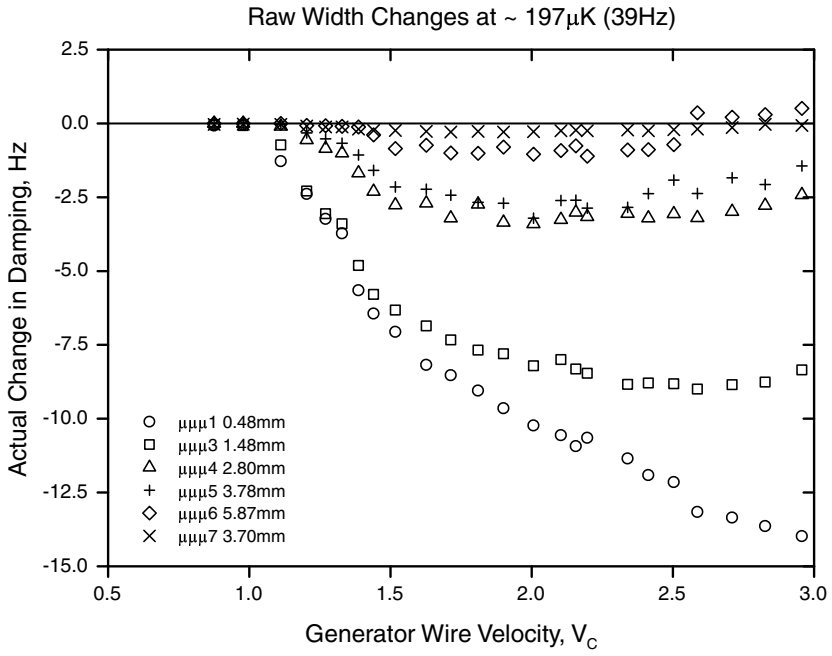

Figure 5.6: The raw response of the detector wires to linear vortex production at 39Hz.

have seen a shielding effect including the seventh detector located at the side of the array. One clearly noticeable feature is that the detectors closest to the source wire have seen the greatest shielding effect. This would indicate that the density of the vortex lines diminishes as they travel away from the source. Also observable is the confirmation that there was no pair breaking or vorticity before the source wire exceeded its critical velocity. Another interesting feature is that the detector located at the side of the source wire has seen a much lesser effect than the detector in the array with a comparable separation. This would indicate that the vorticity is highly directionalised

along the axis of the wire motion.

If we now compensate for the quasiparticle beam effect and convert the actual changes in damping into a fractional change we can look more closely at how the damping changes and from this observe changes in the vortex line density. Fig 5.7 shows the fractional change in the damping. As can be seen

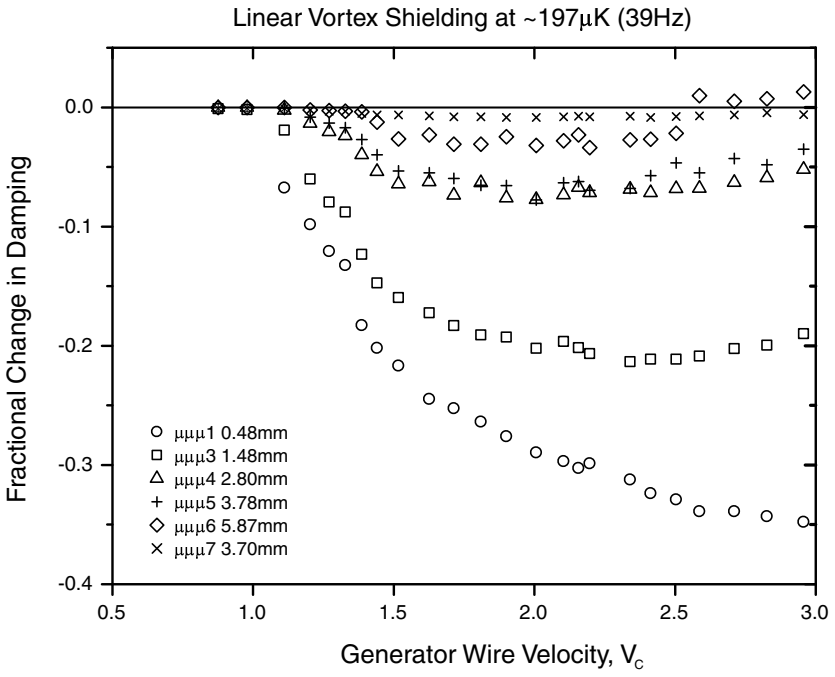

Figure 5.7: Development of a vortex tangle at a temperature of $\sim 197\mu$K or width of $\sim$ 39Hz.

in Fig 5.7 there is no observable change in the damping experienced by the detector wires until the source wire approaches the critical velocity. Upon reaching this criteria there is a rapid increase in the density of the shielding and hence vortex lines until the velocity reaches approximately 1.5 times the critical velocity or $1.5V_c$. At this velocity the rate of increase decelerates and for the distant detectors the damping experienced begins to increase.

At around $3V_c$ the heating effect of the quasiparticle beam becomes so great that only the wires in direct proximity to the source wire are still seeing an increase in vortex density. At velocities greater then this, the changes in vortex line density are no longer measurable due to the beam cataclysmically dominating the response of the wires.

5.3.3 Transverse Vortex Production

Instead of using a wire in the linear array to generate the quasiparticle beam the seventh wire which is located to the side of the array, as shown in Fig 5.1, will be used. As before this effect is more accurately measured at the beginning of a demagnetisation run when there has been no heat applied to the cell and the quasiparticle density in the bulk superfluid is at a minimum. The six wires in the linear array are used to detect the beam. The actual changes in the damping are measured for varying source wire drive velocities between $< V_c$ and $\sim 3V_c$. The changes are shown in Fig 5.8 as a function of the source wire velocity. The source wire velocity is again scaled with the critical velocity of this wire so that pair breaking occurs at $\frac{V}{V_c} = 1.0$.

The most obvious difference between the linear quasiparticle beam and the transverse quasiparticle beam effects is that the detectors do not see any effects of the beam immediately after pair breaking occurs. One possible reason for this could be that the effect of the quasiparticles on the detector wires is lessened due to the detector motion being perpendicular to the motion of the quasiparticles. Experiments conducted by Fisher[53], also show the angular dispersion of the quasiparticle beam increasing as the source wire velocity increases. This could result in the beam having a smaller effect on

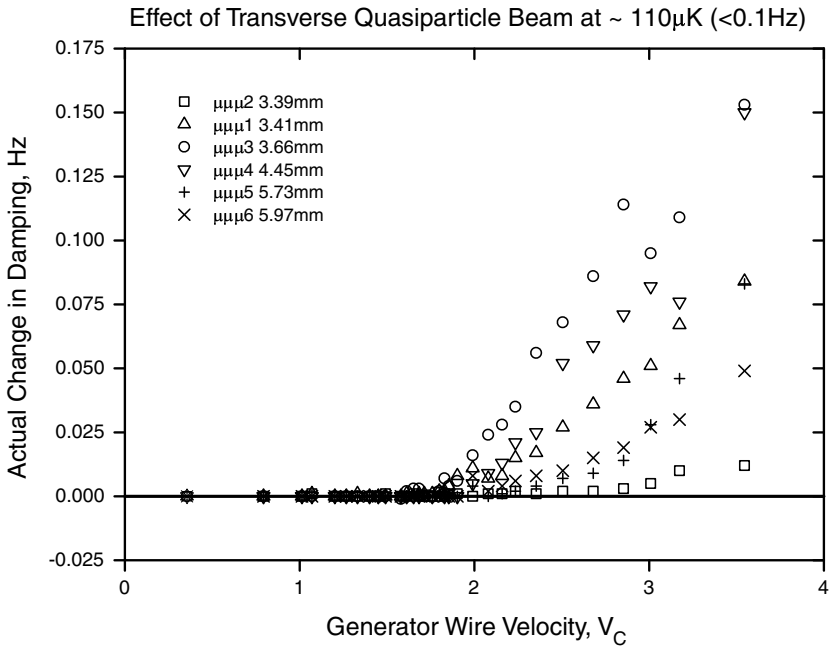

Figure 5.8: The effect of the transverse pair breaking quasiparticle beam on the detector damping.

the resonators directly in its path as the density the of quasiparticles reduces. The detectors begin to see an extra damping effect once the source wire velocity exceeds $1.5\,V_c$. As can be seen in Fig 5.8 the first detector wire to experience the extra damping is $\mu\mu\mu 3$. This would indicate that the source wire is not exactly perpendicular to the array but slightly orientated towards this detector.

The second interesting feature is that the detector we would expect to experience the most damping, $\mu\mu\mu 2$ sees much less extra damping than the other wires in the array despite it being the closest spatially and directly in front of the beam producing wire. One hypothesis for this is that the majority of the quasiparticles, being highly ballistic, travel past this resonator without interacting. Also the angular distribution of the beam increases with

the source wire velocity causing the density of the quasiparticles to reduce directly inline with the source wire motion. The responses for the three of the resonators furthest away from the source, $\mu\mu\mu 4$ to $\mu\mu\mu 6$, behave as would be expected with the detectors closest to the source wire experiencing more extra damping due to the beam than the resonators farther away.

The measurements with the source wire being within the array shows the region of vortex lines propagating in the axis of wire vibration but does the vorticity stretch to the side? As can be seen in Fig 5.7 the resonator located at the side of the array, $\mu\mu\mu 7$, sees the vorticity and experiences a shielding effect but on a much smaller scale compared to a resonator at a similar, but linear, separation. This adjacent wire will now be used to create the vorticity and the six wires in the linear array will be monitored for any evidence of the shielding effect. This showed that the beam is highly directionalised with the largest effect on the detectors directly in front of the source wire with the exception of $\mu\mu\mu 2$ for an unknown reason. So with the beam effect measured, the source wire is, similar to the linear investigations, driven through a range of velocities between $< V_c$ to $\sim 3V_c$ where V_c is once again the pair breaking critical velocity of our source wire. The raw results before correcting for the beam effect are displayed in Fig 5.9.

As can be seen, the actual changes in the response of the detectors even before corrections for the effect of the quasiparticle beam are very small with changes of $\sim 10\%$ in the damping, at a source wire velocity of $3V_c$. The raw data does show nicely however that the vortex cloud is clearly detected by the first two detectors in the array with the other detectors only noticing a heating effect.

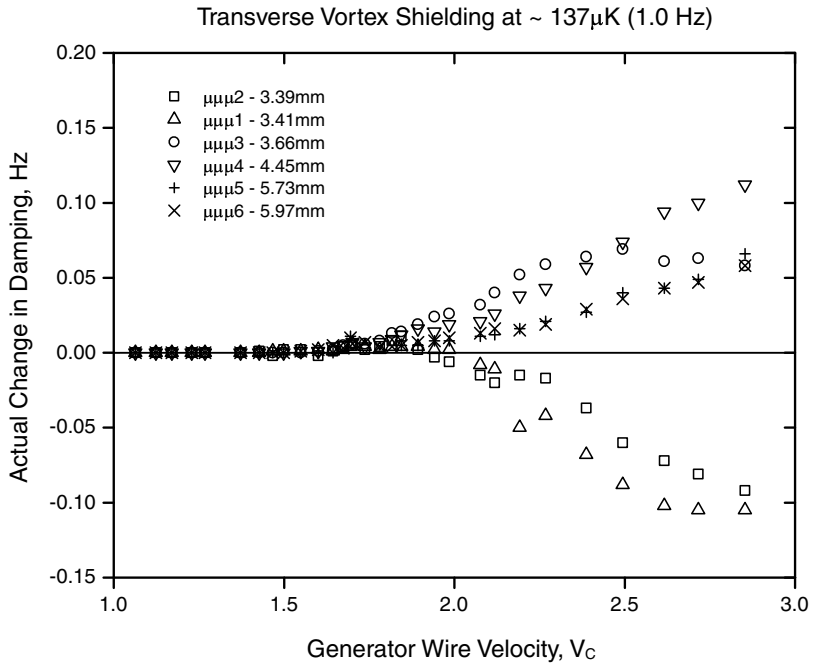

Figure 5.9: The raw response of the detector wires to transverse vortex production.

If we now take away the effect of the quasiparticle beam by subtracting the changes in the actual width measured at the base temperature and convert the changes into the fractional change we can see how the vorticity alone has affected the detectors. The experiment was conducted at two temperatures. Firstly it was conducted at 1.0Hz which corresponds to 137μK. The result for this is shown in Fig 5.10. As was shown before by the quasiparticle beam data the detectors don't see any effect until the source wire velocity is much greater than $V_c = 1$. This is assumed to be due to similar reasons to why the beam did not affect the detectors until a similar drive velocity was reached. Also clearly noticeable is that only three wires in the array experience a shielding effect. The three are the resonators directly in front

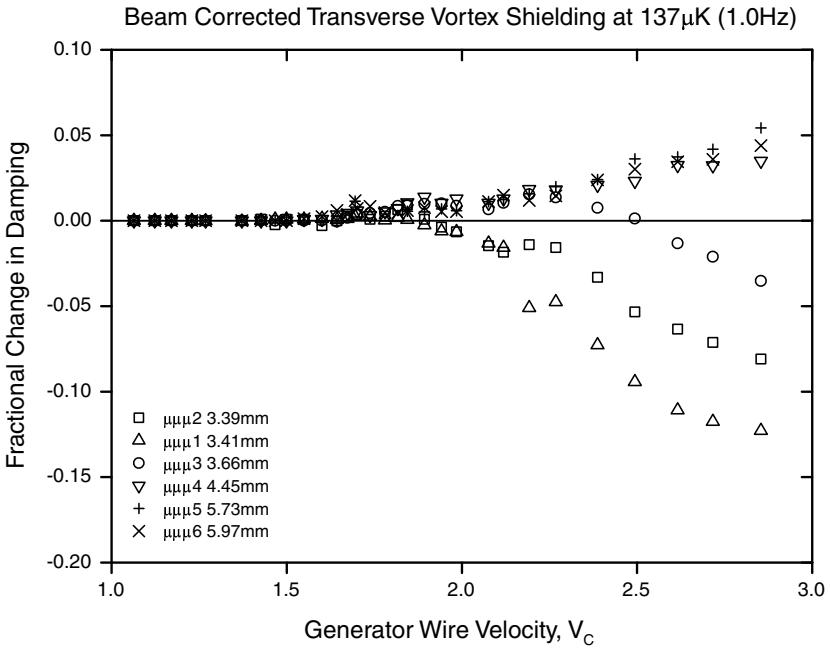

Figure 5.10: The response of the detector wires at 1Hz to transverse vortex production after the quasiparticle beam has been corrected for.

of the source wire. The three resonators set more to the side of the source wire, $\mu\mu\mu 4, 5, 6$, see only a heating effect due to the bulk superfluid being heating during vortex production. From this we can state that the vortex cloud is highly orientated spatially along the direction of the source wire motion. One interesting feature of the results is what happens to the third wire in the array, $\mu\mu\mu 3$. Initially this detector sees a heating effect similar to the outer three wires. At about $2.25V_c$ however the heating experienced decreases and at $2.5V_c$ this detector now shows the shielding effect. This indicates that the source wire needs to be driven at high velocities to cause the region of vorticity to grow sideways.

The superfluid temperature is next raised to $\sim$ 30Hz or 191μK. Unfortunately this time the sixth detector, $\mu\mu\mu 6$, was lost through a software error

and so no results for this detector are available. The detector drives were increased to give a similar signal height to the lower temperature measurements and the source wire was driven through a range of velocities again between $< V_c$ to $\sim 3V_c$. The same quasiparticle beam correction is applied to the correction used with the 1.0Hz data. The results are shown in Fig 5.11. The data appears to show a similar trend to the low temperature data

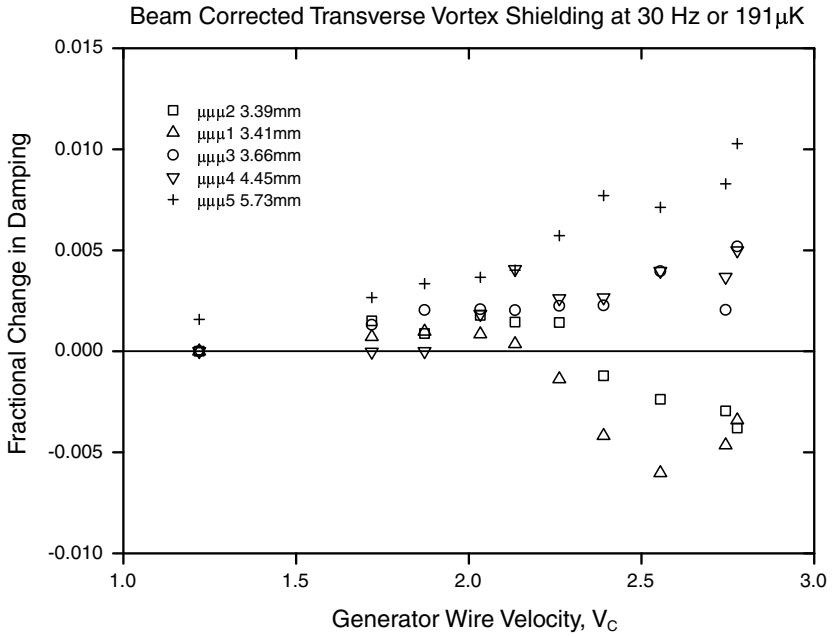

Figure 5.11: The response of the detector wires at 30Hz to transverse vortex production after the quasiparticle beam has been corrected for.

but with a few differences. The first difference is that the detectors see a heating effect much sooner after the critical velocity is reached. The reason for this may be that with the bulk superfluid being warmer the source wire has to be driven at a higher drive current than before so the heat deposited into the superfluid during a pulse is greater. This idea is supported by the observation that the fifth wire in the array sees the heating effect before the

other wires despite it being the furthest away from the source wire. The second difference from the earlier measurements is that the third wire in the array no longer shows any shielding although the heating it detects does drop after the source velocity reaches $\sim 2.6V_c$.

5.3.4 Temperature Dependence of Decay Length

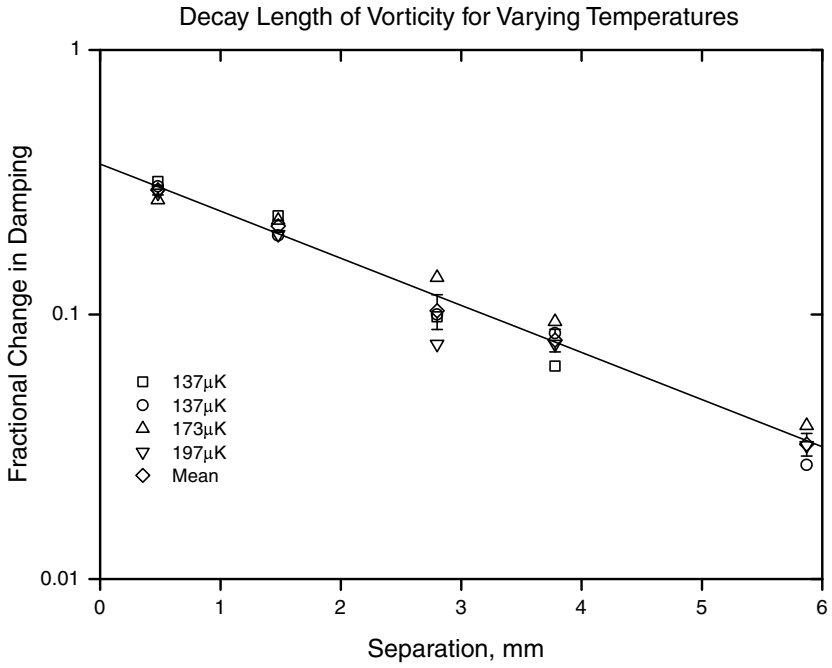

Figure 5.12: The response of the detector wires at various temperatures.

To be able to investigate the effect the bulk superfluid temperature has upon the decay length of the vortex cloud the linear investigations described in section 5.3.2 were repeated at several temperatures between 1.0Hz or 137μK and 39Hz or 197μK. The decay length is measured at a source wire drive velocity of $2.0V_c$ for each temperature by measuring the fractional change in the detector damping at this velocity from the responses of the

detectors. Also the mean average of these results was calculated and added to the plot. The results of this are shown in Fig 5.12.

As can be clearly seen the data at different temperatures are highly consistent with there being no temperature dependence within the temperature range investigated. The line drawn through the mean data assumes simple exponential decay of the change in damping with regards to the separation between detector and source. The error bars added to the mean points are calculated from the standard deviation of the varying temperature data.

5.3.5 The Decay Length

Now that the responses of the detectors have been measured for a variety of cell temperatures it is possible to infer how the vortex line density changes at known values of the generator wire velocity by measuring the fractional change in damping. In figs 5.13(a), 5.13(b), 5.13(c) and 5.13(d) the decay length of the cloud of vortex lines at drive velocities of $1.25V_c$ to $3.0V_c$ are shown.

The uncertainty in the data points are calculated from the standard deviation of the four different temperatures at which the data was measured. By measuring the decay length at various drive velocities between $1.25V_c$ and $3.0V_c$, it can be shown that the decay length is a constant $\sim$ 2.25mm until the drive approaches $2.5V_c$ where the decay length noticeably begins to shorten. The full data for the decay length at various source wire velocities can be seen in Fig 5.14.

This shortening effect is assumed to be due to the increasingly dominant effect of the thermal quasiparticle beam, which is generated when the source

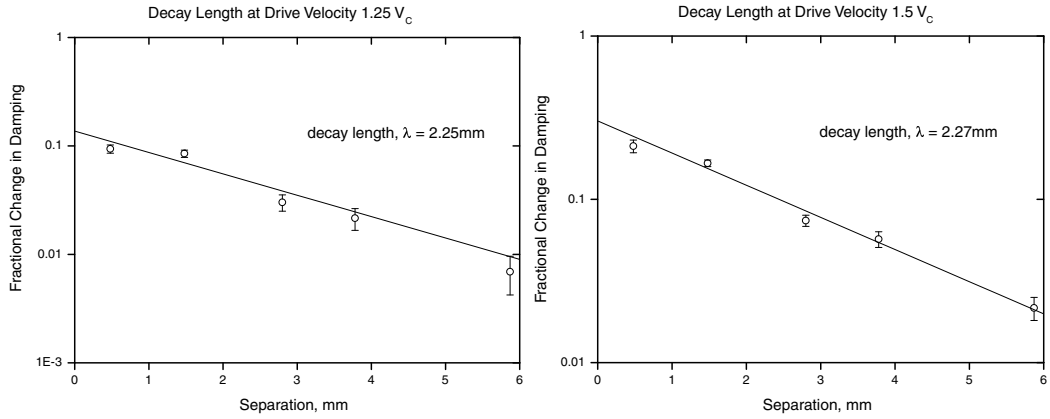

(a) Source wire velocity of $1.25\,\mathrm{V_C}$.

(b) Source wire velocity of $1.5\,\mathrm{V_C}$.

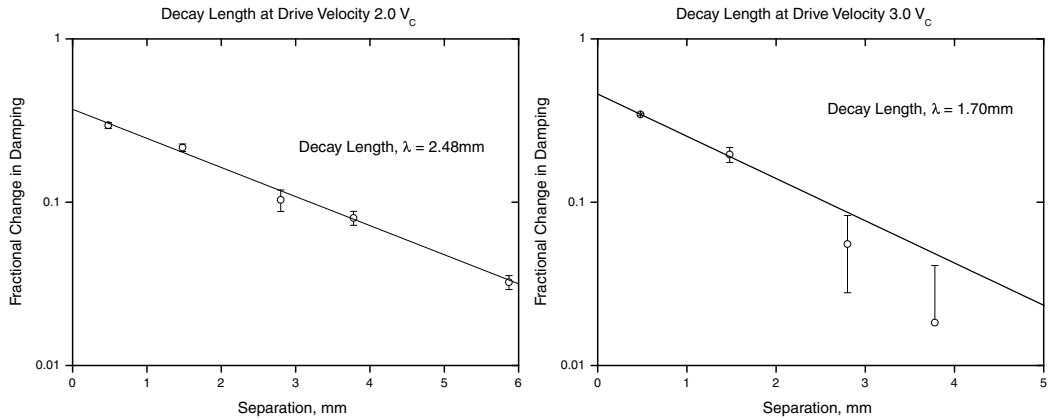

(c) Source wire velocity of $2.0\,\mathrm{V_C}$.

(d) Source wire velocity of $3.0\,\mathrm{V_C}$.

Figure 5.13: Decay lengths of the vortex tangle at varying source wire drive velocities.

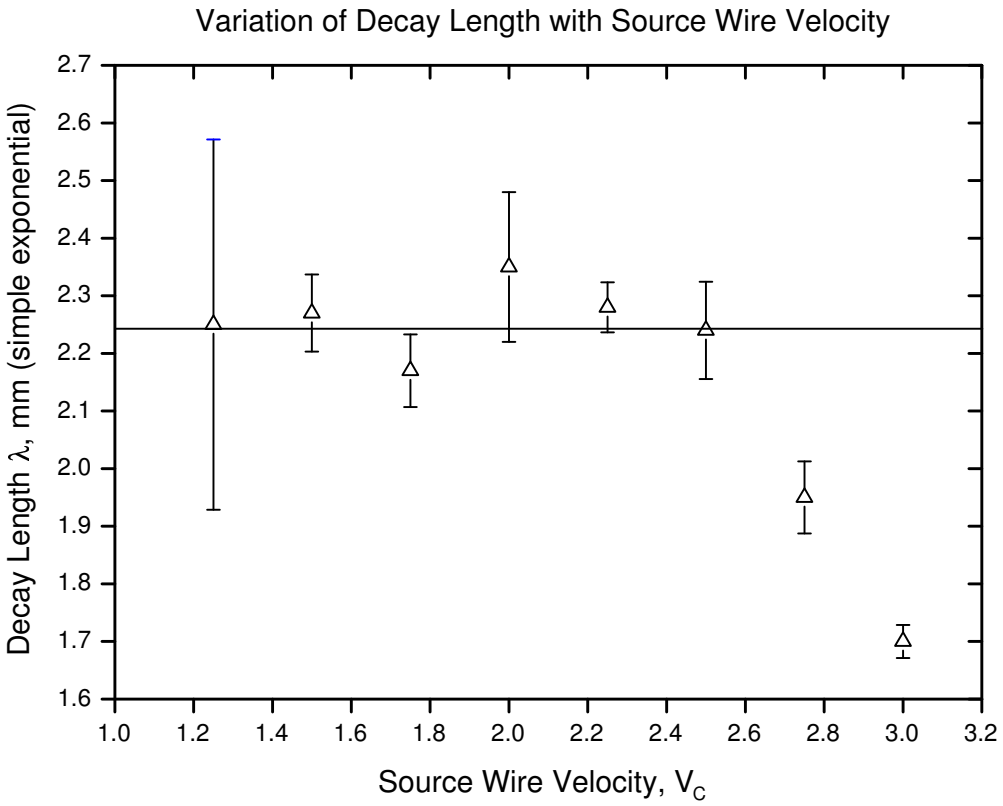

Figure 5.14: The decay length of a non-homogenous region of vorticity assuming simple exponential decay.

wire breaks the superfluid Cooper pairs, increasingly interacting with the vortex lines and increasing their rate of decay. It should be stated clearly however that this decay length should only be considered to be valid for vorticity produced by a vibrating wire resonator and in the orientation of the generating wire motion.

5.4 Conclusions

It has been shown that a vibrating wire resonator driven above its critical velocity will generate a tangle of quantised vortex lines. These vortex lines can be detected by measuring the quasiparticle flux incident upon a secondary vibrating wire resonator in close proximity. By measuring the damping on several detectors placed at different separations it has been possible to observe the development of the tangle at the different separations for a range of source wire drive velocities. Also the shape of the tangle has been investigated in the directions perpendicular to the source wire motion. In these directions the extent of the vorticity has been seen to be greatly diminished in comparison to the vorticity along the axis of wire motion. The reasons for could be that either the vorticity is thrown off the generating wire as it reaches its maximum of displacement or that the quasiparticle beam created along with the vorticity pushes the vortex lines in the direction that this beam is travelling in.

Next by using the fractional change in detector damping, the rate at which the vorticity decays spatially was examined. By measuring this fractional change in the damping a picture of how the vorticity decays spatially was formed. Fitting this data to a simple exponential decay model provided a very good correlation. This experiment was repeated at several temperatures between 137μK and 197μK. The results show that the decay length can be seen to be temperature independent, at least within the temperature range which could be investigated here. The decay length was also shown to be independent of the source wire drive velocity until the velocity reached $\sim 2.5V_c$ where the decay length began to drop rapidly. It is thought that the

violent production of the thermal ballistic quasiparticle beam at this velocity is the contributing factor for this. The decay length for vorticity generated by a vibrating wire resonator in superfluid ^{3}He-B at a temperature between 137μK and 197μK has been measured as 2.2mm.

Chapter 6

Investigating The Vortex Tangle

6.1 Experimental Technique and Theory

The previous chapter has shown a vibrating wire resonator can create a region of vorticity that will shield neighbouring detectors from thermal quasiparticles through Andreev processes. The next experiment shall investigate what happens when the vorticity is used to reflect a beam of quasiparticles emitted by a black body radiator. The simplicity of the premise behind this experiment belies the complicated processes that occur. The black body radiator is heated so that a clearly defined beam of thermal quasiparticles is emitted from an orifice. By placing a vortex generating wire adjacent to the orifice a fraction of the beam of quasiparticles will be retro reflected back into the radiator when there is vorticity in the beam's path. These reflected quasiparticles will then raise the temperature inside the radiator or 'box' and with the black body radiator being well characterised, the power returning into

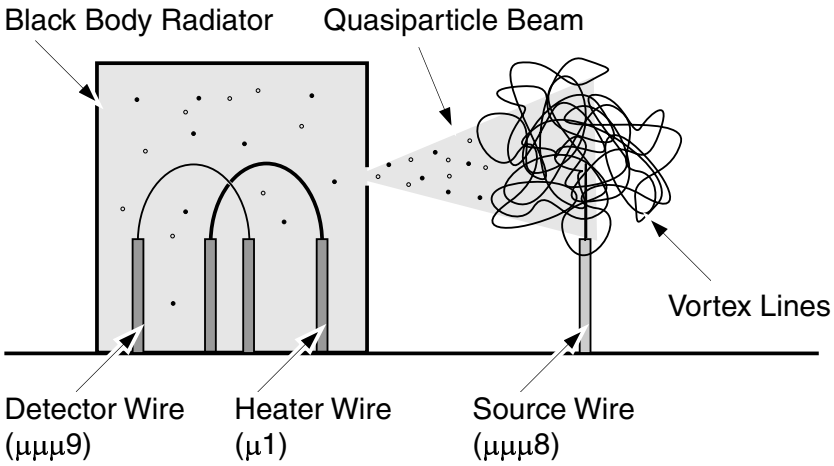

Figure 6.1: Diagram of the Black Body Radiator and generator wire.

the box can be calculated. By analysing the results with a mathematical model the vortex line density created by the source wire can be calculated and shall be investigated for several beam and bulk superfluid temperatures.

This experiment is similar in premise to an experiment conducted by Enrico *et al*[8] where a black body radiator was used to measure the localised flow fields around a moving paddle. To avoid the production of thermal quasiparticles, the paddle velocity was kept below its pair breaking velocity and we now know that this also restricted any production of vortices. The experiment I shall discuss varies in how the flow fields are produced. By using a 4.5μm diameter vibrating wire rather than a paddle, the flow fields directly due to the moving object are far smaller than for a $\sim 500\mu$m wide paddle. This enables the flow fields associated with the wire motion to be negligible in comparison with the fields associated with the vortex tangle.

6.1.1 The Mathematical Model

To create a model of the processes happening during these measurements it is necessary to first set up the equilibrium conditions for a black body radiator with a constant applied power at equilibrium where the only other energy entering the box is due to the reflection of the beam.

It is possible to deduce the temperature from the width Δf_2 of the detector resonator ($\mu\mu\mu\,9$) inside the radiator. A power $\dot{Q}_{applied}$ is applied to the superfluid inside the radiator by a second larger diameter resonator ($\mu\,1$). The response of the box can be measured by calculating the 'width parameter' $W = \Delta f_2 \tilde{E} T$ where T is the temperature, deduced from Δf_2, and $\tilde{E} = \Delta + k_B T$ is the average thermal quasiparticle energy. As was shown in section 4.8 by the 'box calibration', the width parameter of the detector wire inside the radiator is found to be directly proportional to the total power entering the box

$$W = \Delta f_2 \tilde{E} T \propto \dot{Q}_{total}. \tag{6.1}$$

We can now consider what happens before the vorticity is being generated and the system is at equilibrium. At the base temperature before any procedures are done to the black body radiator the only power entering the box is due to the heat leak from the paper and stycast walls. This is denoted by $\dot{Q}_{heatleak}$. This must be matched at equilibrium by the power leaving the box $\dot{Q}_{total}$.

$$\dot{Q}_{total} = \dot{Q}_{heatleak} \tag{6.2}$$

If we wish to produce a quasiparticle beam with a higher quasiparticle energy the temperature inside the box is raised by adding an extra power with the heater resonator, $\mu 1$. This power is shown in Fig 6.2 as $\dot{Q}_{applied}$. Now the

total power leaving the box through the quasiparticle beam is given by

$$\dot{Q}_{total} = \dot{Q}_{heatleak} + \dot{Q}_{applied}. \tag{6.3}$$

Now we have a higher energy quasiparticle beam being produced by the radiator we can begin to look at what happens to the radiator when we switch on the vorticity generating wire adjacent to the aperture.

When the vortex generator wire is switched on there are two new power terms to be considered. The first term is an extra power entering the box due to the pair breaking quasiparticle beam created when a vibrating wire resonator exceeds its critical velocity. This power increases the total power exiting the box by an additional term $\dot{Q}_{generator}$. Along with this extra term there is going to be an effect due to the vorticity created by the resonator retro reflecting back some fraction, f, of the quasiparticle beam being emitted by the box. This term is defined as $f\dot{Q}_{total}$. Putting all the powers into equilibrium we now get

$$\dot{Q}_{total} = \dot{Q}_{heatleak} + \dot{Q}_{applied} + \dot{Q}_{generator} + f\dot{Q}_{total}. \tag{6.4}$$

Rearranging equation 6.4 we can write the expression to give the reflected fraction of the quasiparticle beam f.

$$1 - f = \frac{\dot{Q}_{heatleak} + \dot{Q}_{applied} + \dot{Q}_{generator}}{\dot{Q}_{total}} \tag{6.5}$$

6.1.2 Evaluating the Power Terms

If we now consider the four different states of the black body radiator; at base temperature no source wire velocity, base temperature source wire on, high box temperature no source wire velocity and high box temperature source

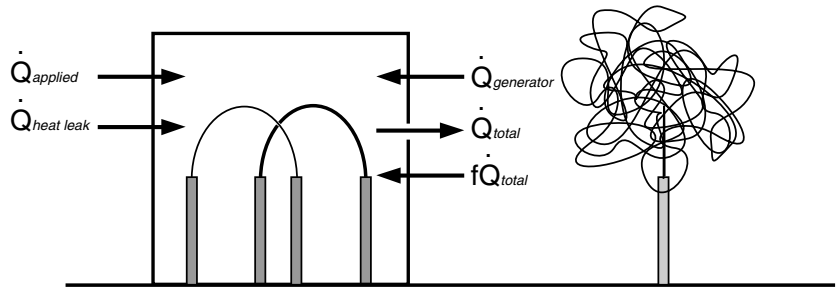

Figure 6.2: Diagram showing powers affecting the black body radiator

wire on, we can use the fact that the black body radiator is sensitive to power changes to evaluate the power inside the box in each of the states. The width parameter of the thermometer wire is written as $W(T, v)$ where T is the box temperature (determined by $\dot{Q}_{applied}$) and v is the generator wire velocity.

The first state is when there is no applied power to the radiator and the source wire is stationary. Under these conditions the width parameter inside the box, $W(0, 0)$ is a given by equation 6.2 and can be written as

$$W(0, 0) = c\ \dot{Q}_{heatleak}. \tag{6.6}$$

The constant c can be calculated from the box calibration shown in section 4.8 but shall be left as c for reasons which shall become apparent later.

The second state we shall now define is when the radiator is above its base temperature but the source wire velocity is still zero. The width parameter inside the box is now written as $W(T, 0)$. By using equation 6.3 the total power in the box at this point can be equated with the width parameter giving

$$W(T, 0) = c\ (\dot{Q}_{heatleak} + \dot{Q}_{applied}) \tag{6.7}$$

where the constant c is the same constant from the box calibration in equation

6.6. Using equations 6.6 and 6.7 the power $\dot{Q}_{applied}$ can be deduced giving

$$\dot{Q}_{applied} = \frac{W(T,0) - W(0,0)}{c}. \tag{6.8}$$

Having defined the ground states for the radiator at the base temperature and a temperature above the base temperature we can now examine what the conditions are inside the radiator when the source wire is driven to create vorticity.

As was defined earlier, when the source wire is driven above its pair breaking critical velocity the resonator will create a pair breaking quasiparticle beam. This beam will deposit a power $\dot{Q}_{generator}$ into the radiator. This gives the width parameter $W(0,v) \propto \dot{Q}_{generator} + \dot{Q}_{heatleak}$. There is however one problem with this simple relationship since it assumes that there is no reflection of the weak quasiparticle beam from the radiator by the vorticity generated. If we examine equation 6.5 it can be clearly shown that

$$W(0,v) = c\ \frac{\dot{Q}_{generator} + \dot{Q}_{heatleak}}{1-f}. \tag{6.9}$$

The final state of the radiator is when there is an applied power into the box causing a raised temperature and the source wire is driven to create vorticity. If we examine equation 6.9 we can see that only an extra term needs to be added to take into account the added power into the box from $\dot{Q}_{applied}$. This gives us this equation,

$$W(T,v) = c\ \frac{\dot{Q}_{generator} + \dot{Q}_{heatleak} + \dot{Q}_{applied}}{1-f} \tag{6.10}$$

where f is assumed to be independent of the beam temperature T and is the same in equations 6.9 and 6.10.

So far we have assumed that the applied power $\dot{Q}_{applied}$ is constant during the experiment. This is found not to be true since when there is an increase

in power and hence temperature inside the resonator the signal voltage, V_x, of the heater wire $\mu 1$ drops. This can be corrected for by measuring V_x when the source wire is being driven, the 'on' state V_{on}, and when it is not, the 'off' state V_{off}. Since the power applied is directly proportional to V_x we can show that

$$\dot{Q}''_{applied} = \frac{V_{on}}{V_{off}} \ \dot{Q}_{applied}. \tag{6.11}$$

This new corrected term for the applied power can now be substituted back into equation 6.10 and by substituting equations 6.6, 6.7 and 6.9 the fraction f is shown to be

$$(1-f) = \frac{V_{on}}{V_{off}} \frac{W(T,0) - W(0,0)}{W(T,v) - W(0,v)}. \tag{6.12}$$

It should be mentioned here that the constant c from the box calibration has been cancelled from the equation. This is why the constant did not need to be evaluated earlier and makes the analysis easier.

6.1.3 Dependance of Bulk Superfluid Temperature

So far we have looked at the physics where there is a negligible quasiparticle density in the bulk superfluid outside of the black body radiator. To increase the density a power is applied into the bulk superfluid to raise the temperature. Resonator $\mu\mu\mu 7$ is used for this since it is orientated perpendicular to the box and generator wire so all the power deposited by this wire will be thermalised. The power entering the radiator from the raised bulk temperature is $\dot{Q}_{bulkbeam}$. Using a similar notation for the width parameter of the thermometer wire inside the radiator we can define the same four states as before but with each state at a raised bulk superfluid temperature. The

width parameter in these states is written as $W(T, \dot{Q}, v)$ where T is the temperature of the Box, $\dot{Q}$ is the applied heat to the bulk superfluid thus raising the cell base temperature and v is the generator wire velocity.

The first state where the radiator is not heated and the generator wire is stationary is defined as

$$W(0, \dot{Q}, 0) = c(\dot{Q}_{heatleak} + \dot{Q}_{bulk\ beam}). \tag{6.13}$$

Similarly when the radiator is heated with $\dot{Q}_{applied}$ and the generator wire is stationary,

$$W(T, \dot{Q}, 0) = c(\dot{Q}_{heatleak} + \dot{Q}_{applied} + \dot{Q}_{bulk\ beam}). \tag{6.14}$$

Now we shall look at what the equilibrium conditions are when the generator wire is moving. The first state is when the radiator is not heated but the bulk superfluid is

$$W(0, \dot{Q}, v) = c(\dot{Q}_{heatleak} + \dot{Q}_{bulk\ beam} + \dot{Q}_{generator} + f(\dot{Q}_{total})) \tag{6.15}$$

and for when both the bulk superfluid and the radiator are heated

$$(1 - f)W(T, \dot{Q}, v) = c(\dot{Q}_{heatleak} + \dot{Q}''_{applied} + \dot{Q}_{bulk\ beam} + \dot{Q}_{generator}). \tag{6.16}$$

where $\dot{Q}''_{applied}$ is corrected for the changes in the heater wire signal voltage as in equation 6.11.

Assuming $\dot{Q}''_{applied}$ and $\dot{Q}_{generator}$ are independent of f and considering equation 6.9 we can say:

$$(1 - f)[W(T, \dot{Q}, v) - W(0, 0, v)] = c(\dot{Q}''_{applied} + \dot{Q}_{bulk\ beam}) \tag{6.17}$$

and

$$W(T, \dot{Q}, 0) - W(0, \dot{Q}, 0) = c(\dot{Q}_{bulk\ beam}). \tag{6.18}$$

Now taking into account effect of heating inside box affecting $\dot{Q}_{applied}$ we can define $\dot{Q}''_{applied}$ as being:

$$\dot{Q}''_{applied} = R''\ \dot{Q}_{applied} = R'' c[W(0,\dot{Q},0) - W(0,0,0)] \tag{6.19}$$

where $R'' = \frac{V_{on}}{V_{off}}$ with criteria as before in equation 6.11. Putting everything into equilibrium equation as before gives:

$$(1-f) = R'' \frac{c[W(T,\dot{Q},0) - W(0,\dot{Q},0)]}{c[W(T,\dot{Q},v) - W(0,\dot{Q},v)]} \tag{6.20}$$

and rearranging results in:

$$f = 1 - R'' \frac{W(T,\dot{Q},0) - W(0,\dot{Q},0)}{W(T,\dot{Q},v) - W(0,\dot{Q},v)} \tag{6.21}$$

which is the equation used to calculate f.

6.2 The Experiment

The experiment consist of a black body radiator containing one 13.5 μm resonator for heating the radiator and one 4.5 μm diameter resonator for thermometry. An aperture of diameter 0.33mm is located in the centre of one side of the radiator to allow the production of a highly thermalised quasiparticle beam. Outside the radiator and adjacent to the aperture is a standard 4.5 μm diameter vibrating wire resonator. The resonator outside the radiator will be used to produce a localised inhomogeneous region of quantised vortex lines. A schematic of this setup is displayed in Fig 6.3.

6.2.1 Varying the Beam Temperature

The experiment consists of two parts. For the first part the cell temperature and hence the bulk superfluid temperature will be kept at or very close to

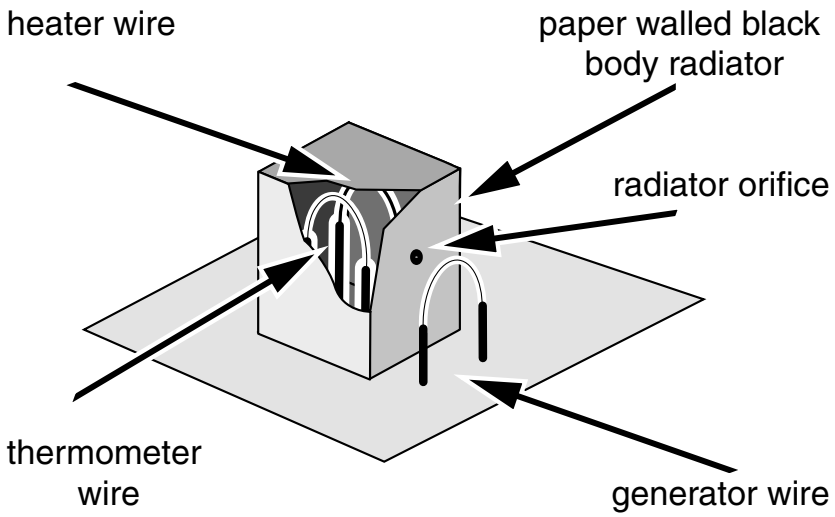

Figure 6.3: Schematic diagram of the Black Body Radiator used for probing a tangle of vortex lines.

the cell base temperature of $\sim$ 110μK. With the bulk superfluid this cold there will be a minimum thermal quasiparticle density. A highly ballistic thermal quasiparticle beam will then be generated by the black body radiator and creating vorticity outside the aperture will cause some fraction f of the emitted quasiparticles to be retro reflected back into the radiator through Andreev processes. These returning quasiparticles will cause an increase of the temperature inside the radiator and from this increase in the temperature the reflected fraction f can be calculated.

Similarly to section 6.1.2 there are four different states in which data needs to be collected. The first states that are investigated are for when there is no applied heat into the radiator. This enables the evaluating of the effect that the generated quasiparticle beam from the source wire will have. To perform this investigation the temperature inside the radiator is logged by measuring the in-phase signal height V_x of the thermometer resonator. This is done

at a resolution of 10 points per second with the National Instruments DAQ card that was also used in section 5.2. Additionally, the source wire in-phase and quadrature voltages are also logged through the DAQ card. Finally a resonator from the array used for the vortex extent experiments will be used to measure the cell bulk temperature. Although the bulk temperature will stay at or very close to its base temperature this information is collected for completeness and in case anything unexpected occurs.

As was described in section 5.2 before any data can be taken with the resonators their parameters need to be measured. All of the resonators to be used, $\mu\mu\mu 8$, $\mu\mu\mu 9$ and $\mu\mu\mu 7$, are frequency swept to calculate their $H \times W/D$ constants. The resonators are then amplitude swept to measure their pair breaking critical velocities. Before the data taking commences though there is a new step which must be performed. The reason for this box calibration is to ensure that the relationship between the width parameter inside the box and power entering the box is linear. A box calibration is not performed for each demagnetisation as the calibration does not change. Fig 4.7 shows the box calibration for three different demagnetisations over a period of $\sim$ 24 months. The full details behind a box calibration can be found in section 4.8.

Now that the resonators are fully characterised and ready, the data can be collected. The thermometer inside the radiator is operated at a signal voltage approximately 10% its critical velocity. Once again this is to ensure that the resonator is operating well within its linear limit. With the radiator at its base temperature a series of pulses are performed with the source wire. The range of velocities used is between $0.5V_c$ and $3.0V_c$ where V_c is the source wire

pair breaking critical velocity. Typically around 40 to 50 pulses are conducted with each pulse lasting around 50 seconds. This allows the radiator to attain an equilibrium. When a pulse is removed the radiator is left to recover for around 100 seconds. This enables the effect of the generated quasiparticle beam from the source wire to be measured.

Once this data is collected the temperature inside the radiator is increased by applying a power with the heater resonator inside the radiator, $\mu 1$. This heater wire is kept on resonance and driven above its pair breaking critical velocity. The effects of any vorticity created by the heater wire will not be considered since the vorticity is assumed to decay quickly within the radiator. The increase in the temperature inside the box increases the intensity of the thermal quasiparticle beam emitted. The driving current of the thermometer wire will need to be increased at this point back to $\sim$ 10% of its critical velocity since the increased temperature inside the radiator will reduce its signal voltage.

The source wire is now used to create vorticity by driving the wire at various velocities again between $0.5V_c$ and $3.0V_c$. The thermometer wire inside the radiator measures the increase in power inside the box and from this the fraction of the quasiparticle beam reflected back into the radiator is calculated. This is repeated for several radiator temperatures and hence beam temperatures.

6.2.2 Varying the Bulk Superfluid Temperature

The second part of the experiment to similar to the first part. The difference is that to investigate the effect that the bulk superfluid temperature has on

the production of the vorticity, power is added to the bulk superfluid with a resonator from the vortex extent arrangement. The resonator elected to do this is $\mu\mu\mu 7$. The reason for choosing this resonator is that the quasiparticle beam it creates for heating is orientated perpendicular to all the other resonators in the cell. This will enable the quasiparticle beam to thermalise with the cell walls without affecting directly any other resonators used. This extra heat added to the superfluid will enable the 'base' temperature to be raised.

The experiment is conducted as before with the same resonators used with the addition of the heater resonator. The signal height V_x of the heater is logged via the DAQ card along with the other resonators. The base temperature of the cell is raised with the heater in the bulk and with no applied heat into the radiator. Due to the heat leak from the radiator walls and the quasiparticle flux from the bulk superfluid the temperature inside the radiator will increase to a temperature just above the temperature of the bulk.

The generator wire is now driven for a multitude of pulses at varying drive velocities similar to the range used before. Once these are collected the radiator is heated with the heat wire $\mu 1$ so that there is a significant increase inside the radiator but the bulk superfluid temperature does not change. The wire drives are increased inside the radiator to compensate for the increased quasiparticle flux. The source wire is again used to create pulses of vorticity within the usual range of velocities. Because of this each temperature requires two exclusive sets of measurements unlike the one exclusive and one shared measurements of the first part. The experiment also took three separate

demagnetisations, 14 to 16, to collect all the data which will be presented here.

6.3 Results

The data collected from the DAQ program is read into the Microcal Origin program. The corrections for zero field cross talk and deviation from the resonant frequency are applied identically to those described in section 5.3. The signal voltages for the thermometer resonator are converted into a damping width, Δf_2, with equation 5.5. Next, this width is converted into a 'width parameter', $\Delta f_2 T\tilde{E}$, which is directly proportional to the power in the black body radiator as shown in equation 4.32. The width parameter of the thermometer resonator is calculated for each of the four states available in each part of the experiment. These parameters are then used to calculate the reflected fraction of the emitted quasiparticle beam from the black body radiator that is retro reflected by Andreev processes and returns power back into the radiator.

The equations used to calculate the fractions are

$$f = 1 - \frac{V_{on}}{V_{off}} \frac{W(T,0) - W(0,0)}{W(T,v) - W(0,v)} \tag{6.22}$$

for the constant bulk superfluid temperature measurements

$$f = 1 - \frac{V_{on}}{V_{off}} \frac{W(T,\dot{Q},0) - W(0,\dot{Q},0)}{W(T,\dot{Q},v) - W(0,\dot{Q},v)} \tag{6.23}$$

for the varying bulk superfluid temperature measurements. The heater wire signal voltages are measured before and during each pulse.

6.3.1 Constant Bulk Superfluid Temperature

The first width parameters to be calculated are the $W(0,0)$ and $W(0,v)$ parameters. This base parameter is found to change slightly for each demagnetisation due to small changes in the actual measured base temperature of

the radiator. The parameter $W(0,0)$ is the initial width parameter inside the box before the source wire outside the box or the heater wire inside the box are operated. This parameter gives us a measure of what the heat leak is into the radiator from the paper walls of the radiator and is assumed to be constant during the demagnetisation. This heat leak is due to the fact that the paper walls of the radiator do not cool during the demagnetisation process and so are at a higher temperature than the bulk superfluid.

The next parameter $W(0,v)$ is measured for a range of source wire velocities between $< 0.5V_c$ and $3V_c$ where V_c is the generator source wire velocity. This is measured by calculating the difference between the width parameter before the pulse and the width parameter after. The results of this for each demagnetisation are shown in figure 6.4(a).

If we examine the results we can see that that for each demagnetisation the base width parameter of the radiator is slightly different. This is due to having a different heat leak from the paper walls. This need not to be a great concern as long as the base effect is measured for each demagnetisation and used respectively. What can be seen clearly however that the source wire velocity has no effect on the radiator until the velocity exceeds the pair breaking critical velocity. This is to be expected as there are no quasiparticles or vortices created until this occurs. The width parameter then increases with source wire velocity until around $1.2V_c$. At this velocity the increase slows and becomes roughly linear with V_c until $2.0V_c$. At this velocity there can be seen another change in the rate of increase which is particularly visible for demagnetisations 15 and 16 which had a slightly lower base temperature than demagnetisation 14. This may be due to the decay length of the vor-

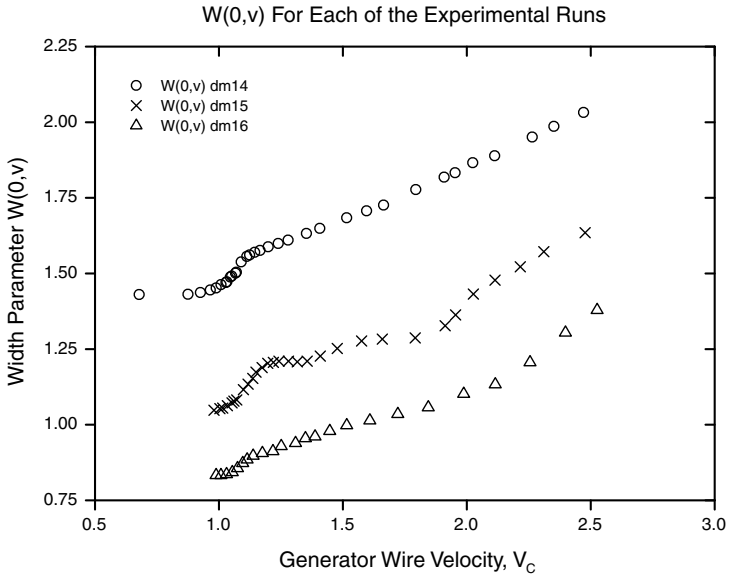

(a) The width parameter $W(0, v)$.

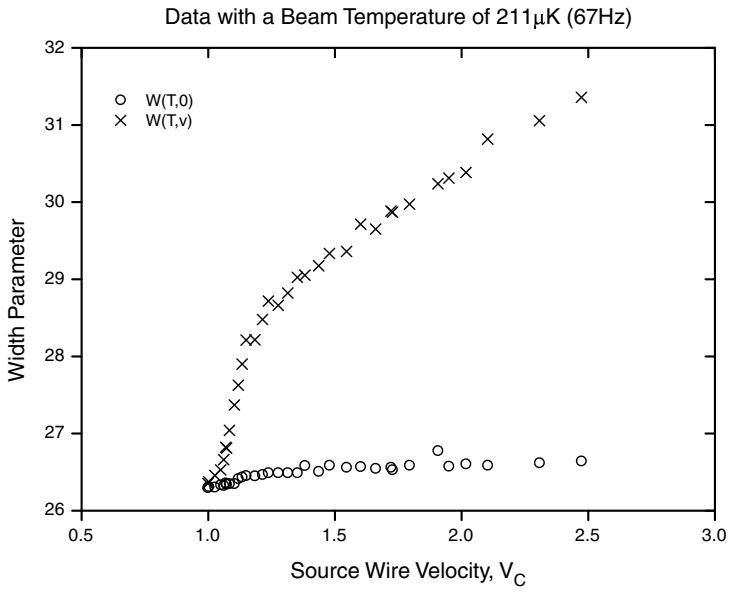

(b) The width parameters $W(T, 0)$ and $W(T, v)$ measured at a temperature of 211μK.

Figure 6.4: Example width parameters for beam temperature experiments.

ticity around the source wire shortening and allowing a higher intensity of generated quasiparticles to reach the radiator. Fortunately the way in which the model was created can take into account these features when calculating f.

The radiator is now heated to various temperatures ranging between 177μK (15Hz) and 275μK (150Hz) with the heater wire inside the radiator. The source wire is again used to create vorticity for short pulses at various drive velocities within the range used for the $W(0, v)$ measurements. The results from this will allow the calculation of $W(T, 0)$ and $W(T, v)$ where $W(T, 0)$ is the width parameter of the thermometer wire inside the radiator before the vorticity is 'switched on' and $W(T, v)$ is the width parameter during the pulse. The results for $W(T, 0)$ and $W(T, v)$ for a beam temperature of 67Hz or 211μK are shown in Fig 6.4(b). Again the results show some features that we have come to expect. There is no effect on the width parameter until the source wire velocity exceeds its critical velocity. There is then a rapid increase in the width parameter until a source wire velocity of $\sim 1.2V_c$. Here the rate of increase of the width parameter reduces. After this velocity the width parameter $W(T, v)$ can be seen to change proportionally with the source wire velocity. This would indicate that the effect of the generated quasiparticle beam and the reflection from the vorticity is proportional to the source wire velocity.

Using these results we can now calculate what the reflected fraction of thermal quasiparticles from the beam is for each different beam temperature using equation 6.22. The reflected fraction results can be seen to follow the shape of the results for $W(T, v)$. There is a sudden onset of reflection as

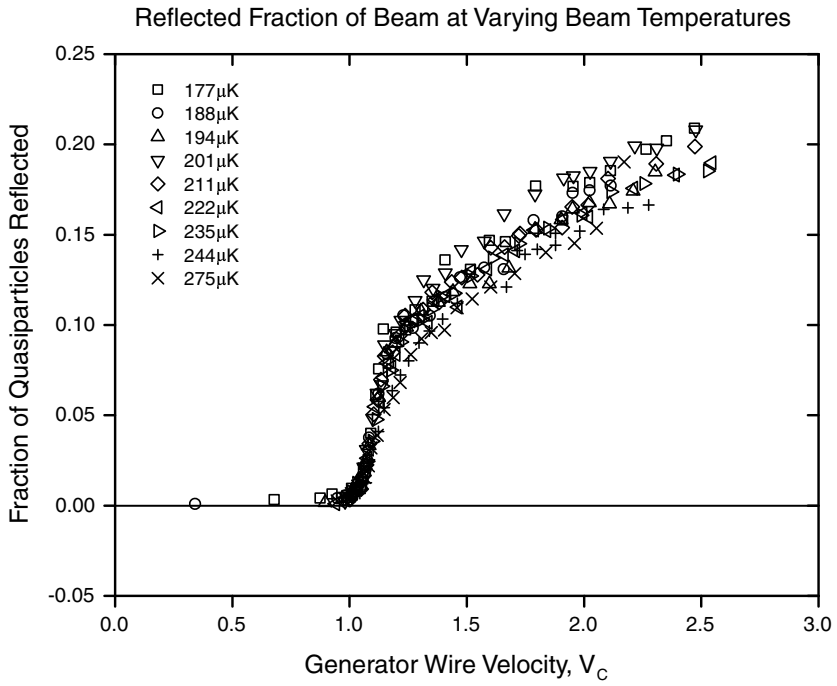

Figure 6.5: The raw reflected fraction of quasiparticles for different beam temperatures.

the source wire velocity exceeds the critical velocity. This reflected fraction increases rapidly to around 10% at $\sim 1.2V_c$. Above this velocity the rate of increase appears to be linear with the source wire velocity. What is interesting is that there is no observable difference in the results for the different temperatures.

6.3.2 Varying Bulk Superfluid Temperature

As we can see from equation 6.23 to calculate the fraction of reflected quasiparticles we need to measure the four different width parameters of the thermometer wire inside the radiator. The first two parameters to be measured, $W(0, \dot{Q}, 0)$ and $W(0, \dot{Q}, v)$, are measured in the same way as for the varying

beam temperature measurements with no applied power directly into the radiator. There is, however this time, an applied power into the bulk superfluid which will cause a power into the radiator from the bulk superfluid through the aperture. Once the bulk superfluid has reached the required temperature and is at equilibrium with the radiator the width parameters are measured with for a source wire velocity within the range of $0.5V_c$ to $3V_c$. The results are shown in Fig 6.6(a) for a bulk superfluid temperature of 171μK.

The results show the expected onset of an effect detected by the radiator at $1.0V_c$ and the rapid increase in width parameter $W(0, \dot{Q}, v)$ up to a velocity of $1.2V_c$. Above this velocity the width parameter increases at a slower rate with generator wire velocity. The width parameter $W(0, \dot{Q}, v)$ remains at a near constant level through the entire range of velocities but shows a slight increase with velocity attributed to the radiator experiencing some collateral heating from the pulses. These results shown in Fig 6.6(b) show the onset of an effect at $1.0V_c$ and the change in rate of increase at $1.2V_c$ for width parameter $W(T, \dot{Q}, v)$. The width parameter $W(T, \dot{Q}, 0)$ remains at a near constant level with a small increase with generator wire velocity due to collateral heating.

The final measurement before f is calculated is the ratio of the signal voltages of the heater wire inside the radiator before and during a generator pulse, R''. This ratio factor allows the correction of the power applied to the radiator. It is clear to see in Fig 6.7 that the heater wire is unaffected until the generator wire begins to pair break. Once this velocity is exceeded the heater wire velocity is reduced during a pulse. At higher source wire drive velocities the heater wire velocity drops by a greater amount showing

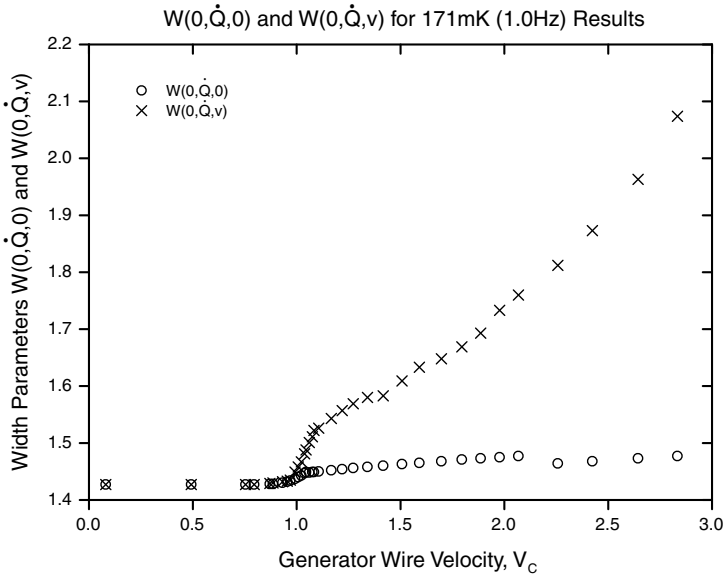

(a) The width parameters $W(0, \dot{Q}, 0)$ and $W(0, \dot{Q}, v)$.

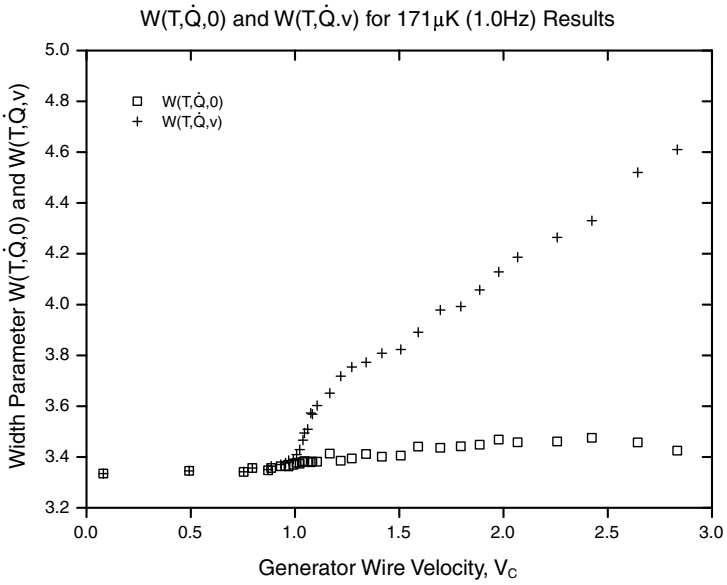

(b) The width parameters $W(T, \dot{Q}, 0)$ and $W(T, \dot{Q}, v)$.

Figure 6.6: Width Parameters for varying bulk temperature of 171μK

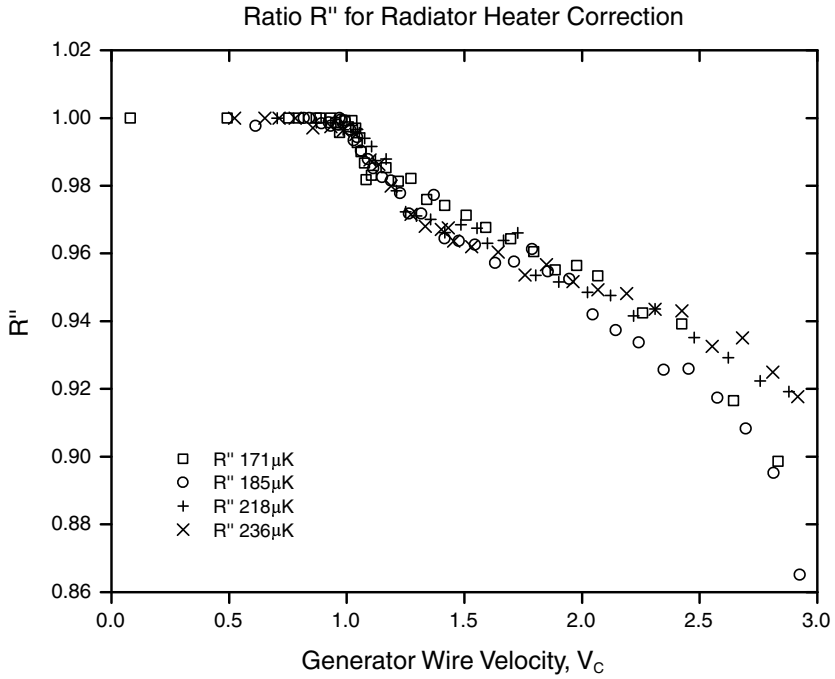

Figure 6.7: The ratio factor R'' for all the bulk superfluid temperatures measured.

an increased heating inside the radiator. It is interesting to see however that the ratio of the heater wire signals is independent of the base temperature inside the radiator.

Now all the results have been analysed the reflected fraction of the quasiparticle beam can be calculated. The fraction is calculated using equation 6.23 with b enumerated by the decay length of vorticity created by a resonator. The results for the reflected fraction f for varying bulk superfluid temperatures shown in Fig 6.8 displays some clear similarities and differences to the results shown in Fig 6.5 for the varying quasiparticle beam temperatures. The obvious similarities are that there is no reflection until the generator wire reaches its critical velocity. Then there is the similar rapid increase

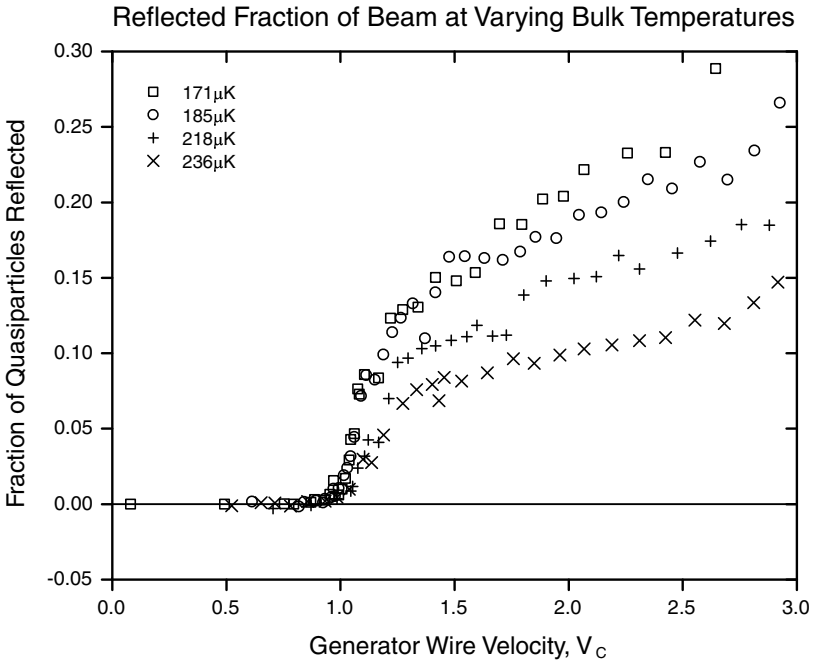

Figure 6.8: The raw reflected fraction of quasiparticles for various bulk superfluid temperatures.

until a velocity of $\sim 1.2V_c$ where upon the rise in reflection slows to a rate proportional to the generator wire velocity. The differences however are even more striking. Where for the different beam temperatures the results showed no variation with temperature the results for the different bulk temperatures are clearly affected by the temperature. At a velocity of $2.0V_c$ the reflected fraction for the lowest temperature of 171μK is 0.21 whereas for the hottest temperature of 236μK the fraction is merely 0.10, a clear indication of the temperature dependence where, as the temperature increases the fraction of the incident quasiparticles being reflected reduces.

6.4 Calculation of L_0, The Vortex Line Density

Here I shall discuss how the model to calculate the vortex line density, L_0 was calculated. The model developed is currently highly simplified and shall need to be refined by later work.

First we define the vortex line density as the total length of vortex line, in metres, per unit volume, in cubic metres. Hence L_0 has units of m^{-2}. Consider a volume filled completely with vortex lines which has a cross sectional area of unit cross section and an effective depth b, where b is given by the decay length of the region of vortex lines. This gives the total length of vortex line inside the volume of $l = L_0 b$. To simplify the model, the vortex lines within this volume are considered be cylinders of radius r. Examining the projection of the vortex lines onto the plane of the cross sectional area gives a surface area of

$$\sigma = 2rl = 2rbL_0 \tag{6.24}$$

assuming $\sigma \ll 1$. A quasiparticle is assumed to be scattered if it gets to within r of a vortex line core and hence equation 6.24 now gives us the probability of a quasi-particle getting to within r of a core. The velocity of the flow around the vortex core is given by

$$v = \frac{\hbar}{2m_3 r} \tag{6.25}$$

and it can be shown that a quasiparticle is scattered if its energy, ϵ, is less or equal to the Fermi energy $p_F v$.

$$\epsilon \leq p_F v. \tag{6.26}$$

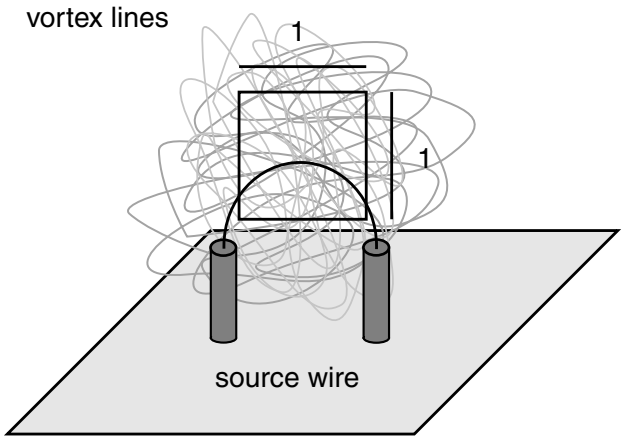

Figure 6.9: Defined box used to define vortex line density.

If we substitute equation 6.25 into equation 6.26 we get

$$\epsilon \leq \frac{p_F \hbar}{2m_3 r}. \tag{6.27}$$

Rearranging this equation in terms of the flow radius,

$$r \leq \frac{p_F \hbar}{2m_3 \epsilon}. \tag{6.28}$$

The mean quasiparticle energy $< \epsilon > \sim k_B T$ where k_B is the Boltzmann constant and T is the temperature. Therefore scattering can be said to occur if

$$r \leq \frac{p_F \hbar}{2m_3 k_B T}. \tag{6.29}$$

Combining equation 6.24 with equation 6.29 results in

$$f \simeq a \frac{p_F \hbar}{2m_3 k_B T} b L_0 \tag{6.30}$$

where a is an added geometric factor. This geometric factor added in equation 6.30, a is inserted to account for approaches by the quasiparticles from different angles. If we consider that a vortex line is tilted by and angle θ it

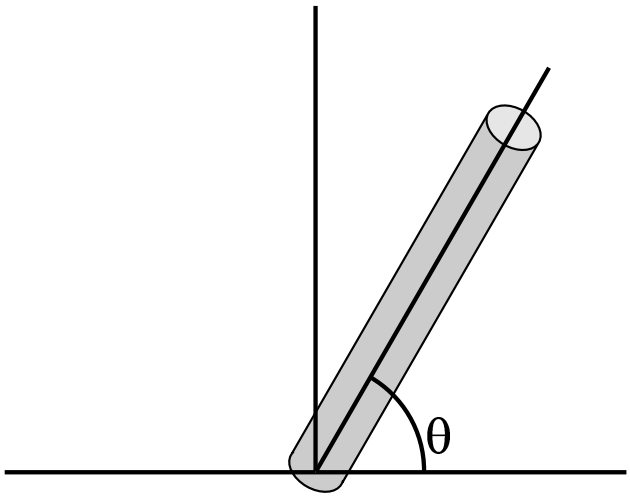

Figure 6.10: The geometric factor.

can be shown that the vector $\underline{p} \cdot \underline{v}$ will undergo a transformation to a scalar quantity

$$\underline{p} \cdot \underline{v} \rightarrow pv \sin\theta. \tag{6.31}$$

If we now substitute this into equation 6.30 this replaces the geometric factor with an integral $\int_0^{2\pi} \sin^3\theta \, \mathrm{d}\theta$ where θ is the angle at which the vortex line is orientated in cartesian coordinates.

$$f = \frac{p_F \hbar}{2m_3 k_B T} b L_0 \int_0^{2\pi} \sin^3\theta \, \mathrm{d}\theta \tag{6.32}$$

The term $\sin^3\theta$ is because the vortex line can by rotated in three dimensions. Solving this integral gives

$$f = \frac{2}{3} \frac{p_F \hbar b L_0}{2m_3 k_B T}. \tag{6.33}$$

We now have a mathematical model to link the reflected fraction of incident quasiparticles upon a region of vortex lines with the line density of the region of vorticity. This equation will be used to build a picture of how the vortex

line density created by a vibrating wire resonator is affected by changes in the incident quasiparticle energy and bulk superfluid temperature.

6.4.1 L_0 for Varying Quasiparticle Beam Temperatures

The reflected fraction of quasiparticles calculated in section 6.3.1 can now be converted into a vortex line density by using equation 6.33 where the term b is the decay length for an inhomogeneous tangle of vortex lines produced by a supercritical vibrating wire resonator, calculated in chapter 5.

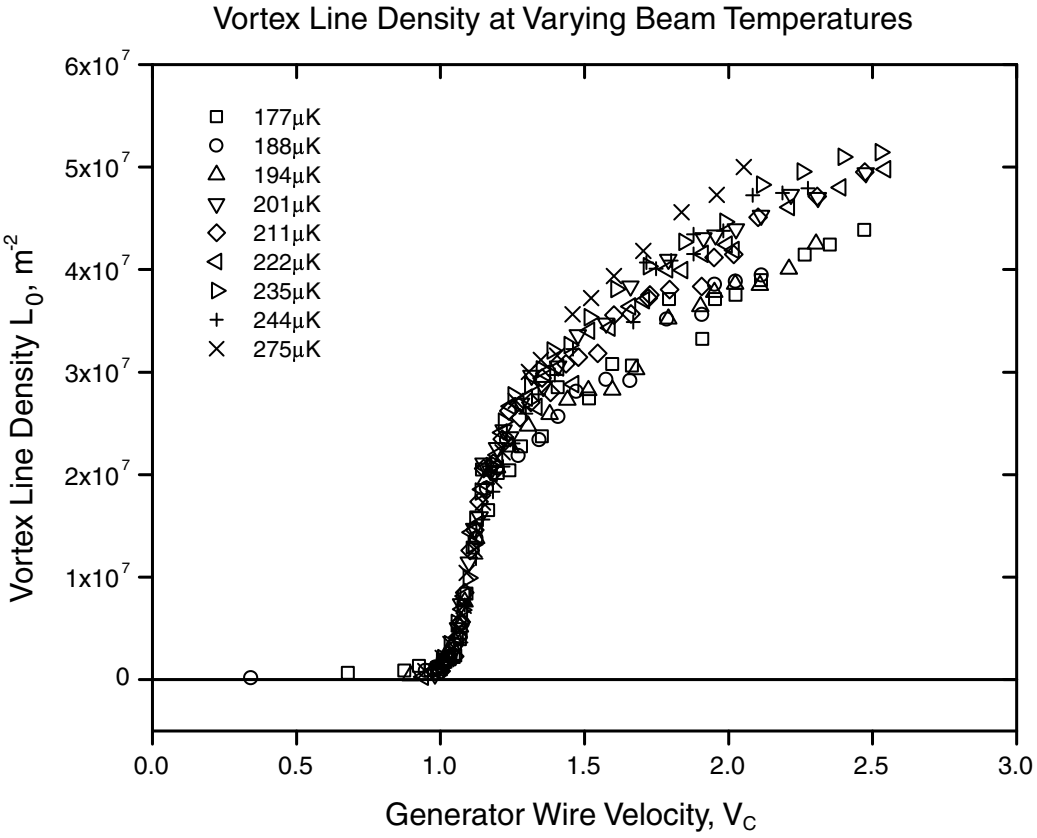

Figure 6.11: The calculated vortex line density for various quasiparticle beam temperatures.

Figure 6.11 shows the calculated vortex line density for the different probe quasiparticle beam temperatures. The vortex lines are seen to be created when the source wire velocity reaches its critical velocity. The vortex line density then rapidly increases until $\sim 1.2V_c$. This is in good agreement with the fraction of quasiparticles reflected shown in Fig 6.5. Above $1.2V_c$ the line density then increases at a slower rate. The scatter in the results indicates a small temperature dependence that was not shown by the reflected fraction. This is assumed to a consequence of our simplified mathematical model since the vortex line density should not be affected by the quasiparticle beam temperature, unless the beam is depositing enough energy into the vortex lines to accelerate decay or inhibit their production. This is not presumed to be the case though. At a source wire velocity of $2.0V_c$, the lowest beam temperature of 177μK measures a vortex line density of $3.8 \times 10^7\,\mathrm{m}^{-2}$ and the hottest beam temperature of 275μK measures a vortex line density of $4.9 \times 10^7\,\mathrm{m}^{-2}$ an increase of 34% for a temperature increase of 55%.

6.4.2 L_0 for Varying Bulk Superfluid Temperatures

Now using equation 6.33 the fraction of quasiparticles reflected measured in section 6.3.2 are converted into a measure of the vortex line density L_0.

Calculating the line density from the reflected fraction shows an interesting feature. Whereas with the reflected fraction there was a clear dependence on the bulk superfluid temperature, the line density dependence on temperature is not so well defined. For the two lowest temperatures 171μK and 185μK, the results show no clear dependence. The second highest temperature 218μK can be seen to have a slightly reduced vortex line density and the

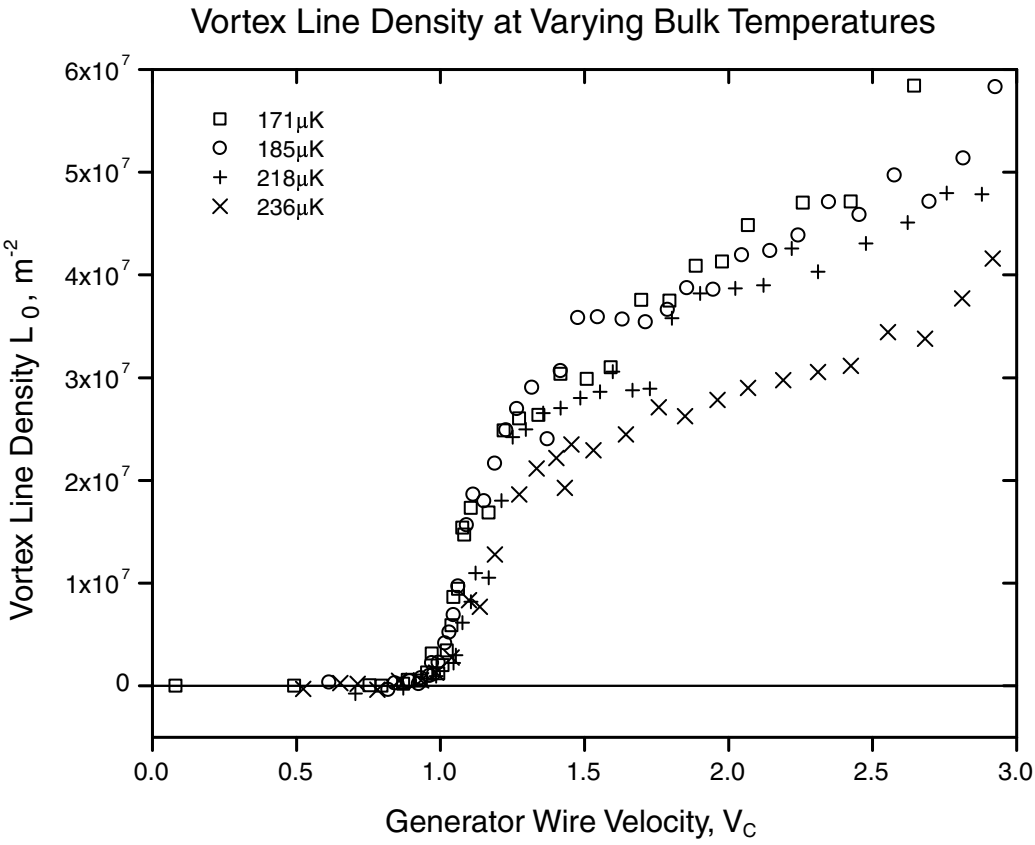

Figure 6.12: The calculated vortex line density for various bulk superfluid temperatures.

highest temperature 236μK is clearly affected. This would appear to show that when factoring in the quasiparticle beam the dependency on the bulk superfluid temperature is reduced but still noticeable. The results also show a high level of scatter especially for the higher temperature results.

6.5 Conclusions

The effect of varying the temperature of an incident quasiparticle beam on a localised vortex tangle has been measured. Initially the fraction of the quasiparticle beam that is retro reflected back into a black body radiator by Andreev processes was measured. The results for this showed no dependence on the temperature of the quasiparticle beam. Converting this fraction into a vortex line density with a simple mathematical model provided an interesting result. Even though the reflected fraction was shown to be beam temperature independent the model containing a term for the quasiparticle energy and hence temperature introduced a temperature dependence.

The second part of this experiment investigated the effect that altering the bulk superfluid temperature would have on the reflected fraction and hence vortex line density. Calculating the reflected fraction of the incident quasiparticles with the results for this showed that the reflected fraction appears to be bulk superfluid temperature dependent. The results clearly show the fraction of the quasiparticles being reflected reducing as the temperature of the superfluid is increased. The hypothesis that perhaps the mean free path is reduced at these higher temperatures is shown to be untrue since even at the hottest temperature investigated of 236μK the mean free path of a quasiparticle is $\sim$ 10mm. The hotter vortex lines must therefore be either less effective at reflecting quasiparticles or lesser in number. Again using the simple mathematical model to calculate the vortex line density this temperature dependence is still seen. However for the lower temperatures the dependence is less dramatic.

For both experiments the value calculated for the vortex line density

falls within the values proposed by theoretical work[60]. The vortex line density does show for both experiments a linear dependence on the source wire velocity after the velocity reaches $\sim 1.2V_c$. Extrapolating this line back it is seen to pass through the origin of $L_0 = 0$ at $0.0V_c$. This would indicate that the vortex line density is directly related to the source wire velocity. This is probably due to the fact that it is the source wire motion that is the mechanism behind vortex creation by a vibrating wire resonator. This result appears to contradict the findings of Vinen *et al*[29] shown in equation 2.18 where the vortex line density is proportional to V_c^2. Whether this is a consequence of the differing methods of turbulence production, the lack of a normal fluid component at low temperatures or a deficiency within the model used to calculate L_0 is currently unclear. It is hoped that current investigations by Nichol *et al*[61] in ^{4}He vortices at very low temperatures will provide further information with regards to the effect of having no normal fluid component to consider.

The experiment could be improved upon with a few small changes. Firstly a black body radiator with a faster time constant could be built. If the radiator could resolve power changes at a fast enough speed the evolution of the vortex tangle could theoretically be measured. The problems with this are that the vibrating wire resonators have problems with signal noise if the time constant on the controlling electronics are set too low. Secondly the effect that the generated quasiparticle beam has on the radiator can be removed by orientating the generator resonator perpendicular to the radiator aperture so that the radiator beam is incident on the 'side' of the generated vortices or perhaps several radiators at different angles around the source

wire. If this was to be built then the value for the 'angular' decay length would have to be measured and this would necessitate the construction of a second linear array with source wire perpendicular to and within a linear array. The experiment which has been performed has validated the technique and has proven the concept but more work needs to be done on the finer details of the procedures and the simplified mathematical model will need to be refined much further.

Chapter 7

Summary

The work presented within this thesis is an account of the research I have conducted on vortices within B phase superfluid helium-3 during the three years of my Ph.D. The initial chapters provide some background into the physics of superfluid ^{3}He at low temperatures and the complex equipment that allows such low temperatures to be investigated. The fourth chapter details the manufacture, operation and theory behind the vibrating wire resonators that feature heavily in the experiments conducted.

The vibrating wire resonator is a group favourite for investigating ultralow temperature helium. A vibrating wire resonator is highly sensitive to changes in the thermal quasiparticle density and so makes an ideal thermometer since it can be operated without perturbing the superfluid to a great extent. Vibrating wire resonators are also highly efficient at detecting any quantised vortex lines within their locality. This is because vortex lines in ^{3}He will interact with the thermal quasiparticles, which the vibrating wires rely on, by scattering the quasiparticles through Andreev processes. Recently however an experiment investigating glasses showed that a vibrating wire resonator

driven above its critical velocity will create vorticity itself[6]. The experiment in which this was discovered was not intended to look for this and its discovery was a pleasant surprise.

Shortly after this discovery a new experiment was planned to investigate this new phenomenon further. This experiment is described in chapter 5. The experimental cell for this consists of seven vibrating wires arranged in an array. The results for this experiment were greatly encouraging. It was shown that the density of vorticity generated by a supercritical resonator can be investigated for the direction of the wire motion. From these results the decay length of the vortex tangle was measured assuming the vorticity decays with a simple exponential relationship. The data fitted the exponential model well. This decay length was calculated for different temperatures of the bulk superfluid. The temperature range which could be investigated was unfortunately limited as the mean free path of the quasiparticles is temperature dependent so the generated quasiparticle beam correction could only be applied for bulk temperatures below 250μK where the mean free path is greater than the cell dimensions.

The shape of the vorticity was also investigated in directions orthogonal to the wire motion. In these directions it was shown that the extent of the vorticity produced is greatly diminished. This suggests that the vorticity is either shaped by the quasiparticle beam, also created by the supercritical resonator, or that the vortices are ejected from the wire surface where they are created when the wire displacement is at a maximum and propagate in this direction. It has been proposed that a new cell could be built containing more closer spaced resonators or the quartz tuning forks, used in Nottingham[62]

for mixture experiments, be used. The advantage that these tuning forks would have over a resonator is that the footprint of the fork is much smaller than the footprint required by a resonator, providing an increased spatial resolution, although tuning forks have not yet been used in pure ^{3}He for vorticity detection.

The second experiment, which is described in chapter 6, involves using a low temperature black body radiator to produce a highly directionalised beam of thermal quasiparticles. The vorticity created by a vibrating wire is then used to reflect this beam back, through Andreev processes, into the radiator. By using a well defined beam of thermal quasiparticles, instead of the background thermal quasiparticles of the first experiment, a model was able to be formulated to quantify the density of the vortex lines generated. The dependency of the temperature of the quasiparticle beam and the temperature of the bulk superfluid in which the vortices were created was measured. The results from this indicate that the vortex line density is dependent on the superfluid temperature with a hotter superfluid causing a lower density. Whilst examining this it was observed that the vortex line density, independently of the temperature, exhibited a linear relationship with the generating wire velocity. This has provided much interest from the field of theoretical vortex dynamics and it is hoped this discovery will provide a greater insight into the dynamics of quantised turbulence. This is in comparison to the early experiments on turbulence produced by counterflow in HeII[27][28][29][30], where the vortex line density was shown to have a quadratic relationship with the flow velocity.

The reasons why the vortex line density is linear with flow velocity is

currently not clear. The experiments in HeII where $L_0 \propto V^2$, used a different method of generating the turbulence to the experiments conducted in ^{3}He. Also the original experiments in HeII were conducted at temperatures where there was a significant normal fluid component which is not present at the temperatures investigated in ^{3}He. Recent work performed by Nichol *et al*[61] on creating turbulence in superfluid ^{4}He with a vibrating grid at temperatures where there is no normal fluid may be able to provide more insight as to whether it is the normal fluid component that provides the V^2 relation, or the differences in the superfluid investigated.

Currently the Lancaster low temperature research group are not conducting further studies on quantised vorticity but there are plans to investigate the dynamics of vortex tangles in the future. Having operated the same experimental cell for three years, current efforts are being directed elsewhere. Experiments were attempted to measure the development of a vortex tangle with time but unfortunately the equipment available could not provide a high enough temporal resolution. Hopefully in the future either the equipment or new experimental techniques will allow this work.

Bibliography

[1] R.C.Weast *The Handbook of Chemistry and Physics* CRC Press, Cleveland (1976)

[2] K.Mendelssohn *The Quest for Absolute Zero* 2nd edn. Taylor and Francis, London (1977)

[3] R.J.Donnelly *Quantum Vortices in Helium II* Cambridge University Press, Cambridge (1991)

[4] R.P.Feynman *Prog. Low Temp. Phys.* **I** North Holland, Amsterdam (1955)

[5] D.I.Bradley *Phys. Rev. Lett.* **84**, 1252 (2000)

[6] S.N.Fisher, A.J.Hale, A.M.Guénault and G.R.Pickett *Phys. Rev. Lett.* **86**, 244 (2001)

[7] J.Kopu, R.Schanen, R.Blaauwgeers, V.B.Eltsov, M.Krusius, J.J.Ruohio, and E.V.Thuneberg *J. Low Temp. Phys.* **120** 213 (2000)

[8] M.P.Enrico, S.N.Fisher, A.M.Guénault, G.R.Pickett and K.Torizuka *Phys. Rev. Lett.* **70** 1846 (1993)

[9] L.Landau *Sov. Phys. JETP* **3**, 920 (1956)

[10] L.Landau *Sov. Phys. JETP* **5**, 101 (1957)

[11] D.Vollhardt and P.Wölfle *The Superfluid Phases of Helium 3.* Taylor & Francis, London (1990)

[12] D.R.Tilley and J.Tilley *Superfluidity and Superconductivity.* Institute of Physics Publishing, Bristol and Philadelphia (1996)

[13] A.J.Leggett *Rev. Mod. Phys.* **47** 331 (1975)

[14] J.Bardeen, L.N.Cooper and J.R.Schrieffer *Phys. Rev.* **108** 1175, (1957)

[15] R.Balian and N.R.Werthamer *Phys. Rev.* **131** 1553 (1963)

[16] P.W.Anderson and P.Morel *Physica* **26** 671 (1960)

[17] P.W.Anderson and P.Morel *Phys. Rev.* **123** 1911 (1961)

[18] P.W.Anderson and W.F.Brinkman *Phys. Rev. Lett.***30** 1108 (1973)

[19] D.D.Osheroff, R.C.Richardson and D.M.Lee *Phys. Rev. Lett.* **29** 920 (1972)

[20] D.S.Greywall *Phys. Rev. B* **29** 4933 (1984)

[21] P.G.Saffman and G.R.Baker *Annual Rev. of Fluid Mech.* **11** Annual Reviews Inc., Palo Alto (1979)

[22] A.F.Andreev *Sov. Phys. JETP* **19** 1228 (1964)

[23] L.Onsager *Nuovo Cimento Suppl.* **6** 249 (1949)

[24] W.F.Vinen *Proc. Roy. Soc.* **A260** 218 (1961)

[25] S.N.Fisher, A.M.Guénault, C.J.Kennedy and G.R.Pickett *Phys. Rev. Lett.* **63** 2566, 1989.

[26] C.F.Barenghi, C.E.Swanson and R.J.Donnelly *Phys. Rev. Lett.* **48** 1187 (1982)

[27] W.F.Vinen *Proc. Roy. Soc. A* **240** 114 (1957)

[28] W.F.Vinen *Proc. Roy. Soc. A* **240** 128 (1957)

[29] W.F.Vinen *Proc. Roy. Soc. A* **242** 493 (1957)

[30] W.F.Vinen *Proc. Roy. Soc. A* **243** 400 (1957)

[31] M.Tsubota, T.Araki, S.K.Nemirovskii *Phys. Rev. B* **62** 11751 (2000)

[32] D.F.Brewer *Phil. Mag.* **7** 721 (1962)

[33] R.P.Slegtenhorst, G.Marees, H.van Beelen *Physica B* **113** 367 (1981)

[34] D.R.Ladner, R.K.Childers, J.T.Tough *Phys. Rev. B* **13** 2918 (1976)

[35] K.P.Martin and J.T.Tough *Phys. Rev. B* **27** 2788 (1983)

[36] D.J.Melotte and C.F.Berengi *Phys. Rev. Lett.* **80** 4181 (1998)

[37] K.W.Schwarz *Phys. Rev. B* **31** 5782 (1985)

[38] K.W.Schwarz *Phys. Rev. B* **38** 2398 (1988) and references therein.

[39] C.Caroli and J.Matricon *Phys. Kondens. Mater.* **3** 380 (1995)

[40] N.B.Kopnin, G.E.Volovic and Ü.Parts *Europhys. Lett.* **32** 651 (1995)

[41] N.B.Kopnin and M.M.Salomaa *Phys. Rev. B* **44** 9667 (1991)

[42] C.F.Barenghi and D.C.Samuels *Phys. Rev. Lett.* **89** 155302 (2002)

[43] M.Krusius, M.Niemetz, W.Schoepe *Phys. Rev. Lett.* **87** 059601 (2001)

[44] M.Niemetz, W.Schoepe, J.T.Simola and J.T.Tuoriniemi *Physica* (Amsterdam) **280B** 599 (2000)

[45] M.Niemetz, H.Kerscher and W.Schoepe, cond-mat/0009299

[46] D.I.Bradley and G.R.Pickett *Phys. Rev. Lett.* **87** 059602 (2001)

[47] D.I.Bradley *et al Cryogenics* **6** 296 (1982)

[48] D.I.Bradley *et al J. Low Temp. Phys.* **57** 359 (1984)

[49] T.Guénault, *Basic Superfluids* (Taylor & Francis, London) (2003)

[50] A.Kent, *Experimental Low-Temperature Physics* (Macmillan, London) (1993)

[51] O.V.Lounasmaa, *Experimental Principles and Methods Below* $1K$ (Academic Press, London) (1974)

[52] D.I.Bradley *et al Phys. Rev. Lett.* **75**, 1887 (1995)

[53] S.N.Fisher, *PhD Thesis* (1992)

[54] Y.Kondo *et al., Physica* (Amsterdam)**178B**, 90 (1992)

[55] T.W.B.Kibble, *J. Phys. A* **9**, 1387 (1976)

[56] E.Varoquaux and O.Avenel, *Physica* (Amsterdam), **197B**, 306 (1994)

[57] S.N.Fisher, A.M.Guénault, C.J.Kennedy, G.R.Pickett, *Phys. Rev. Lett.* **69**, 1073 (1992)

[58] K.F.Coates, A.M.Guénault, S.G.Mussett and G.R.Pickett *Europhys. Lett.* **2** 523 (1986)

[59] A.I.Ahohen, J.Kokko, M.A.Paalanen, R.C.Richardson, W.Schoepe and Y.Takano *J. Low Temp. Phys.* **30**, 205 (1978)

[60] M.Tsubota, T.Araki, W.F.Vinen *Physica B* **329-333**, 224-225 (2003)

[61] H.Nichol, P.V.E.McClintock, P.Hendry, L.Skrbek *In preparation*

[62] D.O.Clubb, *PhD Thesis* (2003)